PHOSPHITE MODIFIED COBALT COMPLEXES FOR OLEFIN HYDROFORMYLATION

by

BATSILE MOSAI MOGUDI

DISSERTATION

Submitted in accordance with the requirements for the degree

MAGISTER SCIENTIAE

in

CHEMISTRY

in the

FACULTY OF NATURAL AND AGRICULTURAL SCIENCES

in the

DEPARTMENT OF CHEMISTRY

at the

UNIVERSITY OF THE FREE STATE

SUPERVISOR: Prof. Andreas Roodt

CO-SUPERVISOR: Dr. Reinout Meijboom

September 2008

Acknowledgements

I would like to express my gratitude to the following:
First and foremost I express my gratitude to the Almighty for giving me the aptitude and strength to accomplish the work I have managed to do.

Prof. Andreas Roodt, for all his expertise in the course and being able to impart his knowledge and his never ending patience and support.

Dr. Reinout Meijboom, for all your assistance, imparting of your knowledge on the course as well as your patience. I thank you for all your endless support.

To Dr Gideon Steyl, for all the NMR and other assistance, Dr Alfred Muller for crystal structure analysis and all the help they have given me during my study your assistance is highly appreciated. Dr Thato Mtshali, thank you very much for your tireless assistance and patience.

Mr. Leo Kirsten and Mr. Inus Janse van Rensburg, for all the patience they had with me.
I appreciate all the assistance you gave me Leo thank you very much for always being available to assist me with any problem I might have encountered.

To my colleagues (inorganic group), the personnel and staff of the Department of Chemistry in the University of the Free State, I express my gratitude and appreciation to everyone who was a part of my success to obtaining this degree.

To my husband, Howard thank you very much for your support, love, encouragement and understanding, my children, Mpaballe, Thale, Ntebogeng and Modisi, for their support and love. I would also like thanking my mother, Emily Marokoane for being there for my children whilst I was away. Dieketseng, I thank you and appreciate all the assistance you gave my family whilst I was away in Bloemfontein.

C change, who has given financial support for our research group and this study*
Prof Andreas. Roodt, I thank you once more for all your financial assistance.

Table of Contents:

Abbreviations and Symbols

δ	chemical shift
ν	stretching frequency on IR
M	metal
n/*i* ratio	linear to branched ratio
Abs	absorbance
k_{obs}	observed rate constant
T	temperature
ppm	parts per million
NMR	nuclear magnetic resonance
CO	carbonyl
^{t}Bu	tertiary butyl
DMF	N,N-Dimethylformamide
$P(OR)_3$	Tertiary phosphite
Syn-gas	Synthesis gas
TPP	Triphenylphosphite
HP-IR	High pressure infra red
GC	gas chromatography
α	alpha
β	beta
γ	gamma
λ	wavelength
σ	sigma
Z	number of molecules per unit cell
TMS	trimethyl silane
F(hkl)	structure factor
H_2/CO	syn gas
°C	degrees Celsius
1°	primary
2°	secondary
Å	angstrom(100 ppm)
θ	theta
4-TBPP	Tris(4-tertiarybutyphenyl)phosphite
2-TBPP	Tris(2-tertiarybutyphenyl)phosphite
2-iPrPP	Tris(2-isopropylphenyl)phosphite
2-EtPP	Tris(2-Ethylphenyl)phosphite

IR	infra red
CO	carbon monoxide
L	phosphite/phosphine ligand
[M]/[L]	metal to ligand concentration
[M]	metal concentration
[L]	ligand concentration
TON	turnover number
TOF	turnover frequency
TBP	trigonal bipyramidal
SP	square planar
cm^{-1}	per centimeter
mg	milligram
M	(mol/L)

Summary

Several dinuclear complexes of the form $[Co_2(CO)_6L_2]$ with L being an aromatic phosphite ligand were varied as follows: L = $P(OPh)_3$, $P(O\text{-}4\text{-}^tBuC_6H_4)_3$, $P(O\text{-}2\text{-}^tBuC_6H_4)_3$, $P(O\text{-}2\text{-}EtC_6H_4)_3$, $P(O\text{-}2\text{-}^iPrC_6H_4)_3$. These dinuclear complexes have been synthesised and characterized by IR and NMR. The dinuclear complexes which were successful in being characterized by X ray crystallography were the ones with L = $P(O\text{-}4\text{-}^tBuC_6H_4)_3$ and $P(O\text{-}2\text{-}EtC_6H_4)_3$. These two dinuclear complexes including the complex with $P(OPh)_3$ as a ligand were used as precursors as active catalysts in the hydroformylation of 1-octene. High pressure spectroscopy was used to detect hydride intermediates. High pressure infra red (HP-IR) studies revealed the formation the monophosphite hydrides ($[HCo(CO)_3L]$) for all the studied ligands, as well as the formation of bisphosphite hydrides $[HCo(CO)_2L_2]$ and the unmodified hydride $[HCo(CO)_4]$. At 140 °C both the unmodified and the bisphosphite had disappeared and the only specie present was the monophosphite hydride which is the active hydride catalyst in hydroformylation reactions.

This study has proven the importance of the stability of the hydride in the hydroformylation reaction along with the selectivity and conversion rate of the 1-octene to the aldehyde. The stability of the hydride was tested in the presence of 1-octene and in the absence of 1-octene. Catalytic activity of the studied cobalt phosphite complexes was tested at the end of the stability runs.

Opsomming

'n Aantal bikernige bis-metaal komplekse met die algemene vorm $[Co_2(CO)_6L_2]$ is gesintetiseer, waar L aromatiese fosfiete is wat as volg gevariëer is: L = $P(OPh)_3$, $P(O\text{-}4\text{-}^tBuC_6H_4)_3$, $P(O\text{-}2\text{-}^tBuC_6H_4)_3$, $P(O\text{-}2\text{-}EtC_6H_4)_3$, $P(O\text{-}2\text{-}^iPrC_6H_4)_3$. Hierdie komplekse is gesintetiseer en gekarakteriseer deur IR en KMR. Die bikernige komplekse wat suksesvol deur X-straal kristallografie gekarakteriseer was die met L = $P(O\text{-}4\text{-}^tBuC_6H_4)_3$ en $P(O\text{-}2\text{-}EtC_6H_4)_3$. Hierdie twee bikernige komplekse, insluitend die kompleks met $P(OPh)_3$ as ligand, was gebruik as voorgangers in die hidroformilering van 1-okteen. Hoë-druk spektroskopie was gebruik om die hidried tussengangers spesies op te spoor. Hoë-druk infra-rooi (HD-IR) studies het die forming van mono-fosfiet hidried ($[HCo(CO)_3L]$) aangedui vir all die bestudeerde ligande, ek ook vir die vorming van bisfosfiet hidriede ($[HCo(CO)_2L_2]$) en die ongemodifiseerde hidried $[HCo(CO)_4]$. By 140 ˚C het beide die ongemodifiseerde en die bisfosfiet spesies verdwyn en die enigste spesie teenwoordig was die mono-fosfiet hidried wat die aktiewe hidried katalis is in die hidroformileerings reaksies.

Hierdie studie het die belangrikheid van die stabiliteit van die hidried in die hidroformilerings reaksie bewys saam met die selektiwiteit en omskakelings tempo van 1-okteen na die aldehied. Die stabiliteit van die hidried was getoets in die teenwoordigheid van 1-okteen en in die afwesigheid van 1-okteen. Katalitiese aktiwiteit van die gestudeerde kobalt fosfiet komplekse was getoets na die stabiliteits lopies.

Chapter 1
Aim of study

1.1 Introduction

Hydroformylation of alkenes (also known as the *oxo synthesis*) is one of the most important industrial processes which involve a transition metal complex as a catalyst. In order to develop and optimize the capability of novel homogeneous catalyst systems, it is essential that the nature of the interaction between metal complexes and organic reactants, substrates as well as potential feedstock poisons, is understood. A key part of this understanding lies in knowing how catalysts can be designed and how particular metal–ligand systems can activate hydrocarbon-based feedstock (both functionalized and unfunctionalized) in a beneficial manner.

Cobalt is not one of the abundant elements, but it is widely diffused in nature.[1] Both cobalt and rhodium are used in catalytic hydroformylation reactions however, cobalt is less susceptible to catalyst poisoning than its rhodium counterpart. Rhodium complexes are used as industrial catalysts for propene hydroformylation,[2,3,4] and although the cobalt complexes are less reactive, they have been in use much longer and predominate.[5] These cobalt catalysts are currently mainly used for long-chain alkenes.[5] Cobalt has also proved to be a cheaper metal.

Otto Roelen discovered the hydroformylation of alkenes on the 26th of July 1938 during his study of the Fischer-Tropsch (FT) reaction (syn-gas conversion to liquid fuels).[6] The hydroformylation reaction is responsible for the production of aldehydes from alkenes. Aldehydes produced by hydroformylation are usually reduced to alcohols, which are useful as solvents, plasticizers[7] and in the synthesis of detergents.[8] In the cobalt-catalyzed-hydroformylation, a significant amount of branched aldehydes are formed. The addition of the hydride is influenced by the steric bulk of the ligand; it has an influence whether the hydride adds *anti*-Markovnikov or Markovnikov. The hydride addition must preferentially be *anti*-Markovnikov when linear aldehydes are preferred; as in the synthesis of biodegradable detergents. Isomerisation of the alkenes also has to be prevented. It was discovered that the addition of an alkylphosphine[9] to the reaction mixture gives higher selectivity for the linear product.

Hydroformylation is the reaction of an alkene in the presence of synthesis gas (CO/H_2) and a transition metal catalyst. Heck and Breslow proposed the general mechanism of cobalt-carbonyl-catalyzed hydroformylation[10] in 1961. In the hydroformylation reaction the CHO generated from H_2 and CO is added across the alkene C=C to form the linear or branched aldehyde. In the event where hydrogenation occurs, the alkene may also be hydrogenated. (see Reaction 1.1).

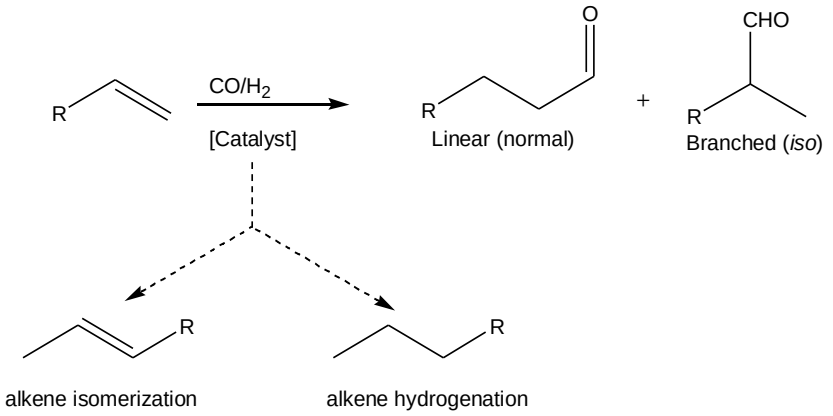

(1.1)

Mono-, di-, tri-, and tetra-substituted derivatives can be obtained by direct replacement of carbon monoxide by phosphine ligands (L) when using the metal carbonyl method in chemistry (reaction 1.2).[11]

$$[Co_2(CO)_8] + nL \rightarrow [Co_2(CO)_{8-n}L_n] + nCO \uparrow \quad \textbf{(1.2)}$$

Phosphites only afford mono- and di-substituted cobalt carbonyl derivatives when using this method.[11] Cobalt as a metal is not attacked by oxygen or water at ordinary temperatures, but at elevated temperatures it is oxidized in moist air.

1.2 Aryl phosphites

Phosphites relative to phosphines decrease the electron density on the cobalt centre therefore they are expected to produce less hydrogenated products.[12,13] At low ligand concentrations the results which were obtained for the hydroformylation of triphenylphosphite and triphenylphosphine were similar.[14] The disadvantages of phosphites include side reactions such as hydrolysis, alcoholysis, *trans*-esterification and Arbusov rearrangement.[15] The side reactions are restricted to alkyl phosphites, acids, carbenium ions and metals catalyze the Arbusov rearrangement.

The aryl phosphites are preferred because they do not have the previous side reactions and bond cleavage of O—C or P—C. The phosphites are also easier to synthesise and are less prone to oxidation than phosphines. The first publication on the use of phosphites is from Pruet and Smith, from the Union Carbide.[16]

It was discovered that manipulation of the phosphite cone angle[12] and using more steric bulk gave the better active monophosphite cobalt carbonyl hydride $[HCo(CO)_3L]$ **(2)**. Both the monophosphite cobalt carbonyl hydride **2** and bisphosphite cobalt carbonyl hydride **3** formed when triphenylphosphite[13] was used as a ligand with a cone angle[17] of 128º. The bisphosphite carbonyl hydrides $[HCo(CO)_2L_2]$ **(3)** were proposed to be inactive as catalysts. When the ligand tris(2,4-di-*tert*-butylphenyl)phosphite was used, formation of the bisphoshite hydride $[HCo(CO)_2L_2]$ **(3)** was not observed. Only the monophosphite hydride $[HCo(CO)_3L]$ **(2)** formed presumably due to the larger cone angle (175º). The larger steric bulk prevented the formation of the bisphoshite hydride.

1.3 Aim and objectives

The aim of the study was to investigate the intimate relationship between the catalytic activity and steric factors of phosphites in modified cobalt carbonyl complexes. These complexes are used as catalyst models in hydroformylation reactions, with a special emphasis on reaction mechanism. The aim was to prepare cobalt complexes modified with phosphite ligands. The focus lies on specifically manipulating the steric demand at the P–donor atom. The aim of the Masters dissertation was to study structural factors of cobalt catalysts with respect to the activity and stability in hydroformylation of higher alkenes, in this case 1-octene. Thus we were investigating the influence of steric properties of the ligand on catalytic activity, while keeping the electronic properties constant.

1.4 Work plan

The initial work plan was to test the solution behaviour of the hydrides during hydroformylation. Instead it was noticed that there were changes in the carbonyl region of the IR spectra where the hydride absorbs (1900 - 2100 cm^{-1}), Which brought about a base for investigation of this region.

1.4.1 Procedure

The phosphites have the same electronic effects, thus varying the steric bulk in order to improve the reaction rates in the hydroformylation catalytic cycle.

Part 1:

Synthesis and characterization of:

Aromatic phosphite ligands, L, of the type $P(O\text{-}2\text{-}RC_6H_4)_3$, (R = Et) and L, of the type $P(O\text{-}4\text{-}RC_6H_4)_3$, (R = ^{t}Bu), were synthesised. These phosphites were selected because they give a range of Tolman cone-angles (variations between 128º - 180º). The phosphites were used in the synthesis of the cobalt carbonyl phosphite complexes $[Co_2(CO)_6L_2]$ **(1)**. $P(OPh)_3$ **(a)** was commercially available, and was purchased and used for the synthesis for the dimer.

Part 2:

Synthesis and characterization of:

Intermediate species e.g. $[HCo(CO)_2L_2]$ **(3)**, $[HCo(CO)_4]$ **(5)** and $[HCo(CO)_3L]$ **(2)**. Reaction of the unmodified hydride $[HCo(CO)_4]$ **(5)** with excess phosphite ligand was performed in order to determine which hydride forms, the monophosphite hydride $[HCo(CO)_3L]$ **(2)** or bisphosphite hydride $[HCo(CO)_2L_2]$ **(3)**.

The monophosphite hydride $[HCo(CO)_3L]$ **(2)** will be synthesised for all the ligands. The hydrides were synthesised in order to be able to identify them when using HP-IR under high temperature and pressure reaction conditions. In addition the synthesis of the modified cobalt carbonyl hydrides will be performed in order to try to find the minimum cone angle which would prevent formation of the bisphosphite hydride $[HCo(CO)_2L_2]$ **(3)**.

Part 3:

HP-IR spectroscopic investigations

Using the dimeric species as precursors in the preformation of the hydrides under high-pressure infrared reaction conditions, performing the hydroformylation of 1-octene in the presence of syngas CO/H_2 = 1. Preformation of the catalyst and allowing it to be aged in catalytic reaction conditions in the absence of 1-octene using a new batch. Eventually testing of the monophosphite cobalt carbonyl hydride $[HCo(CO)_3L]$ **(2)** which was allowed to age in the hydroformylation of 1-octene. Observe the catalytic changes after the ageing of the cobalt carbonyl hydride species

2, comparing the results obtained with those obtained for the hydroformylation of 1-octene without the aged catalyst.

Part 4:

Evaluate the rate of catalysis, i.e.

- Hydride appearance
- Hydride change in the presence of alkene during the hydroformylation reaction
- Change of the cobalt phosphite carbonyl catalyst in the presence and absence, of 1-alkene
- Rate of conversion of 1-octene infrared spectra at (1822 and 1639 cm^{-1}) to the formation of the aldehyde with infrared spectra at (1734 cm^{-1}) with the two different hydrides i.e. the hydride which was not allowed to age and the hydride that was not allowed to age.

1.5 References to the identification of the cobalt carbonyl complexes

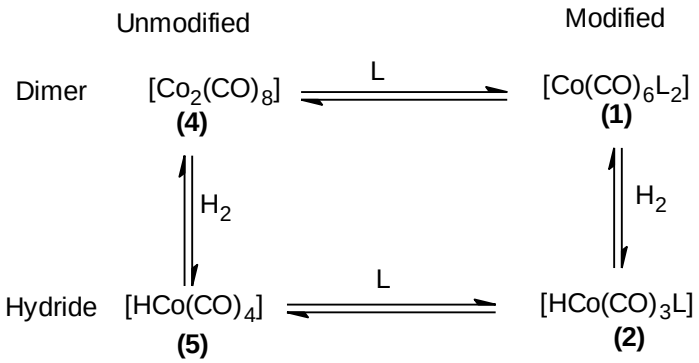

Scheme 1.1: Reaction scheme and identification of the cobalt carbonyl complexes[18] L represents the phosphite ligands $P(OPh)_3$ ***(a)****, $P(O\text{-}4\text{-}^tBuC_6H_4)_3$* ***(b)*** *and $P(O\text{-}2\text{-}EtC_6H_4)_3$* ***(c)*** *for the purpose of this study.*

1.6 Representation of complexes and ligands

Cobalt Complexes

The cobalt phosphite complexes, cobalt complexes and ligands which will be mentioned in the following chapters will be identified in the following manner.

Complex **1:** Cobalt phosphite dimer $[Co_2(CO)_6L_2]$

Complex **2:** monophosphite hydride $[HCo(CO)_3L]$

Complex **3:** bisphosphite hydride $[HCo(CO)_2L_2]$

Complex **4:** unmodified cobalt carbonyl dimer $[Co_2(CO)_8]$

Complex **5:** unmodified cobalt carbonyl hydride $[HCo(CO)_4]$

Complex **6:** alkyl species $[RCH_2CH_2Co(CO)_3L]$

Complex **7:** π Complex [$RCH_2{=}CH_2CoH(Co)_2L$]

Complex **8:** acyl species [$RC(O)Co(CO)_3L$]

Ligands (L):

a $P(OPh)_3$

b $P(O\text{-}4\text{-}^tBuC_6H_4)_3$

c $P(O\text{-}2\text{-}EtC_6H_4)_3$

d $P(O\text{-}2,4\text{-}^tBu_2C_6H_3)_3$

e $P(O\text{-}2\text{-}^iPrC_6H_4)_3$

f $P(O\text{-}2\text{-}^tBuC_6H4)_3$

R represents an alky group

References

1 D.S. Roland, "*Cobalt",* Waverly, Baltimore MD, 1948, 108.

2 M.E. Orchin and W. Rupilius, *Catal, Rev.,* 1972, **6**, 85.

3 R. L. Pruett, *Adv. Organomet*. *Chem*., 1979, **19**, 1.

4 J. Falbe, "*Carbon Monoxide in Organic Synthesis*", C. R. Adams, Chapter 1, Springer, New York, 1970.

5 B.C. Gates, "*Catalytic Chemistry",* John Wiley and Sons Inc, 1992, p.93.

6 O. Roelen, *Ger. Pat*., 1938, **949**, 548.

7 D.F. Foster, D. Gudmunsen, D.J. Adams, A.M. Stuart, E.G. Hope, D.J. Cole-Hamilton, G.P. Shwarzand and P. Pogorzelec, *Tetrahedron,* 2002, **58**, 3901.

8 D.F. Shriver and P.W. Atkins, "*Inorganic Chemistry"*, Oxford University Press, 3rd Edition, 1999, p.593.

9 L. H. Slaugh and R. H. Mullineaux, *J. Organomet. Chem*., 1968, **13**, 469.

10 (a) R.F. Heck and D.S. Breslow, *Chem. Ind*., *(London)*, 1960, 467.
(b) R.F. Heck and D.S. Breslow, *J. Am. Chem. Soc*., 1961, **83**, 403.

11 M.S. Arabi, A. Maisonnat, S. Attali and R. Poilblanc, *J. Organomet. Chem*., 1974, **67**, 109.

12 R. Meijboom, M. Haumann, A. Roodt and L. Damoense, *Helv. Chim. Acta*., 2005, **88**, 676.

13 M. Haumann, R. Meijboom, J.R. Moss and A. Roodt, *Dalton Trans.*, 2004, 1679.

14 P.W.N.M. van Leeuwen, "*Homogeneous Catalysis, Understanding the art"*, Kluwer Academic Publishers, Dordrecht, 2004.

15 http://chemistry.lsu.edu/stanley/webpub/4571-chap16-hydroformylationpdf 29/11/07

16 R.L. Pruet and J.A. Smith, *J. Org. Chem*., 1969, **34**, 327.

17 C.A. Tolman, *Chem. Rev*., 1977, **77**, 313.

18 C. Crause, L. Bennie, L. Damoense, C.L. Dwyer, C. Grove, W. Janse van Rensburg, M.M. Kirk, K.M. Mokheseng, S. Otto and P.J. Steynberg, *Dalton Trans*., 2003, 2036.

Chapter 2

Hydroformylation Catalysis

2.1 Introduction

This chapter concentrates on the theoretical aspects of organometallic chemistry and coordination chemistry applicable to catalysis. The general principles applicable in the hydroformylation catalytic cycle will be shown, in which a catalytic species is regenerated in the reaction. A description on both the unmodified and modified catalytic cycles involved in hydroformylation. The different metal types, which are available for the hydroformylation reaction, are preferably cobalt and rhodium. The phosphite and phosphine ligands; ligand influences related to the influence they have on catalysis. The role the hydride has in hydroformylation as well as the influence the steric bulk of the different ligands have on the selectivity towards linear or branched aldehydes will be discussed. The different types of products that is accessible by making use of the hydroformylation reactions.

2.2 Types of catalysts (homogeneous vs heterogeneous)

A catalyst is defined as a substance that increases the rate of a reaction, but is not itself consumed in the process. Catalysts are widely used in nature, in industry and in the laboratory. It is estimated that they contribute to one-sixth of the value of all manufactured goods in industrialized countries.[1] Production of chemicals in industry is based on the catalytic combination of small molecules (C_2H_4, CO, H_2, H_2O and NH_3) to produce larger molecules (ethylene glycol, acetaldehyde, acetic acid and acrylonitrile), which are of economic importance.[2] The two most important characteristics of a catalyst are its activity, which is expressed as its turnover number or frequency, and its selectivity. The turnover number (TON) is the number of product molecules produced per molecule of the catalyst. The turnover frequency (TOF) is the turnover number per unit time. Organometallic compounds are successful catalysts because it is easy to modify the catalyst by changing the ligand environment. Important properties that can be influenced are the rate of the reaction and the selectivity towards desired products. Homogeneous catalysts present a better opportunity for the manipulation of the catalyst by changing the electronic and steric properties. Manipulation of the catalyst is done in order to improve selectivity towards the desired products.

High selectivity is a way to:

- reduce waste
- reduce work-up equipment of a plant

The catalysts can be homogeneous or heterogeneous. A catalyst is referred to as homogeneous if it is in the same phase as the reactants and no phase boundary exists. A heterogeneous catalyst has a phase boundary. The reactions are referred to as homogeneous catalysis and heterogeneous catalysis respectively.[3,4] A catalyst is responsible for a reaction being faster (or in some cases more specific) than a reaction which is not catalyzed. The catalyst can also lower the activation energy. Petrochemical conversion uses both the homogeneous as well as heterogeneous catalysts. Table 2.1 shows the strengths and weaknesses of both methods, making it easy to differentiate homogeneous from the older, successful, heterogeneous catalysis.[5]

Table 2.1: Homogeneous vs. heterogeneous catalysis

	Homogeneous Catalysis	Heterogeneous Catalysis
Activity (relative to metal content)	High	Variable
Selectivity	High	Variable
Reaction conditions	Mild	Harsh
Service life of catalyst	Variable	Long
Sensitivity towards catalyst poisons	High	Low
Diffusion problems	None	May be impossible
Catalyst recycling	Expensive	Cheap
Variability of steric and electronic properties of catalyst	Possible	Not possible
Mechanistic understanding	Plausible under random conditions	More or less impossible

Hydroformylation catalysts consist of a transition metal atom (M) which enables the formation of metal-carbonyl hydride species. The species are optionally modified by substitution of the carbonyl group by ligands (L). A general composition is represented by the types of complexes (see Structure 1)

$$[H_xM_y(CO)_zL_n] \quad \textbf{(1)}$$

Where (x, y, z, n = 0, 1 , 2, etc). When n = 0 the catalyst is referred to as ‘unmodified’, whereas if the metal centre is coordinated to ligands other than CO or hydrogen it is referred to as ‘modified’. Control of the selectivity, chemo-, *regio*- and

stereo-selectivity is the most important problem in the hydroformylation reaction. *Chemo*selectivity is concerned with such competition reactions as isomerisation, hydrogenation of the alkene and aldehyde hydrogenation that occur under hydroformylation conditions.[6]

The following types of selectivity can be distinguished in a chemical reaction.[7]

- *Chemoselectivity* When more than one reaction can take place for the same substrate. Chemoselectivity indicates which of the two will be hydrogenated e.g. hydrogenation or hydroformylation.
- *Regioselectivity:* e.g. Hydroformylation reaction, the aldehyde group can be attached either to primary, terminal carbon or the secondary, internal carbon atom. This would lead to either the linear or branched product. This predicts the type of product that will be obtained.
- *Diastereoselectivity:* The substrate would contain a stereogenic center and this together with the catalyst can direct the addition of the hydrogen in hydroformylation to give one of the two diasteriomers.
- *Enantioselectivity*: This time the substrate is achiral, but the enantiopure or enantio-enriched catalyst may give rise to the formation of one specific pure enantiomer product (See Figure 2.1).

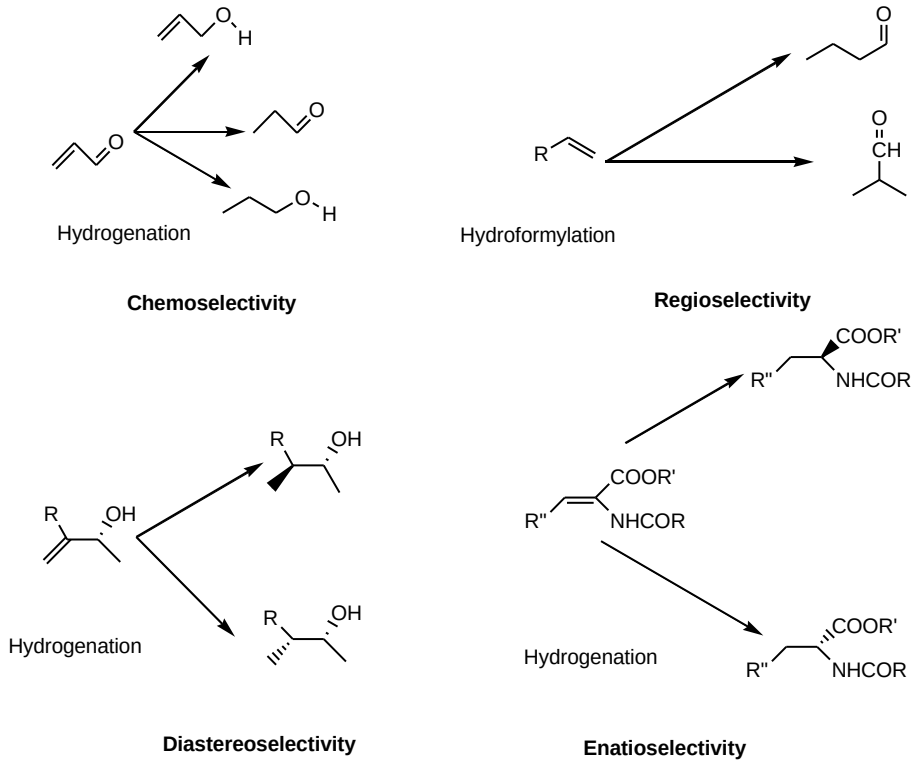

Figure 2.1: Selectivity of chemical conversions.

Production of fine chemicals uses a variety of sophisticated homogeneous catalysts.

The following are the requirements for a successful catalytic process:

- The reaction being catalyzed must be thermodynamically favourable.
- The catalyzed reaction must be fast enough.
- The catalyst must have an appropriate selectivity towards the desired product.
- The catalyst must have a life time long enough to be economically viable.

2.2.1 Application of hydroformylation catalysts

The major application of cobalt complexes is in the hydroformylation reactions. Today hydroformylation is the most important application of homogeneous catalysis on an industrial scale,[8] with worldwide production capacities of about 6 million ton/yr.[8] The products of hydroformylation are valuable precursors for plasticizers and detergents.[1] The perfect hydroformylation reaction is more selective towards linear aldehydes than branched aldehydes and in high yield. It also minimizes reagents and solvents, as well as byproducts. The types of ligands used in industrial hydroformylation plants are the phosphines PR_3 (R = C_6H_5, *n*-C_4H_9), triphenylphosphine oxide and in some special cases phosphites, $P(OR)_3$.[8] The compounds accessible by the production of aldehydes are represented in (Figure 2.2)

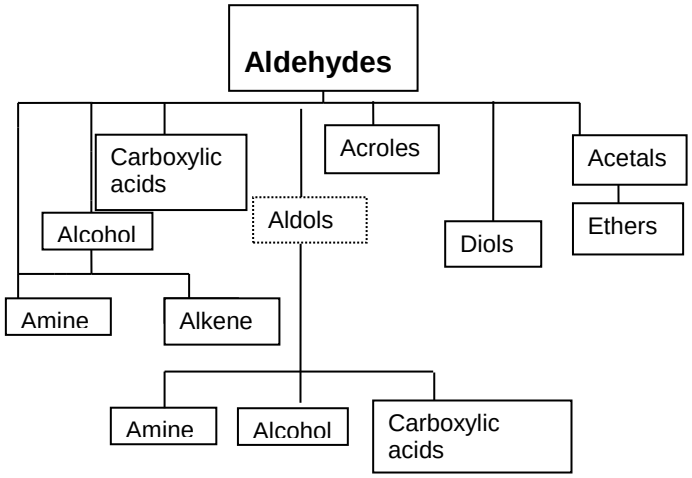

Figure 2.2: Chemical business bandwidth of compounds accessible by hydroformylation.[5,9]

The number of homogeneously catalyzed processes has been steadily growing in the eighties and nineties. It was the work of Adkins and Krsek,[10] Storchl,[11] Berty and Markó[12] and Natta[13] that confirmed the hydroformylation process to be homogeneous in nature.

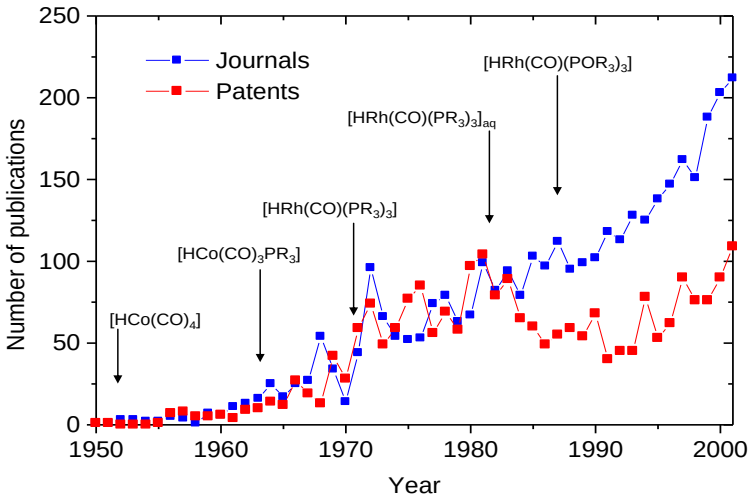

Figure 2.3: Publications on 'hydroformylation' (SciFinder)

The discovery of hydroformylation gained little recognition for the first 20 years[7] (Figure 2.3) after Otto Roelen discovered it. In the mid 1950's two main developments made a contribution to the steady increase on the importance of hydroformylation. The first development was the rapid growth of the petrochemical industry. It managed to switch the alkene away from natural or FT alkenes to a broad variety of cheap and pure petroleum-based alkenes. This presented improved feedstock availability and quality.

The second development was the emergence of at least two markets, the PVC and the detergent industries. Even today these sectors have remained the most significant customers for alcohols produced *via* hydroformylation or hydrogenation from aldehydes formed in hydroformylation. The Low Pressure Oxo (LPO) process took a leading role in the hydroformylation reaction processes. The third hydroformylation catalysts generation was concerned with reaction engineering. The idea was to use a water soluble phosphine as a ligand thus transferring hydroformylation into the aqueous medium (reaction 2.1).

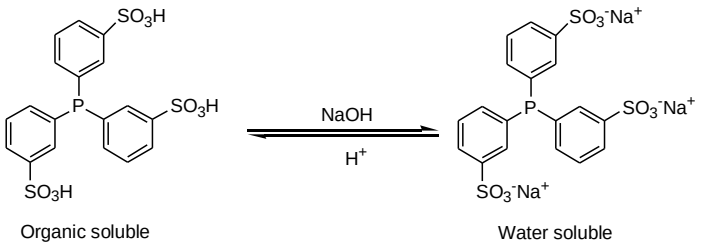

(2.1)

The usage of rhodium compared to cobalt is more attractive because of the high selectivity and mild reaction conditions for the manufacture of n-butylaldehyde. When using rhodium as a catalyst, it is important to be able to recover the metal due to it being an expensive metal. A method for the recovery of the metal was developed by Ruchrchmie/Rhone-Poulenc based on using water-soluble phosphines. The phosphorus ligand used was trisulphonated triphenylphosphine, commonly referred to as TPPTS[14] (reaction 2.1).

When using higher molecular weight olefins, which are less volatile such as 1-octene, dodecene and styrene, they also tend to be less soluble in water. Should Rh-TPPTS be used in the catalytic cycle, low rates of hydroformylation are obtained. The Union Carbide reported a technique that made use of the monosulphonated triphenyl phosphine (TPPMS).[15] Solubilising agents such as N-methylpyrrolidone, polyalkylene glycols, etc, make alkali metal salts of TPPMS which is soluble in the non polar organic phase. Rh-TPPMS complexes can be used for the hydroformylation of higher alkenes. When the reaction is completed the single phase is then separated into a non-polar and a polar phase by the addition of water or methanol, or by changing the temperature.

The biphasic, but homogeneous, reaction system exhibited distinct advantages over the conventional one-phase process and the extension of the principle has been studied since then. A variety of complexes have been observed under syn-gas pressure. The complexes formed depend on the conditions they were subjected to, a wide range of temperatures (25-200ºC) and pressures (1-300 bar) were used. The complexes of the reactions requiring higher temperatures are shown in Figure 2.4 with (L as a phosphine).

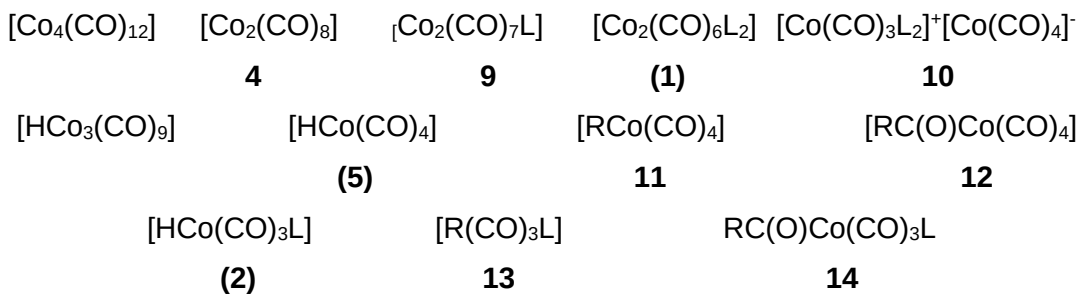

Figure 2.4: Examples of complexes involved in cobalt hydroformylation.

The tetranuclear and trinuclear clusters will only be observed at low pressure[16] but all the other species are common under hydroformylation. Complex **10** is an ionic complex, which is formed in polar solvents.[17] Under these conditions both the dimer and hydride are observed, therefore depending on the hydrogen pressure there will be less or more of the hydride present. The complexes in brackets will be formed during the process of this study of the cobalt phosphite carbonyl hydroformylation, where L represents the phosphite ligands.

2.3 Variations of ligands and their properties

The properties of the catalyst can be changed by modification of the ligands. By modifying the ligand the selectivity towards the desired products can either be increased or decreased.

2.3.1 Unmodified hydroformylation catalysts.

The first catalysts for hydroformylation were based on the unmodified catalyst $[HCo(CO)_4]$ **(5)** with only carbon monoxide as a ligand.[18] The cobalt carbonyl hydrides require harsh reaction conditions: the pressure ranged between 200 and 350 bar to avoid the decomposition of the catalyst and deposition of the metallic cobalt. The temperature was adjusted according to the pressure and the concentration of the catalyst between 150ºC and 180ºC to ensure an acceptable rate of reaction.

The metal carbonyls are amongst the most common organotransition metal complexes. The carbonyls tend to be very high-field ligands forming strong M-L bonds. Carbonyl group, CO, can bond to the metal because it has empty orbitals which overlap with the filled $d\pi$ orbital of the metal. The acceptor orbital in CO is π^*. The carbon atom in CO has a lone pair of electrons, which is the filled orbital, an *anti*-bonding π^* orbital, which is the empty orbital. The combination of the filled

orbital d_π and an empty π^* orbital on the metal constitutes the σ^* bond. The CO is simultaneously an electron donor as well as an electron acceptor.

This type of interaction is referred to as back bonding; because electrons are transferred from CO to the metal and back to the CO. Ligands that are capable of backbonding are referred to as π–acids. Back bonding stabilises the "nonbonding" *d* electrons, making them susceptible to reaction. It also makes the C–O bond weaker making the ligand more reactive than an uncoordinated CO. Other π–acid ligands are the alkenes; they undergo back bonding with transition metals. Figure 2.5 shows how overlap takes place to form the M-C π bond.

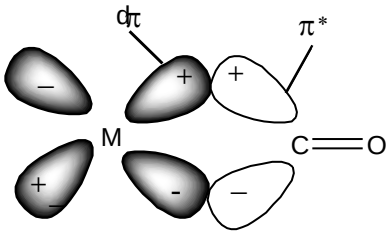

Figure 2.5: The overlap between a filled d_π orbital and an empty COπ^* orbital to give the π component of the M–CO bond. The shading refers to the occupancy of the orbital and the negative and positive signs to the symmetry.[19]

There are two modes of π–back bonding and two types of π–acceptor ligands see Figure 2.6:

- Longitudinal acceptors, such as carbon monoxide, isonitriles and linear nitrosyls
- Perpendicular acceptors, such as alkenes and alkynes

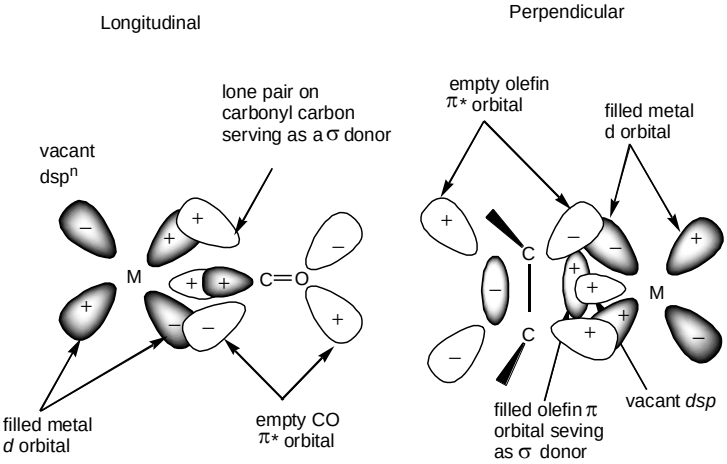

Figure 2.6: Types of π acceptors

The reactivity of π–acceptor ligands is affected to a certain degree by π–back bonding. The importance of carbon monoxide is due to its reactivity; the carbonyl group is susceptible to nucleophilic attack at carbon and as well as electrophillic attack at oxygen.

2.4 Ligand properties

The different types of ligand systems will be discussed with emphasis on the properties they have. The ligands have an effect on the properties of the catalyst depending on their electronic and steric properties. Electronic effect is as a result of transmission along bonds, changing from $P(4\text{-}C_6H_4OCH_3)_3$ to $P(4\text{-}C_6H_4)_3$. Steric effects are as a result of forces (usually non bonding) between parts of the molecule *e.g*. changing from $P(4\text{-}C_6H_4CH_3)$ to $P(2\text{-}C_6H_4)_3$ (see Figure 2.7).

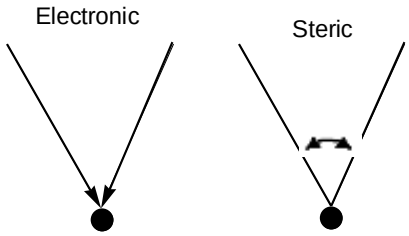

Figure 2.7: Schematic definition of the electronic and steric parameters

2.4.1 Electronic effects

The electronic properties of the phosphites have a large effect on the rate and selectivity of the reaction. Strohmeier[20] showed that the carbonyl stretching frequencies could be used to measure the electronic properties of the ligands. He showed that the electronic parameter (ν), could be used as a measure of the electronic effects of the complex. Tolman[21] introduced an approach to describe the electronic parameter (χ) based on the reference compound $[Ni(CO)_3(P\text{-}^tBu_3)]$, similar to the method introduced by Strohmeier.

2.4.2 Phosphines and phosphites: steric effects

In order to measure steric bulk of the phosphine/phosphite ligand Tolman[21] proposed the Tolman's parameter θ (theta). The steric bulk was measured by using the CPK models. The measurements were taken from the central metal, which is situated at a distance of 2.28 Å from the phosphorus atom in the appropriate direction. For symmetric phosphor ligands (PX_3) the Tolman cone angle is defined by the apex angle of a cylindrical cone, centered 2.28 Å from the center of the P

atom, which just touches the van der Waals radii of the outermost atoms of the model, shown in Figure 2.8(a). When unsymmetrical ligands $PX^1X^2X^3$ are considered a model can be defined that minimises the sum of the cone half-angles Figure 2.8(b) shown by equation 2.1.

$$\theta = (2/3)\sum_{i=1}^{3} \theta_i/2 \qquad \textbf{2.1}$$

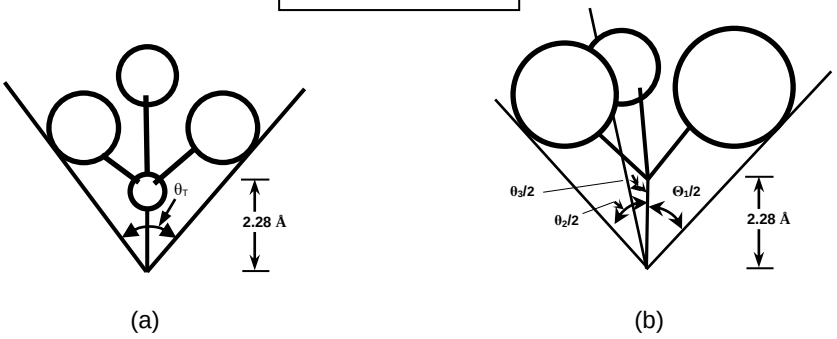

(a) (b)

Figure 2.8 (a) Measurement of the cone angle of symmetrical ligands (b) Cone angle measurement of unsymmetrical ligands.[21]

2.5 Mechanism of hydroformylation

There are major differences between the modified and unmodified systems in industrial hydroformylation. In the early 1960's Heck and Breslow formulated the generally accepted hydroformylation cycle depicted in Scheme 2.2.[22] The Scheme was originally formulated for unmodified cobalt catalysis. The unmodified and modified hydroformylation will be discussed separately.

2.5.1 Introduction

Hydroformylation catalysis involves reactions which involve the consumption of reactants, products and regeneration of the products in the catalytic cycle. Under reaction conditions of hydroformylation, an equilibrium mixture between $[Co_2(CO)_8]$ **(4)** and $[HCo(CO)_4]$ **(5)** exists. The rhodium and cobalt catalysts have only one important difference between their respective mechanisms. The cobalt-catalyzed process does not have the oxidative addition or reductive elimination step, which are present in the rhodium-catalyzed hydroformylation reaction. Cobalt was used as the metal; which was later substituted by rhodium as a metal. Rhodium was susceptible to metal poisoning and was also very expensive, causing recovery of the metal to be important. Spectroscopic investigations led to more detailed insight

into the hydroformylation mechanism and the role of the ligands with respect to activity and steric selectivity (induced by chirality).

2.5.1.1 Unmodified cobalt and rhodium catalytic cycle

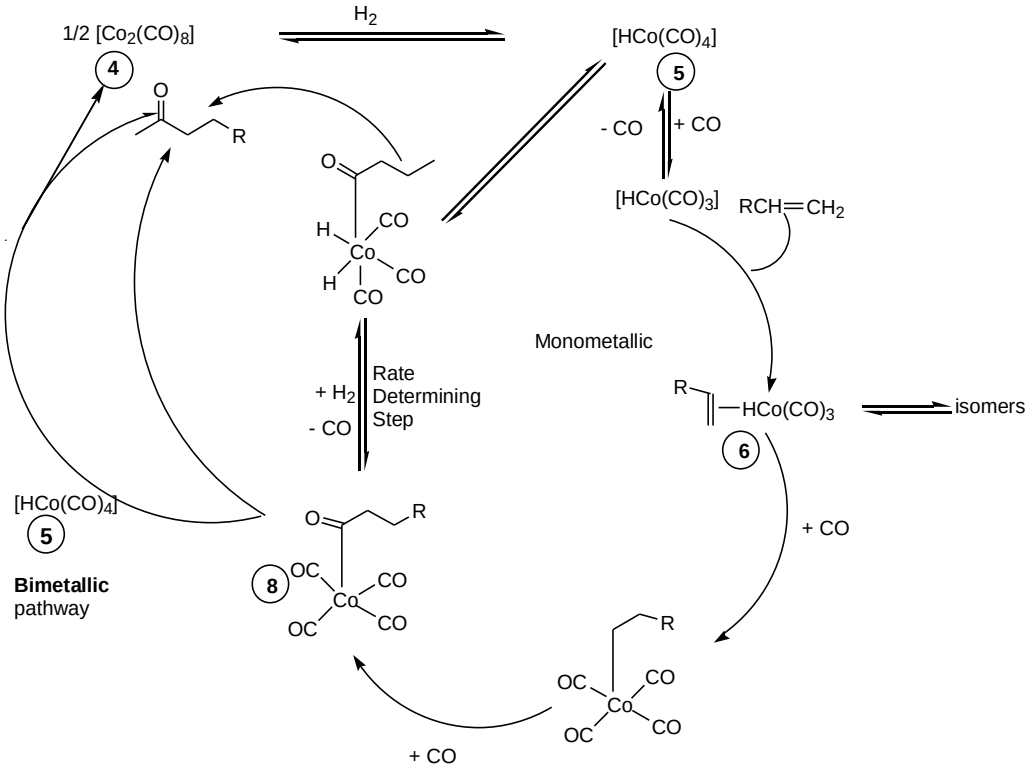

Scheme 2.1: Hydroformylation catalytic cycle with the use unmodified cobalt catalyst.

Scheme 2.1 represents the catalytic cycle for the unmodified hydroformylation. The metal can be rhodium or cobalt. The elemental steps for Scheme 2.2 are:

1) Reaction of the metal carbonyl $[Co_2(CO)_8]$ **(4)** with hydrogen to form the metal hydride carbonyl species $[HCo(CO)_4]$ **(5)**
2) Dissociation of CO to generate the unsaturated 16e species $[HCo(CO)_3]$
3) Coordination of the alkene $RCH=CH_2$ (18e) refers to the electron count of the species.
4) Formation of the alkyl metal carbonyl species (16e) **(6).**
5) Coordination of CO (18e).
6) Insertion of CO to form the acyl metal carbonyl $[RCH_2CH_2C(O)Co(CO)_3]$ (16e) **(8).**
7) Cleavage of the acylmetal species by hydrogen to form the aldehyde and regeneration of the metal hydride carbonyl $[HCo(CO)_4]$ **(5).**

A competing bimetallic cycle was suggested but was not recognised by Heck and Breslow.[23] In this cycle it was suggested that the acyl intermediate could react with $[HCo(CO)_4]$ **(5),** to give the *inter*molecular hydride transfer, this would be followed by reductive elimination of the aldehyde to produce the Co-Co bonded dimer $[Co_2(CO)_8]$ **(4)**. The reaction conditions of hydroformylation when using the unmodified hydride are largely influenced by the thermal instability of the unmodified hydride, which produces metallic cobalt if the CO partial pressure is not high enough. With an increase of the temperature the CO partial pressure required to maintain the stability of $[HCo(CO)_4]$ **(5)** increases. The temperature required to enable reasonable reaction rates is between 110 and 180º, when using syngas (H_2/CO) pressures of 200 – 300 bar.

It was discovered that the reaction was not catalyzed by the supported cobalt[5] but rather by the unmodified hydride $[HCo(CO)_4]$ **(5)** which was formed in the hydroformylation reaction and is responsible for the ratio of the linear and branched product that is being produced. Scientifically it is an interesting question on how to influence the kinetics and the changing of ligands. The first processes for hydroformylation were based on cobalt carbonyl complexes. The only ligand present was carbonyl. The mechanism was later generalised and applied to ligand modified systems as well in which the catalysts precursor proposed to be the mono substituted hydride, $[HCo(CO)_3L]$ **(2).**

When $[Co_2(CO)_8]$ **(4)** is in solution, an equilibrium exists between the bridged and the non bridged isomers. It is thermally unstable and decomposes at temperatures above 50°C. In addition it dimerises to the tetranuclear cluster $[Co_4(CO)_{12}]$. Dicobalt octacarbonyl $[Co_2(CO)_8]$ is a useful starting material *e.g*. when it is reacted with pyridine it gives $[Co(py)_6][Co(CO)_4]_2$ when this complex is reacted with sulphuric acid it produces $[HCo(CO)_4]$ **(5).**[24] Similarly, reaction with DMF gives $[Co(DMF)_6][Co(CO)_4]_2$ (see Scheme 3.4).

Two main equilibrium reactions exist when using $[Co_2(CO)_8]$ **(4)**.[25] This indicates sensitivity of the chemico-physical behaviour of cobalt carbonyls to small changes in their immediate environment, such as change in CO partial pressure, addition of hydrogen, presence of a base or application of a vacuum. The first is the equilibrium reaction of $[Co_2(CO)_8]$ **(4)** with H_2 to yield $[HCo(CO)_4]$ **(5)**. Both the kinetics and the equilibrium of this reaction are greatly influenced by the CO pressure in the system.

The second is the equilibrium of decomposition of $[Co_2(CO)_8]$ **(4)** to $[Co_4(CO)_{12}]$. When $[Co_2(CO)_8]$ **(4)** is placed under medium or high hydrogen pressure, the formation of cobalt tetracarbonylhydride from dicobalt octacarbonyl can be observed according to reaction 2.3.

$$[Co_2(CO)_8] + H_2 \longrightarrow 2[HCo(CO)_4] \qquad \textbf{(2.2)}$$

Reaction 2.2 is the key step in the hydrogen activation of cobalt (carbonyls). Carbon monoxide has a retarding effect on the synthesis of $[HCo(CO)_4]$ **(5)** from $[Co_2(CO)_8]$ **(4)**. In order to account for this observation, a series of equilibria were suggested (reactions. 2.3 - 2.6).

$$[Co_2(CO)_8] \longrightarrow [Co(CO)_7] + CO \qquad \textbf{(2.3)}$$

$$[Co_2(CO)_7] + H_2 \longrightarrow [H_2Co_2(CO)_7] \qquad \textbf{(2.4)}$$

$$[H_2Co_2(CO)_7] \longrightarrow [HCo(CO)_4] + [HCo(CO)_3] \qquad \textbf{(2.5)}$$

$$[HCo(CO)_3] + CO \rightleftharpoons [HCo(CO)_4] \qquad \textbf{(2.6)}$$

There was a general need for improvement, milder reaction conditions were required. Increased selectivity for linear aldehydes and reduced by-product formation were the main objectives for the hydroformylation reaction.

2.5.1.2 Modified hydroformylation catalytic cycle

The properties of the catalyst can be changed by modification of the spectator ligands. By modifying the ligand the selectivity towards the desired products can either be increased or decreased. The hydridocobalt carbonyl reaction with alkene has selectivity *via* Markovnikov and *anti*-Markovnikov addition to give rise to linear and branched alkylcobalt carbonyl isomers.[7] The sterically less demanding nature of $[HCo(CO)_3]$ favours the formation of the branched isomer, whereas the $[HCo(CO)_4]$ (5) predominantly generates the linear isomer.

When using phosphines or phosphites to modify the ligand, selectivity towards the linear aldehyde increases. Disadvantages of phosphites include side reactions such as hydrolysis, alcoholysis, *trans*-esterification, Arbusov rearrangement (restricted to alkyl phosphites, hence the predominant use of aryl phosphites) and O—C or P—O bond cleavage.[23,26]

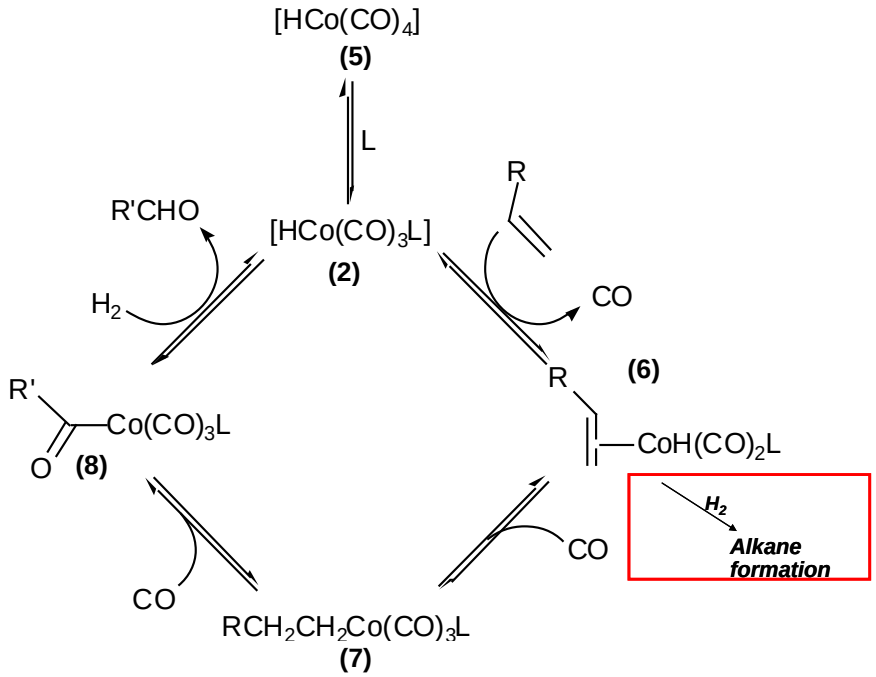

Scheme 2.2: Generalised Heck-Breslow hydroformylation mechanism.[22]

From Scheme 2.2 the unsaturated $[HCo(CO)_2L]$ **(2)** species is formed by loss of a CO ligand, and the addition of an alkene to this 16e species is quick resulting in the π complexes **(6**). Hydrogen transfer to the alkene is influenced by the steric demand of the ligand leading either to the Markovnikov or preferentially *anti*-Markovnikov addition. The addition of CO produces the alkyl species $[RCH_2CH_2Co(CO)_3L]$ **(7).** Alkyl migration to a coordinated CO ligand results in the acyl species $[R'C(O)Co(CO)_3L]$ **(8)** which is cleaved by hydrogen to form the aldehyde and regenerate the monophosphite hydride **(2)**.

The linear to branched aldehyde ratio which are formed by the unmodified metal carbonyl catalysts are influenced by the catalyst concentration (slightly), temperature (strongly) and partial pressures $p(H_2)$ (slightly) and p(CO) (very strongly).[7]

2.6 Cobalt vs Rhodium

2.6.1 Cobalt-phosphines

Phosphine cobalt catalysts of the type $[Co_2(CO)_6(PR_3)_2]$ have been extensively used as hydroformylation catalysts.[27] In 1966, Shell[28] reported a system where the addition of tertiary alkyl phosphines stabilized the catalyst to such an extent that reaction pressures below 100 bar were possible. The Shell researchers discovered that phosphines could replace carbon monoxide as an electron donating ligand.

This was a fundamental step in metal-carbonyl catalyzed reactions. Alkylphosphines due to their electron donating properties, usually lead to lower reaction rates and thus requiring higher temperatures.[29,30,31] Due to the donating of electrons by phosphine to the electron deficient cobalt carbonyl Co-CO the bonds are strengthened. The phosphine complex is less active than the unmodified tetracarbonyl complex; therefore the reaction was carried out at higher temperatures (170ºC vs 140ºC). Alkyl phosphines have an influence on the reaction which becomes much slower.[32,33] The catalysts improved the selectivity towards linear aldehydes; it also acquired activity towards hydrogenation. The monophosphine hydride $[HCo(CO)_3L]$ **(2)** which is much more stable, was the dominant species. Catalysts were tailor-made *via* electronic and steric properties of the ligand. Slaugh and Mullineaux[28] made a commercially important discovery that the addition of phosphines, such as $P(^nBu)_3$, would give a catalyst that is much more active but would require less pressure (5 - 100 bar) than the unmodified hydride.[34] The catalyst would also favour primary rather than secondary aldehydes to the extent of 8:1 *vs.* 4:1. It was believed that the steric bulk of the phosphine would encourage the formation of the less hindered primary alkyl complex (see Scheme 2.3) and speed up migratory insertion. Although tributylphosphine was reported as a selective and active catalyst, the phobane derivatives proved to be more effective.[35]

The Shell process, the only process using a cobalt-phosphine catalyst, may be considered the final step in the development of the first generation process. The second-generation process combined the advantages of the ligand modification with the transition from cobalt to rhodium as catalyst metal. The alkyl phosphines were the ligands of choice for cobalt, but led to slow reactions when applied to rhodium catalysts.[36] Arylphosphines are weaker electron donors, therefore they tend to form less stable complexes compared to CO. Arylphosphines also decompose quickly at higher temperatures. If the aryl group is more electron withdrawing, the decomposition would occur faster.

There are two routes to enter the modified hydroformylation cycle (Fig 2.9), with L = Phosphine ligand, one is *via* the cobalt (II) carboxylate precursor, and the other *via* the dicobalt octacarbonyl. The route from dicobalt octacarbonyl proceeds *via* a dicobalt bis(phosphine) salt $[Co(CO)_3L_2]^+[Co(CO)_4]^-$. The $[Co_2(CO)_7L]$ proceeds directly to the dimer $[Co_2(CO)_6L_2]$ **(1)** and hydride $[HCo(CO)_3L]$ **(2)** (Fig. 2.2) under syngas pressure. These carbonyl species are unstable in the absence of CO

pressure. In the absence of carbon monoxide there is cobalt plating. In the presence of excess ligand, the equilibrium may shift to the di- and tri-substituted cobalt species (e.g. $[HCo(CO)_2L_2]$ **(3).** Should the species be "ligand starved" the following species may be formed: $[Co_2(CO)_7L]$. The catalyst is more hydritic in nature. More paraffin's are formed and fewer products such as aldols are formed.

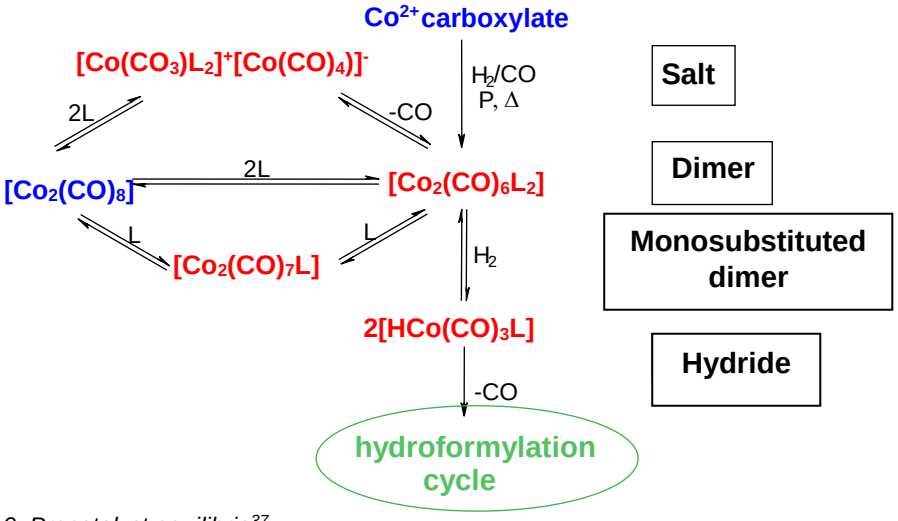

Figure 2.9: Precatalyst equilibria[37]

2.6.2 Rhodium-phosphines

The work of Wilkinson[38] in the mid sixties showed that arylphosphines should be used for rhodium and that even at mild conditions active catalysts can be obtained. On a laboratory scale there was great progress with the application of rhodium-phosphine catalysts. Many industries started to use phosphine ligands in rhodium catalyzed processes. The first commercial process was launched in 1974. This was ascribed to the former Celanese Corporation (today the Hoechst-Celanese Corporation), which mentioned the successful operation of a butylaldehyde, a rhodium phosphine catalyst plant at Bishop, Texas, in their business report the same year.[39] The Union Carbide Corporation followed in 1976; in the following years an aggressive license policy changed the picture of propylene hydroformylation drastically. In 1978 Mitsubishi Chemical Cooperation also started using triphenylphosphine as a ligand in the synthesis of rhodium catalysts.

2.6.3 Cobalt-phosphites

Since the Shell process that utilized trialkylphosphines was introduced, a variety of phosphine ligands have been studied. Recently the use of tertiary phosphine ligands in which the phosphorus atom is incorporated into a limonene bicycle has been reported.[33] More publications are available on phosphite ligands which are

used in hydroformylation catalysis since the patent in 1967. Since phosphites relative to phosphines, should decrease the electron density on the cobalt center they are expected to yield less hydrogenation products. In a previous publication which reported results on triphenylphoshite modified cobalt hydroformylation of 1-pentene, it was found that a large amount of the bis-phosphite cobalt hydride was formed, which was believed to be catalytically inactive.[40] Isomerisation of the 1-alkenes occurred resulting in the formation of the less reactive internal alkenes.

Subsequently it was also reported on the findings on phosphite modified cobalt catalyzed hydroformylation using a ligand with a significantly larger cone angle tris(2,4-di-*tert*-butyl phenyl) phosphite.[41] The increased cone angle of tris(2,4-di-*tert*-butyphenyl)phosphite **(d)** (175º)[41] compared to $P(OPh)_3$ **(a)** (128°) is presumed to prevent the formation of the catalytically inactive bis(phosphite) cobalt hydride. In a previous publication of the bisphosphite cobalt hydride $[HCo(CO)_2\{P(OPh)_3\}_2]$ **3a** it was noted that it was indeed inactive under hydroformylation conditions.[40]

In Scheme 2.3 the Heck and Breslow mechanism was used to explain the results obtained from the study of triphenylphoshite used as a ligand in modified hydroformylation. The bisphosphite hydride proved to be the dominant species involved in hydroformylation. The coordination of 1-pentene is followed by hydride insertion to form the alkyl species $[(C_5H_{11})Co(CO)_2\{P(OPh)_3\}_2]$. Alkyl migration to form the acyl species was less favoured, thus shifting the equilibrium back to the π-complex **6a**. According to the Scheme 2.3 it can be seen that the monophosphite hydride **2a** is the active catalyst in the Heck and Breslow mechanism.

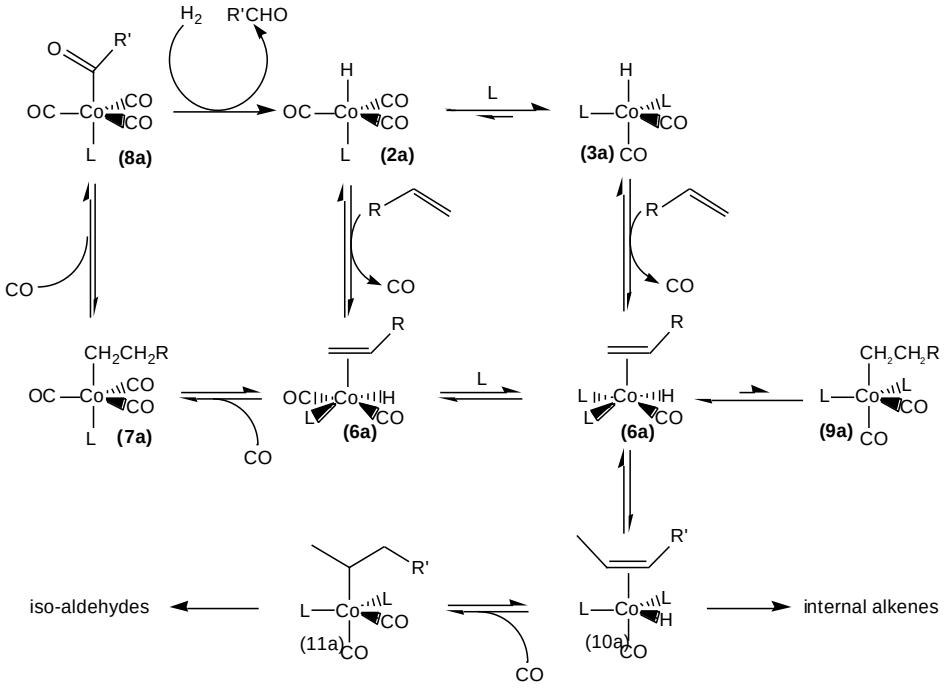

Scheme: 2. 3: Proposed mechanism for P(OPh)$_3$ ***(a)*** *modified cobalt hydroformylation*

Pruet and Smith studied a variety of phosphite and phosphine ligands.[42] They discovered that ligands with increasing electron withdrawing properties had a general trend of having an increase in selectivity towards the formation of the linear aldehyde. Donating substituents such as 4-methoxy resulted in a decrease of linear to branched aldehyde. The 4-chloro substituted phenyl phosphite gave high l:b ratio The use of *ortho*-substituted aryl phosphites gave lower selectivity for the linear product.

For a ligand modified catalyst (M = Rh, Co) the following general equilibrium is observed (reaction 2.7):

$$HM(CO)x + yPR_3 \rightleftharpoons HM(CO)x\text{-}y(PR_3)y + y(CO) \qquad \textbf{(2.7)}$$

At low pressure of CO the equilibrium is shifted to the right hand side; with the coordination of the ligands to the metal center it becomes sterically congested. Should the pressure of carbon monoxide CO increase, the n:*i* ratio diminishes immediately. Only at higher partial pressure [(pCO) > 15 bar)] is the catalytic cycle dominated by [HM(CO)$_3$L] **(2)** species, this favouring linear products

2.6.4 Rhodium-phosphites

In the late sixties phosphites were considered as ligands for rhodium hydroformylation. Triphenylphosphite turned out to be the ligand of choice. In the eighties Van Leeuwen and coworkers had discovered the effects of a bulky monophosphite that gave very high rates.[43]

A bulky phosphite such as tris(2-tert-butylphenyl)phosphite (cone angle 180°) yields an unstable rhodium complex. A rhodium complex containing tris(2-*tert*-butyl-4-methylphenyl)phosphite as a ligand catalyzed the hydroformylation of 1-octene with good selectivity and high reaction rates.[44] The rate constant was *pseudo* first-order in $[H_2]$ and 1/[CO]. The bulky phosphites give rise to an active species which contains one ligand, resulting in the formula $[HRh(CO)_3L.]$[7,43] (see Structure 2).

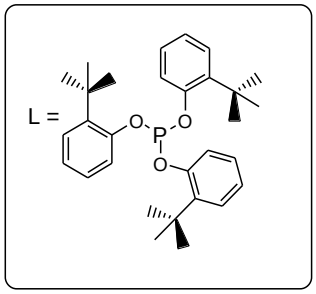

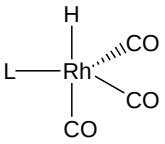

(2)

It was indicated that the ligands containing bulky phosphite were not applicable for 1-alkenes, due to the high rates of isomerisation that resulted.[45] In this study it was proven that using the bulky phosphite in the hydroformylation of 1-octene an extremely fast reaction was achieved. High linearity and a low rate of isomerisation were obtained. The monophosphite phosphite rhodium hydride complex could only be observed under pressure of CO and H_2 and could not be isolated.[46]

2.7 Spectroscopic studies

Homogeneous catalytic intermediates have been identified both by infrared and multinuclear NMR. HP-IR is usually used as a way of identifying *in situ* hydroformylation intermediates, but only identification of the carbonyl ligands is obtained and complete characterization can not be achieved. The construction material and design of the spectroscopic cell is very important, considering that these reactions take place at high temperatures and pressures (see Chapter 5). The hydroformylation process requires reactor designs that would be applicable to catalysis by transition metal complexes. The design must be able to allow efficient

transfer of the reactants from the gas phase to the liquid phase, because the reactants are in both the gas as well as the liquid phase.[47] More details on the HP-IR spectroscopy are available in Chapter 5.

Acyl tetracarbonyl metal complexes have been identified as intermediates by the use of infrared spectroscopy under the hydroformylation conditions. The acyl tetracarbonyl metal complex is in equilibrium with the tricarbonyl metal complex.[48]

High pressure infrared (HP-IR) spectroscopy has been used for over 30 years for the study of transition metal catalysed processes.[49] The technique is useful for reactions, which would involve carbon monoxide. The transition metal carbonyl complexes should be key intermediates in the catalytic mechanisms. These complexes have one or more strong ν_{CO} absorptions, the frequency as well as the relative intensities provide information about the geometry and electronic character of the metal center. With the appropriate IR absorptions, HP-IR spectroscopy is capable of being used to monitor the depletion and formation of reactants and products. These reactions make use of high pressures of CO or syn-gas (CO/H_2) and require high temperatures. Due to all these reaction conditions *in situ* spectroscopy requires a cell of an appropriate robust design. Many of the important intermediates in the catalytic mechanism are very reactive and short lived; this makes it impossible to observe them under the catalytic conditions. In order to study these intermediates the following can be done:

- Kinetic studies of stoichiometric reaction step.
- Spectroscopic identification of reactive intermediates at low temperature
- Rapid detection of intermediates generated photochemically.

Whyman carried out early HP-IR studies of cobalt catalyzed alkene hydroformylation.[50] Under catalytic conditions it was shown that in the absence of the alkene, the dimeric catalyst precursors $[Co_2(CO)_8]$ **(4)** and $[Co_2(CO)_6(PBu_3)_2]$ are converted into the hydrides $[HCo(CO)_4]$ **(5)** and $[HCo(CO)_3(PBu_3)]$ respectively. In the absence of phosphine, a mixture of $[Co\{C(O)R\}(CO)_4]$ ($R = C_8H_{17}$) and $[Co_2(CO)_8]$ was observed during the hydroformylation of 1-octene. The proportion of the acyl complex increased with p(CO). For internal alkene substrates only $[HCo(CO)_4]$ **(5)** and $[Co_2(CO)_8]$ **(4)** were observed. During the hydroformylation of the phosphine modified system using 1-octene the acyl species were not observed,

but $[HCo(CO)_3(PBu_3)]$ was the dominant species, while $[HCo(CO)_2(PBu_3)_2]$ and $[Co_2(CO)_7(PBu_3)]$ are formed both at high and low phosphine concentrations.

HP-IR studies by Mirbach[51] and by Pino *et al.*[52] found that hydrogenolysis of the cobalt acyl to be dominant. This conclusion was supported by the kinetic studies of Kovács.[53] Sasol workers reported HP-IR measurements which they did for cobalt-catalyzed 1-dodecene hydroformylation using bicyclic phosphines (see Structure 3) derived from (R)-(+)-limonene.[33] Using the Fourier deconvolution to separate the absorptions due to $[HCo(CO)_4]$ and $[Co_2(CO)_7(Phosphine)]$, it was possible to estimate the ratio "modified" $[Co_2(CO)_7(Phosphine)]$ to "unmodified" $[HCo(CO)_4]$ in the catalytic mixture by using the peak areas.

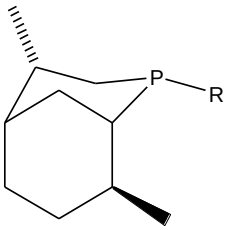

(3)

The values of these ratio's varied from 2 to 20 depending on the R group used in the phosphine ligand, this showed a relation with the catalyst activity as well as the catalyst selectivity. The modified catalysts $[Co_2(CO)_7(Phosphine)]$ ratios were higher when the catalysts were less active but more selective towards the linear products. In a study performed using a Co/triphenylphosphite catalyst system, HP-IR indicated the formation of $[HCo(CO)_3\{P(OPh)_3\}_2]$ **(3a)** at a temperature of 110ºC, but at higher temperatures absorption bands corresponding to $[HCo(CO)_4]$ **(5)** were observed. At higher ligand $P(OPh)_3$ **(a)** concentrations, the inactive bisphosphite hydride $[HCo(CO)_2\{P(OPh)_3\}_2]$ **(3a)** was observed.[40]

2.7.1 Alkyl- and acylcobalt carbonyl complexes

The alkyl and acylcobaltcarbonyl complexes are accepted intermediates in the hydroformylation reaction of alkenes catalyzed by unmodified and modified catalysts. Several authors have attempted to rationalize the factors affecting the isomerisation of these products. A study was performed with its focus on the investigation of rhodium-catalyzed hydroformylation of olefins in order to understand the effect of high-pressure on the conversion rate, aldehyde selectivity and alkene isomerisation.[54] (Scheme 2.4)

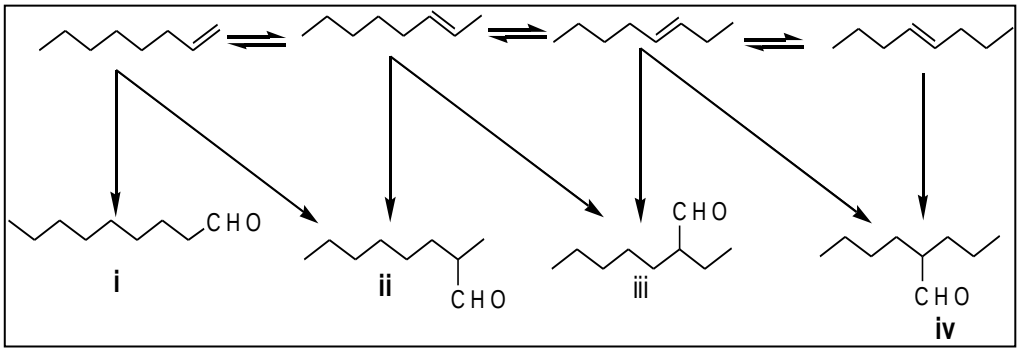

Scheme 2.4: Isomerisation and hydroformylation starting from 1- or 4-octene

In the hydroformylation of linear long chain alkenes there is competition of alkene isomerisation and hydroformylation. This may lead to the four different aldehydes i - iv as outlined in scheme 2.4. The results obtained when starting with 1-octene are 1-nonanal (i) and 2-methyl-octanal (ii) as was expected. The products were a direct representation of the hydroformylation products. The products which were generated after the isomerisation of 1-octene are (iii) and (iv). At a pressure of 70 bar, all the products i – iv are obtained in descending quantities. At a pressure of 500 bar, product selectivity was significantly changed. The aldehydes (iii) and (iv) can not be observed. Under these conditions isomerisation of 1-octane was almost completely suppressed. Extensive isomerisation of the alkyl and acyl derivatives with an inhibiting effect of CO under pressure was found and considered responsible for the low regioselectivity of the hydroformylation reaction.[55]

2.8 Industrial importance of hydroformylation

Hydroformylation reactions that are used in industry are patented. A few selected hydroformylation reactions processes are summarized in Table 2.2. The various processes in Table 2.2 show the different products which are accessible industrially by hydroformylation. In section 2.6.1 it is shown that other important products which are available by hydroformylation are vitamin A, 1,4–butanediol and 3-methyl–1,5–pentanediol. A variety of pharmaceutical products are produced by industrial hydroformylation.

Asymmetric hydroformylation is able to provide a variety of chiral molecules accessible as valuable precursors for pharmaceutical and agrochemicals.[5]

Table 2.2. Industrial hydroformylation Reaction Processes[56]

Manufacturer	Process	Product
Mitsubishi Kasei	Isononyl aldehyde for Isononyl alcohol, which Is used in polyvinyl chloride resin as a plasticizer alcohol. An introduction for Vitamin A synthesis.	Rhodium catalyst with triphenyl phosphine oxide as a weakly coordination ligand; catalyst separated from the products by distillation. Rhodium catalyst without phosphorus ligand; Reaction represented by reaction 2.8.
BASF Hoffman-La Roche ARCO	An intermediate for 1, 4-butanediol.	Rhodium catalyst with chelating phosphorus ligand; Hydroformylation of 2-Methyl butane-4-ol followed by Hydrogenation; Reaction represented by reaction 2.9
Kuraray	An intermediate for 3-Methyl-1,5-pentane diol.	$[Rh_4(CO)_{12}]$ with phosphorus ligand as the precatalyst; Hydroformylation of 2-Methyl butane-4-ol followed by Hydrogenation; Reaction represented by reaction 2.10.

2.8.1 Other hydroformylation reactions.[56]

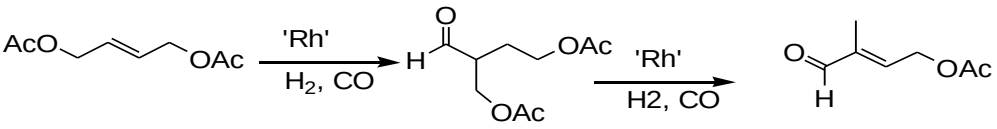

Vitamin A (**2.8**)

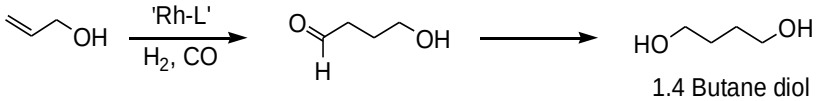

1.4 Butane diol **(2.9)**

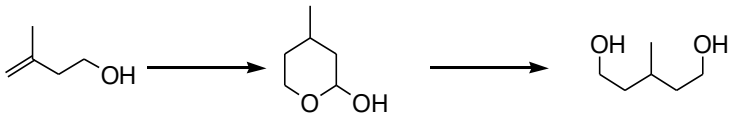

3-methyl 1,5 pentane diol **(2.10)**

The hydroformylation reaction is used in the development of important every day commercial goods, including the synthesis of vitamin A (eq 2.8).[57,11] There is a large annual demand for vitamin A. The major producers are BASF, Hoffman-La Roche and Rhône-Poulenc Animal Nutrition. In the initial synthesis BASF and Hoffman-La Roche are using the hydroformylation step.

2.9 Thermodynamics and kinetics

For the experimental observation of a chemical reaction, it is important that the thermodynamic and kinetic changes should not be too unfavourable. The thermodynamic change in Gibbs free energy (ΔG) and the kinetic requirement is measured by the free energy activation ($\Delta G^{\#}$).

If a reaction is thermodynamically favourable (ΔG<0) and the energy of activation is too high, the reaction will not occur. When the reaction is thermodynamically unfavourable (ΔG>0) the reaction may occur only if the activation energy is low. The conversion of diamond to graphite is thermodynamically favourable but only happens at a considerably small rate at room temperature and pressure. Some knowledge has been gathered about macro-kinetic influences, *e.g*. temperature, pressure, synthesis gas composition and catalyst concentration, predominately in the field of propene hydroformylation. Conclusions about the rate-determining step have been deduced mainly from spectroscopic observations. For the high-pressure hydroformylation catalysts $[Co_2(CO)_8]$ **(4)** and $[Rh_4(CO)_2L_2]$ the equation derived by Natta and Ercoli is generally accepted (eq 2.11)[58,59]

$$R = k \times [\text{substrate}] \times [\text{catalyst}] \times [p(H_2)]/[p(CO)] \quad \textbf{(2.11)}$$

The rate of reaction of the phosphite ligands such as $[HRh(CO)P(C_6H_5)_3]$ depend on the following parameters:

1) It is first order in catalyst concentration.
2) First order in the partial pressure of hydrogen.
3) When there is a low concentration of alkene there is a positive order, and at high alkene concentration there is a negative order (substrate inhibition).
4) At a low CO partial pressure (p(CO) < 10 bar), positive order, and at high ligand concentrations zero th order.

Hydroformylation reactions are significantly influenced by solvents. Polar solvents such as alcohols lead to higher rates of reactions than the non polar solvents such as toluene or hexane.

2.10 Conclusion

This chapter gave a brief review on hydroformylation catalytic reactions in literature. The modified and unmodified catalytic cycles that describe how the different catalytic cycles influence the products obtained. Reaction parameters that may influence the efficiency of the hydroformylation catalytic cycle reactions. Discussion was also on the phosphite and phosphine ligands in comparison with the different metals, cobalt and hydride. Industrial importance of hydroformylation was also part of the review.

References

1 D.F. Shriver and P.W. Atkins, "*Inorganic chemistry"*, 3rd Ed. 1999.

2 K.F. Purcell and J.C. Kotz, "*An introduction to inorganic chemistry*" Saunders College Publishing, Philadelphia, 1980.

3 G.C. Bond, "*Heterogeneous Catalysis*", Claredon Press, Oxford, 1994.

4 J.T. Richardson, "*Principles of Catalyst Development*", Plenum Press, New York, 1989.

5 B. Cornils and W. A. Herrmann, "*Applied Homogeneous Catalysis with Organometallic Compounds"*, A Comprehensive Handbook", VCH, Weinheim, 2000, p.5.

6 P.W.N.M. van Leeuwen and C. Claver (eds.), "*Rhodium Catalyzed Hydroformylation: Catalysis by Metal Complexes*" Kluver Academic Publishers, 200, p.37.

7 P.W.N.M. van Leeuwen, "*Homogeneous Catalysis*, *Understanding the Art*", Kluwer Academic Publishers, Dordrecht, 2004.

8 C.D. Frohning, C.W. Kohlpaintner, in "*Applied Homogeneous Catalysis with Organometallic Compounds"* B. Cornils, W.A. Hermann. Eds; VCH, Weinheim, 2000, **Vol. 2**.

9 B. Cornils in. "*New Synthesis with Carbon Monoxide",* (Ed.: J. Falbe), Springer, Berlin, 1980, **70**, 383.

10 H. Adkins and G. Kresk, *J. Am. Chem. Soc*., 1948, **70**, 383.

11 H.H. Storch, N. Golumbic and R.B. Anderson, "*The Fischer-Tropsch and Related Syntheses"*, Wiley, Chapman and Hall, New York, London, 1951, 441.

12 J. Betty and L. Markó, *Acta Chim*. *Acad. Sci. Hung*., 1963, **3**, 177.

13 G. Natta, *Brenstoff. Chem*., 1955, **36**, 176.

14 S. Bhaduri and D. Mukesh, "*Homogeneous Catalysis, Mechanisms and Industrial Applications",* John Wiley and Sons, Inc., 2000, p. 93.

15 J. Haggin, Chem. Eng. News, April 17, **1995** , p. 25.

16 N. Yoshinura and Y. Tokito*, Eur. Pat*., 1987, 103, 223.

17 B. Cornils and W.A. Humann, "*Aqueous Phase Organometallic Catalysis-Concepts and Applications*", eds, Wiley-VCH, Weinheim, 1998.

18 (a) S. Patailed "*The Chemistry of the Carbonyl Group*", Wiley – Interscience. New York, 1966.
(b) S. Warren, "*Chemistry of the Carbonyl Group"*, Wiley, London, 1974.

19 R.H. Crabtree, "*The Organic Chemistry of the Transition Metals*", Wiley-Interscience, 1948, p13.

20 W. Strohmeier and F.J. Müller, *Chem. Ber.,* 1967, **100**, 2812.

21 C.A. Tolman, *Chem. Rev*., 1977, **77**, 313.

22 a) R.F. Heck and D.S. Breslow, *Chem., Ind. (London)*, 1960, 467. b) R.F. Heck and D.S. Breslow, *J. Am. Chem. Soc*., 1961, **83**, 4023.

23 http://chemistry.lsu.edu/stanley/webpub/4571-chapt16-hydroformylationpdf 29/11/07.

24 H.W. Sternberg, I. Wender and M. Orchin, *Inorg. Synth*., 1957, **5,** 192.

25 R. Tannenbaum and G. Bor*, J. Organomet. Chem*., 1999, **18**, 586.

26 P.W.M.N. van Leeuwen, *Appl. Catal. A: Gen*., 2001, **61,** 212.

27 F.E. Paulik, *Catal. Rev*., 1972, **6**, 49.

28 L.H. Slaugh and R.H. Mullineaux, U.S. Pat., 3,239,569 and 3,239,570, 1966 (to Shell); *Chem. Abstr.*, 1964, **64**, 15 745 and 19 420.

29 A.A. Oswald, D.E. Hendrikse, R.V. Kastrup, K. Irikura, E. Mozeleski and D.A. Young, *Phosphorus and Sulphur*, 1987, **30**, 237.

[30] A.A. Oswald, J.S. Merola, E. Mozeleski, R.V. Kasrup and J.C. Rwisch, *ADV. Chem. Series,* 1961, **104**, 503.

[31] J.K. MacDougal, K.C. Simpson, M. Green, M.J. Green and D.J. Cole-Hamilton*, J. Chem. Soc., Dalton Trans.*, 1996, 1161.

[32] L.H. Slaugh and R.D. Mullineaux, *J. Organomet. Chem*., 2000, **593**, 211.

[33] C. Crause, L. Bennie, L. Damoense, C.L. Dwyer, C. Grove, N. Grimmer, W.J. van Rensburg, M.M. Kirk, K.M. Mokheseng, S. Otto and P. J. Steynberg, *Dalton Trans.*, 2003, 2036.

[34] C.W. Masters, "*Homogeneous Transition Metal Catalysis"*, Chapman Hall, 1981.

[35] J.L. van Winkle, S. Lorenzo, R.C. Morris and R.F. Mason, U.S. Patent, 3,420, 898, 1969. U.S. Abstr. 1964, **64**, 15745 and 19420.

[36] T. Onado, *Chem. Tech.,* 1993, Sept. 31.

[37] C. Dwayer, H. Assumption, J. Coetzee, C. Crause, L. Damoense and M. Kirk, *Coord. Chem. Rev.,* 2004, **248**, 653.

[38] a) J.F. Young, J.A. Osborn, F.A. Jardine and G. Wilkinson, *J. Chem. Soc*., *Chem. Comm*., 1965, 131. b) D. Evans, J.A. Osborn, G. Wilkinson, *J. Chem. Soc*., 1968, 3133. c) D. Evans, G. Yagupsky and G. Wilkinson, *J. Chem. Soc*., 1968, 2660.

[39] Celanese Corp. Annual Business report, 1974, 9.

[40] M. Haumann, R. Meijboom, J.R. Moss and A. Roodt*, Dalton Trans*., 2004, 1679.

[41] R. Meijboom, M. Haumann, A. Roodt and L. Damoense, *Helv. Chim. Acta*, 2005, **88**, 676.

[42] (a) R.L. Pruet and J.A. Smith, *J. Org. Chem*., 1969, **34**, 322. (b) R.L. Pruet and J.A. Smith, S. African Pat. 6804937, 1968, *Chem. Abstr.,* 1969, **71**, 819.

[43] P.W.N.M. van Leeuwen and C.F. Roobeek, *J. Organomet. Chem*., 1983, **258,** 343; Brit Pat. 2,068,377, US Pat. 4,467,116, *Chem. Abstr*., 1984, **101**, 191142.

[44] A. van Rooy, E.N. Orij, P.C.J. Kamer, F. van den Aardweg and P.W.N.M. van Leeuwen, *J. Chem. Soc*., *Chem. Commun*., 1991. 1096.

[45] a) H. Janencko and J.J. Ziolkowski, *J. Mol. Catal*., 1984, **26**, 355. b) A.M. Trzeciak and J.J. Ziolkowski, *J. Mol. Catal*., 1986, **34**, 213. c) A.M. Trzeciak and J.J. Ziolkowski, *J. Mol. Catal*., 1988, **48**, 319.

[46] T. Jongsma, G. Challa and P.W.N.M. van Leeuwen, *J. Organomet. Chem*., 1991, **421**, 121.

[47] B.C. Gates, "*Catalytic Chemistry*", John Wiley and Sons Inc. 1992.

[48] P. Powell, "*Principles of Organometallic Chemistry*", 2nd Edition, Chapman and Hall, 1988.

[49] B. Heaton, "*Mechanisms in Homogeneous Catalysis: A Spectroscopic Approac*", Wiley-VCH, 2005.

[50] a) R. Whyman, *J. Organomet. Chem*., 1974, **66**, 23; b) R. Whyman, *J. Organomet. Chem.*, 1974, **81**, 97.

[51] M.F. Mirbach, *J. Organomet. Chem*., 1984, **265**, 205.

[52] P. Pino, A. Major, F. Spindler, R. Tannenbaum, G. Bor and I.T. Horwath, *J. Organomet. Chem*., 1991, **417**, 65.

[53] K. Kovács, F. Ungváry and L. Markó., *Organometallics*, 1986, **5**, 209.

[54] J. Albers, E. Dinjus, S. Pitter and O. Walter., *J. Mol. Catal. A: Chem*., 2004, **219**, 41.

[55] L. Rosi, A. Salvini, M. Bianchi, P. Frediani and F. Piacenti, *J. Organomet. Chem*., 1997, **535**, 143.

[56] S. Bhaduri and D. Mukesh, "*Homogeneous Catalysis: Mechanisms and Industrial Applications"*, John Wiley and sons, 2000, p. 98.

[57] K. Nagareda, "*Preparation of 2-formyl-4-acyloxy-1-butenes as materials for vitamin A"*, in Jpn. Kokai Tokkyo Koho, 1994.

[58] a) G. Natta and R. Ercoli, *Chem. Ind (Milan).* 1952, **34**, 503. b) G. Natta, R. Ercoli and S. Castellano, *Chem. Ind*., (Milan) 1955, **6**, 31. c) G. Natta, R. Ercoli, S. Castellano and F.H. Barbun, *J. Am. Chem. Soc*., 1954, **76**, 4049.

[59] B. Hal and L. Markó, *Chem. Ber*., 1968, **101**, 2209.

Chapter 3
Synthesis and Characterization of Cobalt Phosphite Compounds

3.1 Introduction

The synthesis of the cobalt phosphite complexes and phosphite ligands used in this study are described in this chapter, and the relevance of these complexes is illustrated in Figures 6.1 – 6.6, **Chapter 6**. Phosphite ligands are used in the synthesis of the cobalt phosphite dimers. The dimers which are synthesised have a variety of Tolman[1] cone angles between 128º and 186.4º. These dimers will be used as precursors in the preformation of the catalysts in hydroformylation of 1-octene (Scheme 6.1, **Chapter 6**).

3.2 Experimental

3.2.1 General experimental

All manipulation of air and moisture sensitive compounds was performed by means of standard Schlenk techniques[2] using argon gas. Dicobalt octacarbonyl was purchased from Strem Chemicals and stored at 0°C and syngas (CO/H_2 = 1:1) was purchased from Afrox. All the other reagents were purchased from Sigma-Aldrich and were of analytical reagent grade and used as received. The ligands were prepared as oxygen sensitive compounds.

The CO stretching frequencies of the complexes were obtained from infrared spectra recorded on a Bruker Tensor FT-IR spectrometer and analysed with the Bruker OPUS – NT software (32 scans, 4 cm^{-1} resolution Blackman – Harris 3 – Term apodisation). Infrared data for solution spectra of the compounds were collected using NaCl windows (optical path length 0.1 nm).

The cobalt phosphite carbonyl dimers were analyzed as KBr disks; solution IR analysis was also done during the synthesis of the dimers using pentane. The IR spectra were taken over a range 2100 – 1600 cm^{-1}. All spectra scans were performed at room temperature, except the spectra taken during hydroformylation which were taken at room temperature at the beginning of the experiment and eventually up to 140°C. The complexes were further characterized using ^{1}H, ^{13}C and

^{31}P NMR on a 300 MHz Bruker nuclear magnetic resonance spectrometer operating at 300 (^{1}H), 121 (^{31}P) and 75 (^{13}C) MHz. In the recording of ^{31}P NMR a capillary tube filled with 80% H_3PO_4 was used for calibration to 0 ppm. The spectra of the NMR were referenced relative to TMS (^{1}H and ^{13}C) or 85 % H_3PO_4 (^{31}P), using residual solvent signals (δ_H 7.24 ppm or 7.16 ppm for $CDCl_3$ and C_6D_6, respectively). ^{1}H and ^{31}P NMR spectra were recorded in C_6D_6 and $CDCl_3$.

Table 3.1: Phosphite ligands and their associated abbreviations

Phosphite name	Chemical formula	Abbreviation
Triphenylphosphite	$P(OC_6H_5)_3$	TPP
Tris(4-^{t}butylphenyl)phosphite	$P(O\text{-}4\text{-}^{t}BuC_6H_4)_3$	4-TBPP
Tris(2-^{t}butylphenyl)phosphite	$P(O\text{-}2\text{-}^{t}BuC_6H_4)_3$	2-TBPP
Tris(2-^{i}propylphenyl)phosphite	$P(O\text{-}2\text{-}^{i}PrC_6H_4)_3$	2-IPPP
Tris(2-ethylphenyl)phosphite	$P(O\text{-}2\text{-}EtC_6H_4)_3$	2-EtPP

3.3 Preparation of phosphate ligands

3.3.1 Preparation of $P(O\text{-}4\text{-}^{t}BuC_6H_4)_3$ (b)

The procedure described is analogous to that of van Leeuwen and Roobeek[3] for the synthesis of tris(2-*tert*-butylphenyl)phosphite.

4-tert-butylphenol (98.2 g; 0.654 mol) was mixed with xylene (5 ml). Triethylamine (0.5 ml) and PCl_3 (19.0 ml; 0.218 mol) were added to the first reaction under an inert atmosphere. The mixture was stirred and heated under reflux for 3 hours. The heat was removed and the reaction was allowed to stir overnight. The reaction product was filtered over celite (pentane was added to the wash). The volatiles were removed *in vacuo*. Pentane was added to dissolve the product and was placed in the freezer for a day. After freezing for one day, precipitation of white crystalline solid was formed and dried *in vacuo* followed by the evaporation of the volatiles. The solid was then purified through recrystallisation from pentane and $P(O\text{-}4\text{-}^{t}BuC_6H_4)_3$ **(b)** was isolated as a white solid. (Yield: 65.46 g, 63%); $\delta_{P\{H\}}$ (121.5 MHz,$CDCl_3$) 128 ppm.

3.3.2 Preparation of $P(O\text{-}2\text{-}EtC_6H_4)_3$ (c)

2-Ethylphenol (50.2 g; 0.411 mol) was mixed with xylene (5 ml), Triethylamine (0.5 ml) and PCl_3 (12.0 ml; 0.137 mol) were added to the first solution under inert conditions and heated under reflux for 3 hours. The heat was removed and the reaction was allowed to stir overnight. Thereafter the reaction was filtered through celite (diethyl ether was added to the wash). The volatiles were removed *in vacuo.*

Pentane was added to dissolve the product and was placed in the freezer. After a day in the freezer the pentane and Et_2O was removed by vacuum. The product which is in a liquid form had the volatiles removed by vacuum thereafter placed in the freezer. $P(O\text{-}2\text{-}EtC_6H_4)_3$ **(c)** was isolated as a clear liquid. (Yield: 48.56 g, 90%); $\delta_{P\{H\}}$(121.5 MHz,$CDCl_3$) 131 ppm.

3.4 Preparation of cobalt phosphite dimeric species

3.4.1 Preparation of $[Co_2(CO)_6\{P(OPh)_3\}_2]$ (1a)

The compound $[Co_2(CO)_6\{P(OPh)_3\}_2]$ **(1a)** was prepared according to literature methods[4,5,6] and similar related complexes.

A solution of $P(OPh)_3$ (2.441 g; 3.22 mmol) in pentane (5 ml) was added to a stirred solution of $[Co_2(CO)_8]$ (0.9981 g; 1.46 mmol) in pentane (10 ml). The immediate evolution of gas was observed and a precipitate formed. After 16 h with stirring the solid was washed with pentane (3 x 10 ml). The straw coloured powder was dried *in vacuo* to give pure dimer. (Yield: 3.478 g, 71%). IR (dodecane) ν_{CO} = 1975, 1993 cm^{-1}. The NMR and IR (KBr) were the same as those obtained in the literature.

3.4.2 Preparation of $[Co_2(CO)_6\{P(O\text{-}4\text{-}^tBuC_6H_4)_3\}_2]$ (1b)

A solution of $P(O\text{-}4\text{-}^tBuC_6H_4)_3$ (1.543 g; 3.22 mmol) in pentane (5 ml) was added to a stirred solution of $[Co_2(CO)_8]$ (0.499 g; 1.46 mmol) in pentane (10 ml). The immediate evolution of gas was observed and a precipitate formed. After 16 hrs with stirring the solid was washed with pentane (3 x 10 ml). The dark red powder was dried *in vacuo* to give pure dimer. Crystals suitable for X-ray diffraction were obtained from the slow evaporation of a solution of the dimer in acetone. (Yield: 1.248 g, 62%); mp 110ºC; δ_H(300 MHz, $CDCl_3$): 7.30, 7.13 (24H; C_6H_4), 1.30 (54H; CH_3); $\delta_{C\{H\}}$(75.5 MHz, $CDCl_3$): 199.4 (CO), 148.9, 148.7, 126.9, 121.6, 34.8, 31.8; $\delta_{P\{H\}}$(121.5 MHz, $CDCl_3$) 170 ppm; IR (pentane) ν_{CO} = 1980, 1997 cm^{-1}. IR (KBr) ν_{CO} = 1974, 1998cm^{-1}.

3.4.3 Preparation of $[Co_2(CO)_6\{P(O\text{-}2\text{-}EtC_6H_4)_3\}_2]$ (1c)

A solution of $P(O\text{-}2\text{-}EtC_6H_4)_3$ (1.272 g; 3.22 mmol) in pentane (5 ml) was added to a stirred solution of $[Co_2(CO)_8]$ (0.499 g; 1.46 mmol) in pentane (10 ml). Immediate evolution of gas was observed and precipitation occurred. After stirring for 16 hrs solid was washed with pentane (3 x 10ml). Resulting in the formation of $[Co_2(CO)_6\{P(O\text{-}2\text{-}EtC_6H_4)_3\}_2]$. Crystals suitable for X-ray diffraction were obtained from the slow evaporation of a solution of the dimer in acetone. (Yield: 1.114 g, 64%); mp 107ºC, δ_H(300 MHz, C_6D_6): 7.53, 6.91 (24H;C_6 H_4); 1.24 (12H; CH_2), 2.59 (24H; CH_3); $\delta_{C\{H\}}$(75.5 MHz, $CDCl_3$): 199.85 (CO), 149.64, 136.37, 130.19, 127.09, 125.67, 120.70, 23.50, 14.46; $\delta_{P\{H\}}$(121.5 MHz,$CDCl_3$) 158 ppm; IR (pentane) ν_{CO} = 1984, 2003. IR (KBr) ν_{CO} = 1998, 1973 cm^{-1}.

3.4.4 Preparation of $[Co_2(CO)_6\{P(O\text{-}2\text{-}^iPrC_6H_4)_3\}_2]$ (1e)

A solution of $P(O\text{-}2\text{-}^iPrC_6H_4)_3$ (1.415 g; 3.22 mmol) in pentane (5 ml) was added to a stirred solution of $[Co_2(CO)_8]$ (0.499 g; 1.46 mmol) in pentane (10 ml). Immediate evolution of gas was observed and a precipitate formed. The solid was stirred for a further 16 hrs and washed with pentane (3 x 10ml). Resulting in the formation of $[Co_2(CO)_6\{P(O\text{-}2\text{-}^iPrC_6H_4)_3\}_2]$. (Yield: 1.633 g, 87%): δ_H(300 MHz, C_6D_6): 7.29, 7.17, 6.88 (30H; C_6H_4), 1.08 (6H; CH), 3.07 (36H; CH_3); $\delta_{C\{H\}}$(75.9 MHz, $CDCl_3$): 199.9 (CO), 149.7, 136.4, 130.2, 127.1, 125.7, 120.7, 23.5, 14.5; $\delta_{P\{H\}}$(121.5 MHz,$CDCl_3$) 157 ppm; IR (pentane) ν_{CO} = 1984, 2003. IR (KBr) ν_{CO} = 1977, 2007 cm^1.

3.4.5 Preparation of $[Co_2(CO)_6\{P(O\text{-}2\text{-}^tBuC_6H_4)_3\}_2]$ (1f)

A solution of $P(O\text{-}2\text{-}^tBuC_6H_4)_3$ (1.548 g; 3.22 mmol) in pentane (5 ml) was added to a stirred solution of $[Co_2(CO)_8]$ (0.499 g; 1.46 mmol) in pentane (10 ml). Immediate gas evolution was observed and a precipitate formed. The precipitate was stirred for a further 16 hrs thereafter washed with pentane (3 x 10 ml). Resulting in the formation of $[Co_2(CO)_6\{P(O\text{-}2\text{-}^tBuC_6H_4)_3\}_2]$. (Yield: 1.483 g, 74%); mp 110 °C; δ_H(300 MHz, C_6D_6): 7.53, 7.36, 7.28, 7.05, (24H; C_6H_4), 1.44 (54H; CH_3); $\delta_{C\{H\}}$(75.5 MHz, $CDCl_3$): 202.9 (CO), 150.6, 139.8, 128.2, 127.3, 124.8, 119.9, 35.2, 30.6; $\delta_{P\{H\}}$(121.5 MHz,$CDCl_3$) 154 ppm; IR (pentane) ν_{CO} = 1988, 2005. ; IR (KBr) ν_{CO} = 1977, 2007 cm^{-1}.

3.5 Synthesis of the cobalt phosphite hydrides

3.5.1 Synthesis of [HCo(CO)$_3${P(O-4-^{t}BuC$_6$H$_4$)$_3$}] (2b)

N,N-dimethylformamide (4.0 ml; 25.8 mmol) was added to a stirred solution of [$Co_2(CO)_8$] (0.2970 g; 0.854 mmol) in pentane (20 ml). A pink precipitate formed and the solution decolourised. At 0°C, 6 M HCl (12 ml) was added to this mixture and an immediate phase separation was observed. The light yellow organic phase was separated from the dark blue aqueous phase. The light yellow organic phase was washed three times with 6 M HCl (2 ml). P(O-4-^{t}BuC$_6$H$_4$)$_3$ (0.4073 g; 0.851 mmol) was added to the organic phase at 0°C and immediate gas evolution was observed. IR spectroscopy showed that the title compound had formed. The solution was concentrated and stored in the freezer. Crystals of **2b** could not be isolated. IR (toluene) ν_{CO} = 2071, 2017, 2002. cm^{-1}.

3.5.2 Synthesis of [HCo(CO)$_2${P(O-4-^{t}BuC$_6$H$_4$)$_3$}$_2$] (3b)

The synthesis of compound **2b** was repeated with two equivalents of [P(O-4-^{t}BuC$_6$H$_4$)$_3$] (0.8147 g, 1.702 mmol). Compound **3b** precipitated immediately from pentane upon addition of P(O-4-^{t}BuC$_6$H$_4$)$_3$. Removal of pentane followed by additional washing with small amounts of pentane afforded pure **3b**. Crystals suitable for X-ray diffraction were obtained by slow diffusion of pentane into a solution of **3b** IR (toluene) ν_{CO} = 2034, 1995, 1975 cm^{-1}.

3.5.3 Synthesis of [HCo(CO)$_3${P(O-2-EtC$_6$H$_4$)$_3$}] (2c)

N,N-dimethylformamide (4.0 ml; 25.8 mmol) was added to a solution of [$Co_2(CO)_8$] (0.2970 g; 0.854 mmol) in pentane (20 ml) and stirred. A pink precipitate formed and the solution decolourised. At 0 °C, 6 M HCl (12 ml) was added to this mixture and an immediate phase separation was observed. The light yellow organic phase was separated from the dark blue aqueous phase. The light yellow organic phase was washed three times with 6 M HCl (2 ml). P(O-2-EtC$_6$H$_4$)$_3$ (0.4504 g, 0.851 mmol) was added to the organic phase at 0°C and immediate gas evolution was observed. IR spectroscopy showed that the title compound had formed. The solution was concentrated and stored in the freezer. Crystals of **2c** could not be isolated. IR (toluene) ν_{CO} = 2074, 2023, 2001 cm^{-1}.

3.5.4 Synthesis of [HCo(CO)$_3${P(O-2-EtC$_6$H$_4$)$_3$}$_2$] (3c)

The synthesis of compound **(2c)** was repeated with relevant masses, two equivalents of P(O-2-EtC$_6$H$_4$)$_3$ (09008 g, 1.702 mmol). Compound **(3c)** precipitated immediately from pentane upon addition of P(O-2-EtC$_6$H$_4$)$_3$. Removal of pentane followed by additional washing with small amounts of pentane afforded pure **(3c)**. Crystals suitable for X-ray diffraction were unfortunately not obtained by slow diffusion of pentane into a solution of **5b** in toluene. IR (toluene) ν_{CO} = 2034, 1995, 1970 cm^{-1}.

3.6 Results and discussion

C_6D_6 was used for the ^{1}H chemical shifts because the chemical shift of the phenyl protons of the dimers were observed in the same region and could not be differentiated. Phosphite ligands which were commercially not available had to be prepared according to Scheme 3.1 and 3.2, using various phenols. These ligands are very sensitive and decomposed at room temperature and had to be stored at 0ºC in the fridge. Triphenyl phosphite was the only ligand which was purchased and used without further purification.

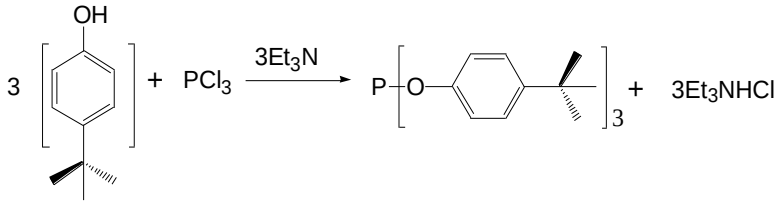

Scheme 3.1: Reaction scheme of P(O-4-^{t}BuC$_6$H$_4$)$_3$ ***(b)***

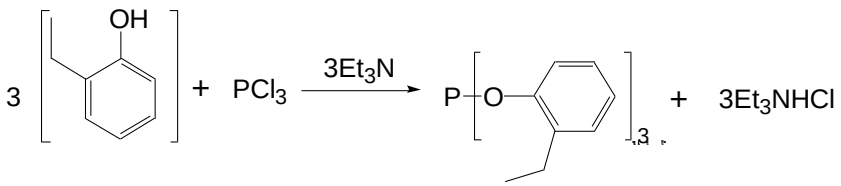

Scheme 3.2 Reaction scheme of P(O-2-EtC$_6$H$_4$)$_3$ ***(c)***

The cobalt complexes [Co$_2$(CO)$_6$L$_2$] **(1)** (where L =P(OPh)$_3$ **(a)**, P(O-4-^{t}BuC$_6$H$_4$)$_3$ **(b),** P(O-2-EtC$_6$H$_4$)$_3$ **(c)**, P(O-2-^{i}PrC$_6$H$_4$)$_3$ **(e)** and P(O-2-^{t}BuC$_6$H$_4$)$_3$ **(f)**) were synthesized in good yield and characterized by means of IR as KBr pallets and in solution as well as NMR spectroscopy. The dimers [Co$_2$(CO)$_6${P(O-4-^{t}BuC$_6$H$_4$)$_3$}$_2$] **(1b)** and [Co$_2$(CO)$_6${P(O-2-EtC$_6$H$_4$)$_3$}$_2$] **(1c)** were structurally characterized by X-ray

crystallography, while the proposed hydride intermediate $[HCo(CO)_3\{P(O\text{-}4\text{-}^tBuC_6H_4)_3\}_2]$ **(2b)** was synthesised and characterized by IR spectroscopy and X-ray crystallography (see Chapter 4). The dinuclear complexes of the cobalt dimers $[Co_2(CO)_6(L)_2]$ **1** (where L = **b** or **c)** as the phosphite ligands) were synthesized from dicobalt octacarbonyl with an excess of the ligand and characterized by IR, NMR and X-ray crystallography where possible. Crystals suitable for X-ray diffraction were obtained from the slow evaporation of a solution of the **3b** and **3c** in acetone (see Figures 4.1 and 4.2).

The dinuclear complex $[Co_2(CO)_6\{P(O\text{-}4\text{-}^tBuC_6H_4)_3\}_2]$ **(1b)** was synthesised from dicobalt octacarbonyl and an excess of tris(4-tertiarybutylphenyl)phosphite as ligand (Scheme 3.3).

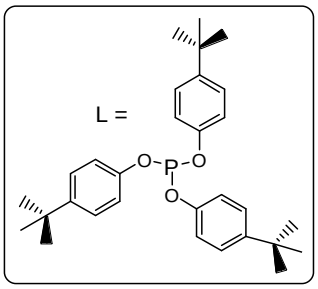

$$[Co_2(CO)_8] + 2L \longrightarrow [Co(CO)_3L]_2$$

Scheme 3.3: Synthesis of dimer $[Co_2(CO)_6\{P(O\text{-}4\text{-}^tBuC_6H_4)_3\}_2]$ ***(1b)***

The infrared spectrum of the formation of (1b) is shown in Figure 3.1. At 2 equivalence the dimer $[Co_2(CO)_6\{P(O\text{-}4\text{-}^tBuC_6H_4)_3\}_2]$ **(1b)** was formed. The formation of the dimer excluded the bridging carbonyls from $[Co_2(CO)_8]$ **(4)**

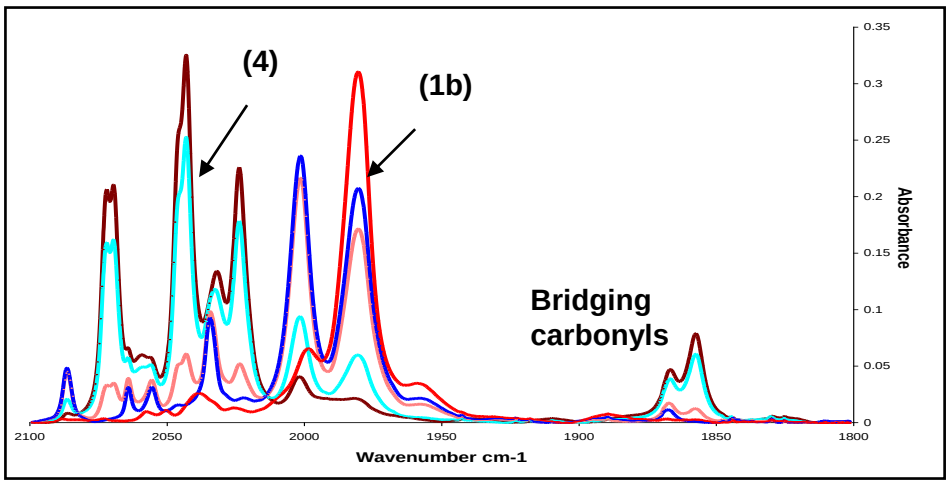

Figure 3.1: Infrared spectrum following the addition of tris(4-tertiarybutylphenyl)phosphite ***(b)*** *from different equivalence of dicobaltoctacarbonyl* ***(4)*** *to give $[Co_2(CO)_6\{P(O\text{-}4\text{-}^tBuC_6H_4)_3\}_2]$* ***(1b)****.*

The formation of the dimer was formed by reacting dicobalt octacarbonyl with the initial addition of P(O-4-^{t}BuC$_6$H$_4$)$_3$ **(b)** at 0.5 equivalence until two equivalence was added. Dicobalt octacarbonyl has bridging carbonyls, but once the dimer has formed the bridging carbonyls have disappeared. The P(O-4-^{t}BuC$_6$H$_4$)$_3$ **(b)** ligands replace two carbonyls on the dicobalt octacarbonyl.

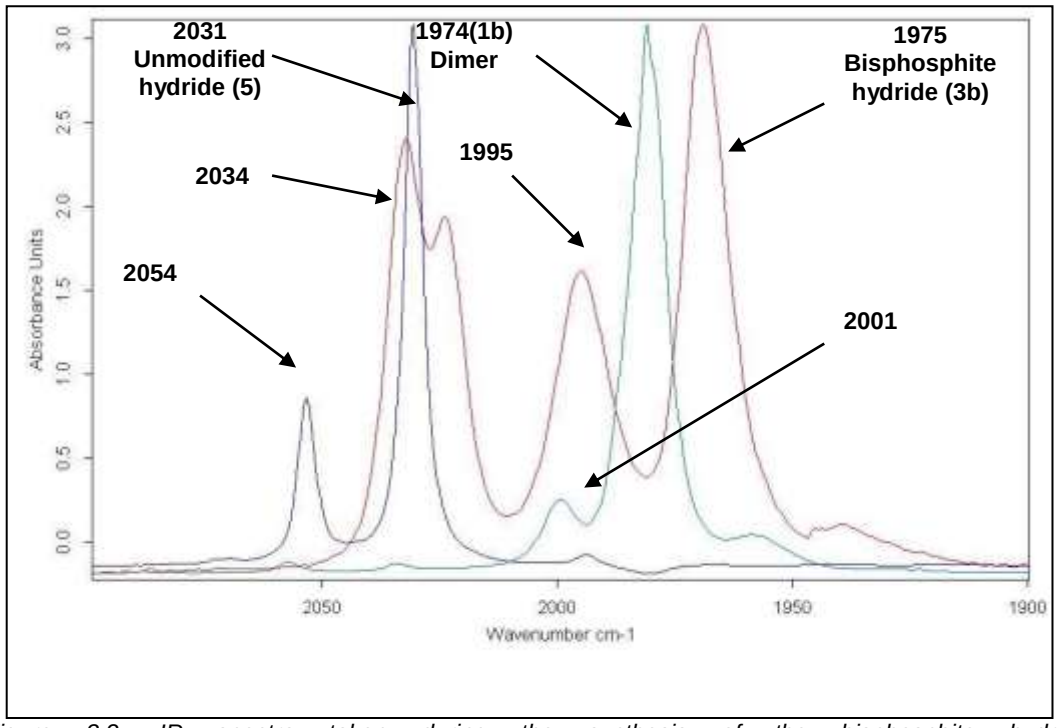

*Figure 3.2: IR spectra taken during the synthesis of the bisphosphite hydride [HCo(CO)$_2${P(O-4-^{t}BuC$_6$H$_4$)$_3$}$_2$] **(3b)** from [Co$_2$(CO)$_8$] **(4)** in pentane at 0℃. **(1b)** represents the IR spectra of the dimer [Co$_2$(CO)$_6${P(O-4-^{t}BuC$_6$H$_4$)$_3$}$_2$]. **(3b)** represents the IR spectrum of [HCo(CO)$_2${P(O-4-^{t}BuC$_6$H$_4$)$_3$}$_2$].*

Figure 3.2 shows the absorbance changes during the reaction between **4** and **b** to form the hydride (see synthetic procedure of **3b**). The unmodified hydride forms first during the reaction and shows two peaks at 2054 and 2031 cm^{-1}. After the addition of the ligand P(O-4-^{t}BuC$_6$H$_4$)$_3$ **(b),** the unmodified hydride peaks disappear and the formation of three new peaks at 2034, 1995 and 1975 cm^{-1} are observed which are characteristic peaks of the formation of bisphosphite hydride **(3b)**.

Figure 3.3 below shows the absorbance changes during the reaction between **4** and **c** to form the hydride (see synthetic procedure of **2c**). Unmodified hydride form first and shows two peaks at 2054 and 2031 cm^{-1}. Upon addition of the ligand, P(O-2-EtC$_6$H$_4$)$_3$ **(c)**, the unmodified hydride peaks disappear and three new peaks at

2074, 2023 and 2001 cm^{-1} are formed which are characteristic peaks of the formation of monophosphite hydride.

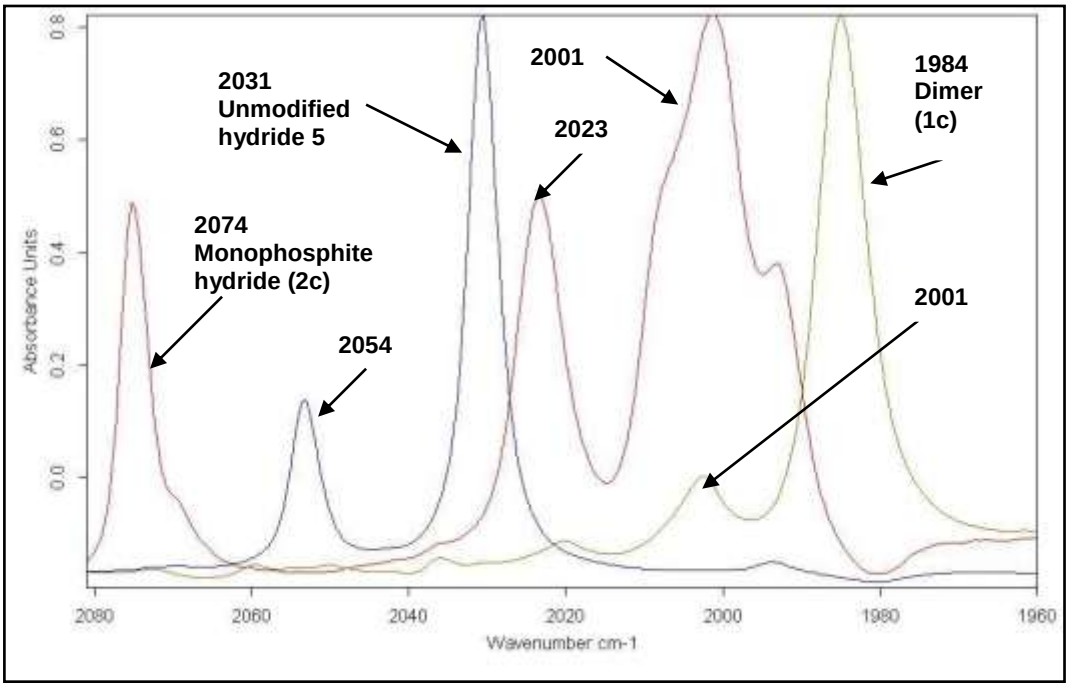

*Figure 3.3: IR spectrum taken during the synthesis of the monophosphite hydride $[HCo(CO)_3\{P(O\text{-}2\text{-}EtC_6H_4)_3\}]$ **(2c)** from $[Co_2(CO)_8]$ **(4)** in pentane. **1c** represents the IR spectra of the dimer $[Co_2(CO)_6\{P(O\text{-}2\text{-}EtC_6H_4)_3\}_2]$. **(5)** Represents the IR spectra of the unmodified hydride, $[HCo(CO)_4]$.*

In the hydroformylation reaction the hydride is formed from the dimer and synthesis gas. The conditions under hydroformylation are stable for the monophosphite cobalt hydride to be formed. Compound **2c** was thermally sensitive at atmospheric pressure. The thermal sensitivity prevented the isolation of crystals of **2c** suitable for X-ray crystallography. Compound **3c** was more stable (decomposed slowly as a solid at 20 °C) but also decomposed rapidly in solution at 20 °C. Complex **2c** and **3c** are both moderately oxygen sensitive, but not sensitive towards water.

The hydrides of the ligand $P(O\text{-}2\text{-}EtC_6H_4)_3$ **(c), 2c** and **3c** could only be synthesized as indicated in Section 3.5.3 and 3.5.4 but could not be isolated as crystals.

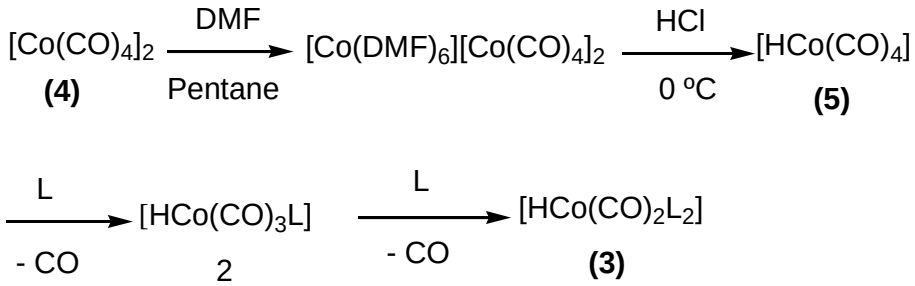

$L = P(OR)_3$

$R = (-4\text{-}^{t}BuC_6H_4, -2\text{-}EtC_6H_4)$

Scheme 3.4: Synthesis of cobalt carbonyl mono- and bisphosphite hydride ***(2)*** *and* ***(3) from*** *$[Co_2(CO)_8]$* ***(5).***

Scheme 3.4 is a representative synthetic procedure for the formation of the mono- and bis-phosphite hydride as observes in Figures 3.2 and 3.3, respectively. These results will help to identify the respective hydrides during the HP-IR study (see Chapter 6).

Table 3.1: IR spectra of the cobalt carbonyl hydrides and the unmodified hydride

Ligands **(L)**	$[Co_2(CO)_6L_2]$ **(1)** $IR\nu_{CO}\ cm^{-1}$	$[HCo(CO)_3L]$ **(2)** $IR\nu_{CO}\ cm^{-1}$	$[HCo(CO)_2L_2]$ **(3)** $IR\nu_{CO}\ cm^{-1}$	Ref
$P(OPh)_3$	1975, 1993	2073, 2021, 1997	2034, 1996, 1971	4
$P(O\text{-}4\text{-}^{t}BuC_6H_4)_3$	1980, 1997	2071, 2017, 2002	2034, 1995, 1975	TW
$P(O\text{-}2\text{-}EtC_6H_4)_3$	1984, 2993	2074, 2023, 2001	2034, 1995, 1970	TW
$P(O\text{-}2\text{-}^{i}PrC_6H_4)_3$	1984, 2993	2075, 2023, 2000		7
$P(O\text{-}2\text{-}^{t}BuC_6H_4)_3$	1988, 2005	2075, 2024, 2004		7
$P(O\text{-}2,4\text{-}^{t}Bu_2C_6H_4)_3$	1984, 2002	2071, 2020, 1998		6

Table 3.1 comprises the results of the IR spectra obtained from the synthesis of the cobalt carbonyl hydrides after having formed the unmodified hydride. The synthesis of the cobalt carbonyl hydrides for all the ligands used in the synthesis when compared to the ones in literature the values are comparable. They all formed the unmodified hydride $[HCo(CO)_4]$ **(5).** With immediate formation of **5** and addition of 1 equivalence of the ligand affords the monophosphite cobalt carbonyl hydride $[HCo(CO)_3L]$ **(2)** and 2 equivalence gave the bisphosphite cobalt carbonyl hydride

[HCo(CO)2L2] **(3)**. The spectra of the unmodified hydride [$HCo(CO)_4$] **(5)** is the same for all the ligands because it is synthesised from dicobalt octacarbonyl for all the ligands.

Table 3.2: Comparison of the ^{31}P NMR data of the phosphite ligands and the dimers

Ligand (L)	Ligand $\delta_{P\{H\}}$(121.5 MHz,$CDCl_3$) ppm	Dimer $\delta_{P\{H\}}$(121.5 MHz,$CDCl_3$) ppm	References
$P(OPh)_3$ **(a)**	126	168.2	4
$P(O\text{-}4\text{-}^tBuC_6H_4)_3$ **(b)**	128.22	169.55	TW
$P(O\text{-}2\text{-}EtC_6H_4)_3$ **(c)**	131.04	158.61	TW
$P(O\text{-}2,4\text{-}^tBuC_6H_4)_3$ **(a)**		156.36	6

Table 3.2 shows a comparison of the ^{31}P NMR of the ligand without the coordination to the metal the results are similar with those in literature. When the ligand is coordinated to the metal an increase in the ^{31}P NMR is seen.

3.7 Conclusion

The phosphite ligands $P(O\text{-}4\text{-}^tBuC_6H_4)_3$ **(b)** and $P(O\text{-}2\text{-}EtC_6H_4)_3$ were successfully synthesised and characterized by ^{31}P NMR. These phosphite ligands were used in the synthesis of the dimeric species, $[Co_2(CO)_6\{P(O\text{-}4\text{-}^tBuC_6H_4)_3\}_2]$ **(1b)** and $[Co_2(CO)_6\{P(O\text{-}2\text{-}EtC_6H_4)_3\}_2]$ **(1c)**.

The complexes **1c** and **1b** were successfully synthesised and characterized by IR and NMR spectroscopy and by crystallography see Chapter 4. The triphenyl phosphite dimer **1a** was synthesised in good yield. All these complexes **1a, 1b** and **1c** were used as precursors in the hydroformylation of 1-octene see Chapter 6.

Hydride intermediate species which were synthesized are comparable to those in literature see Table 3.1. The bisphosphite carbonyl hydride $[HCo(CO)_2\{P(O\text{-}4\text{-}^tBuC_6H_4\}_3\}_2]$ **(3b)** was successfully synthesized and characterized by IR spectroscopy and crystallography. There were no crystal structures for the synthesis of the monophosphite $[HCo(CO)_3L]$ **(2)** and bisphosphite $[HCo(CO)_2L_2]$ **(3)** hydrides for $P(OPh)_3$ **(a)** and for $P(O\text{-}2\text{-}EtC_6H_4)_3$ **(c).** For the monophosphite cobalt carbonyl hydride $[HCo(CO)_3L]$ **(2)** no crystals were obtained for all the ligands **a, b** and **c.** The monophosphite cobalt carbonyl $[HCo(CO)_3L]$ **(2)** was unstable at room temperature.

Due to the monophosphite cobalt carbonyl hydride [$HCo(CO)_3L$] **(2)** being unstable crystals of the hydride were not obtainable.

From Table 3.2 the results obtained from literature and this work for both the ligands and the dimers are similar. The crystal structures of the dimers were also similar and the crystal structures of the hydrides were similar see Chapter 4 for more information.

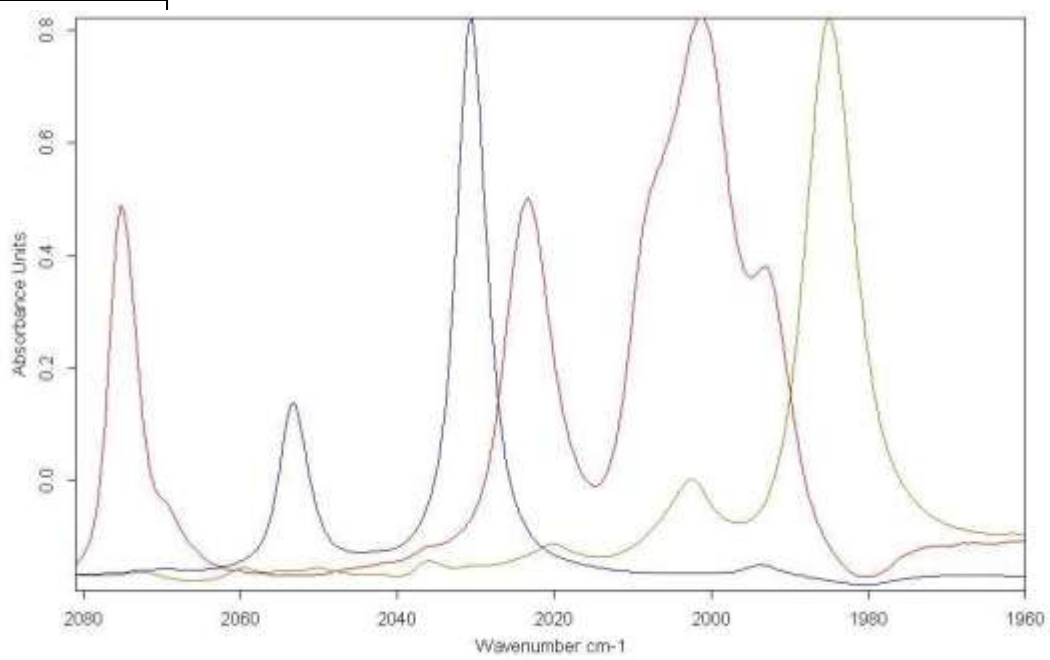

alt phosphite compounds

Compounds", Wiley-

8, 343.

579.

2005, **88**, 676.

Chapter 4

X–ray crystallographic studies of cobalt phosphite complexes

4.1 Introduction

Crystallography is a branch of science which deals with the geometric properties and structures of crystals and crystalline substances. In 1912 von Laue[1] proposed that crystals could diffract X-rays. Following this an experiment was performed which confirmed this theory. The most common crystalline household[2] materials are salt, sugar and washing soda; examples of industrial materials are corundum and germanium. Precious stones such as diamonds and emeralds serve as good examples of crystalline materials. Crystals of a given material tend to be alike in their morphology. A solid compound with atoms arranged periodically in three dimensions is representative of a single crystal. The use of X–rays gives a lot of information in regards to the arrangement of atoms in a crystal. When X–rays are impinged on a crystalline solid, a diffraction pattern is obtained. The diffraction pattern can be related to the inter-atomic spacing.

4.2 The diffraction of X–rays

The electric fields of X–rays, in the same way as those of visible light waves, interact with the electron clouds of atoms. Diffraction effects are important; because X-rays have shorter wavelengths and their rays which are scattered by adjacent atoms in a crystal can interfere. In X-ray diffraction the interest is not only in the direct beam but in the scattered radiation. The diffraction pattern which the X–ray diffraction produces can tell more about the internal arrangement of the crystal.

4.2.1 The Bragg Equation

The number of electrons in an atom determines the scattering characteristics of the X–rays. The atoms in a crystal are lined up in planes, and each plane can diffract the X–rays. Bragg simplified the situation by using near monochromatic X–rays having a narrow wavelength range. They discovered that the X–rays were diffracted only at certain angles that depended at the wavelength and the interplanar spacing of the crystallographic planes.

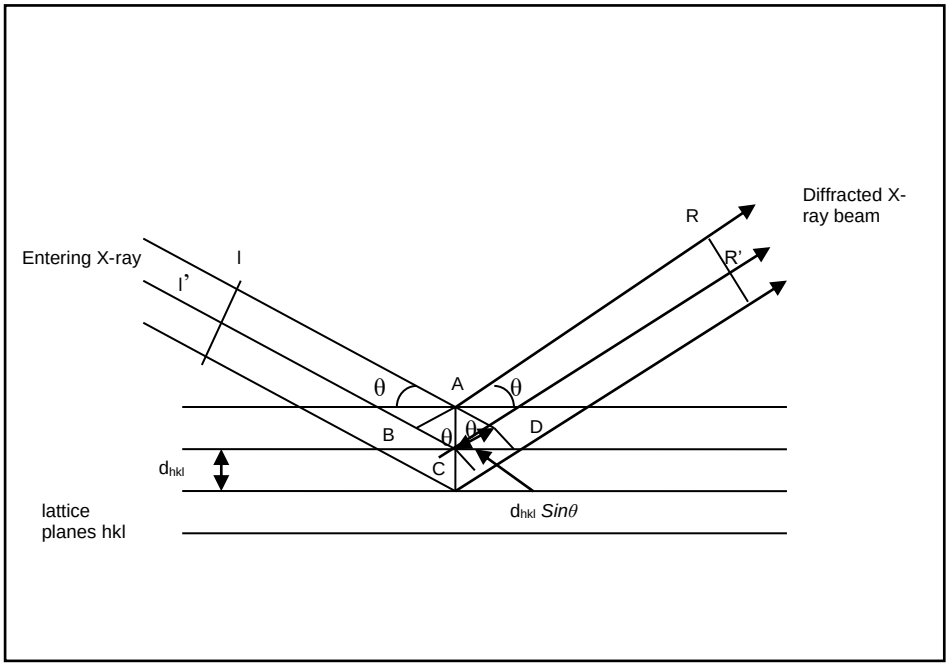

Figure 4.1: Derivation of the Bragg equation, 2d sin θ = nλ. The diffraction of X rays may be considered as reflections from different planes.

From Figure 4.1, W.L. Bragg's explanation for the diffraction is exemplified. Several parallel planes of a crystal are represented. X–rays impinge on the crystal at an angle θ. The incident X–rays of wavelength λ are seen as reflected specularly (as if by a mirror), the angle of incidence being equal to the angle of reflection. The surface atom at point A reflects a small part. Some of the beam will penetrate to the lower part and be reflected. Constructive interference, of the beam at *RR*' occurs only if the difference in distances traveled by the two beams is an integral number of wavelengths, i.e, only if the path, *IAR* differs from that of *I'CR'* by a whole number of wavelengths. Otherwise no diffraction will be observed. The conditions which are necessary for reinforcement are that the distance BC and CD must be equal to an integral number of wavelengths (*nλ*). From figure 4.1, sin θ = CD/d or CD = dsin θ and BC = dsin θ .This condition requires that *nλ* = 2d sin *θ,* which is the **Bragg Equation.** Braggs law $\lambda = 2d_{hkl} \sin\theta$ explains the conditions that should be fulfilled in order to get a reflection from a lattice plane. There is a set of planes in the lattice that gives a reflection hkl in reciprocal space. In the unit cell atoms are given by fractional coordinate's xyz. The three dimensional diffraction patterns are given integer coordinates hkl related to the set of lattice planes. The Bragg law is able to be used in the prediction of the diffraction angle for a given set of planes (hkl). The interpretation of a single crystal experiment requires the reciprocal lattice. It is possible to use the reciprocal lattice to deduce symmetry properties of the direct lattice as well as the crystal structure.

4.2.2 The structure factor

The intensity of the X–ray in the diffraction pattern is affected by a variety of factors. The structure factor F(*hkl)*[3] is one of the factors, and it depends on the crystal structure. The amplitude and phase of the scattered X–ray is determined by the arrangement of the atoms of the crystal relative to the plane in question. The X–ray of the crystals can be expressed mathematically by the structure factor eq. 4.1:

$$F_{hkl} = \sum_{r=1}^{N} f_r \cos 2\pi(hx_r + ky_r + lz_r) \qquad \textbf{(4.1)}$$

The structure factor is expressed in terms of the contents of a single unit cell. The scattering factor is f_r with N atoms, and the position of the rth atom is given by the fractional coordinates (x_r, y_r, z_r).

4.3 Structure determination of compounds

4.3.1 Introduction

The crystals for $[Co_2(CO)_6\{P(O\text{-}4\text{-}^tBuC_6H_4)_3\}_2]$ **(1b)** and $[Co_2(CO)_6\{P(O\text{-}2\text{-}EtC_6H_4)_3\}_2]$ **(1c)** red plates and $[HCo(CO)_3\{P(O\text{-}4\text{-}^tBuC_6H_4)_3\}_2]$ **(3b)**, yellow plate solids suitable for X-ray analysis were isolated as described in **Chapter 3** (see Section 3.4.2, 3.4.3 and 3.5.2) and characterized by means of X-ray crystallography. Complexes **1b** and **1c** were obtained by slow evaporation in acetone, while the yellow complex **(3b)** was obtained by slow diffusion of pentane into a toluene solution of **3b**. A summary of the general crystal data and refinement parameters for all the cobalt complexes **1b**, **1c** and **3b** are provided in Table 4.1.

4.3.2 Experimental

The X–ray data set for $[Co_2(CO)_6\{P(O\text{-}4\text{-}^tBuC_6H_4)_3\}_2]$ **(1b)** were collected on a Bruker SMART CCD 1K area detector diffractometer (Universty of the Witwatersrand), using graphite monochromated Mo-Kα radiation (λ = 0.71073 Å) at 293 K. The structure was solved by conventional Patterson and Fourier methods and refined through full matrix least-squares calculations based on F^2, using the software packages WinGX[4] with SHELXL97.[5] All non hydrogen atoms were refined anisotropically, while the phenyl hydrogen atoms were calculated as riding on the adjacent carbon (aromatic C – H = 0.96 Å). Absorption corrections were performed using SADABS Multi–Scan on

the Bruker, 2005. The program Diamond[8] was used for graphical representation of the crystal structures.

The X–ray data sets for $[Co_2(CO)_6\{P(O\text{-}2\text{-}EtC_6H_4)_3\}_2]$ **(1c)** and $[HCo(CO)_2\{P(O\text{-}4\text{-}^tBuC_6H_4)_3\}_2]$ **(3b)** were collected both at a temperature of 293 K on an *APEX2* (Bruker CCD); cell refinement was done using *SAINT* – Plus;[6] data reduction was performed with *SAINT Plus* and *XPREP*[7]. Programe(s) used to solve the crystal structures was the *SIR97*; program(s) used to refine structure: *SHELX-97;*[5] molecular graphics: Diamond.[8] Computing publication material: WinGX.[4] Absorption corrections were completed using SADABS Multi – Scan on the Bruker CCD.

The structure was solved by conventional Patterson and Fourier methods for reflections and refined through full matrix least-squares calculations based on F^2, using the software packages WinGX[4] with SHELXL97.[5] All non-hydrogen atoms were refined anisotropically, while the phenyl hydrogen atoms were calculated as riding on the adjacent carbon (methyl C – H = 0.96 Å, aromatic C – H = 0.93 Å).

*Table 4.1: Crystallographic data and refinement parameters for **1b**, **1c** and **3b***

Complex identification	**1b**	**1c**	**3b**
Empirical formula	$C_{66}H_{78}Co_2O_{12}P_2$	$C_{54}H_{54}Co_2O_{12}P_2$	$C_{60}H_{79}CoO_8P_2$
Molecular weight (g/mol)	1243.2	1074.8	969.5
Crystal system	Triclinic	Monoclinic	Triclinic
Space group	$P\bar{1}$	P 2(1)/c	$P\bar{1}$
a(Å)	12.1796(19)	18.5777(5)	12.014(5)
b(Å)	12.460(2)	10.5387(2)	12.863(5)
c(Å)	12.990(2)	26.4248(6)	22.050(5)
α(°)	77.552(3)	90.00	92.36(5)
β (°)	65.628(3)	96.62(10)	93.45(5)
γ(°)	80.463(3)	90.00	116.59(5)
Volume (Å^3)/Z	1746.9(5)/1	5139.1(2)/4	3032.7(19)/2
density $_{cal}$ (Mg.m^3)	1.107	1.408	1.175
Crystal colour	Red	Red	yellow
Crystal morphology	block	plate	plate
Crystal size (mm)	0.54 x 0.36 x 0.34	0.29 x 0.20 x 0.05	0.26 x 0.13 x 0.06
θ ranges (°)	2.22 - 26.37	1.10 - 28.32	0.93 - 25.19
R_{int}	0.0782	0.0640	0.0719
Index ranges	-13≤*h*≤15, -15≤*k*≤15, -16≤*l*≤15	-22≤*h*≤22, -12≤*k*≤12, -32≤*l*≤32	-10≤*h*≤14, -15≤*k*≤12, -26≤*l*≤26
Reflections collected/unique	10624 / 7052	63289 / 9754	26888 / 10794
Completeness (%)/ θ(°)	98.5 / 26.37	99.9 / 25.68	98.9 / 25.19
Refinement method	Full matrix least squares F^2	Full matrix least squares F^2	Full matrix least squares F^2
Goodness-of-fit on F^2	1.009	0.981	0.965
Absorption coefficient	0.572 mm^{-1}	0.770 mm^{-1}	0.386 mm^{-1}
F(000)	576	2266	1144
Final R indices [I > 2σ (I)]	R1 = 0.0571, *wR2* = 0.1582	R1 = 0.0553, *wR2* = 0.1306	R1 = 0.0797, *wR2* = 0.1688
Largest diff peak and hole/ e Å^{-3}	0.847 and -0.652	0.833 and -0.596	0.979 and -1.610

1b$[Co_2(CO)_6\{P(O\text{-}4\text{-}^tBuC_6H_4)_3\}_2]$, **1c**$[Co_2(CO)_6\{P(O\text{-}2\text{-}EtC_6H_4)_3\}_2]$, **3b**$[\{HCo(CO)_3\{P(O\text{-}4^tBuC_6H_4)_3\}_2]$

4.4 Crystal structure of $[Co_2(CO)_6\{P(O\text{-}4\text{-}^tBuC_6H_4)_3\}_2]$ (1b)

The partial projection of the title compound **1b** is shown in Figure 4.2, while the molecular diagram showing the numbering scheme of **1b** is presented in Figure 4.3. Selected bond distances and angles of the complex are given in Table 4.2, while those of the phenyl rings are given in Table 4.3. Selected torsion angles of the title compound are presented in Table 4.4. Supplementary data containing a complete list of atomic coordinated, anisotropic displacement parameters, bond distances and angles are given in the **Appendix** in Table **A1 – A4**.

4.4.1 Packing of the crystal structure 1b

The title compound **1b** crystallized in the triclinic space group $P\bar{1}$, with one molecule per unit cell (see Table 4.1), the Co-Co bond is dissected by an inversion centre.

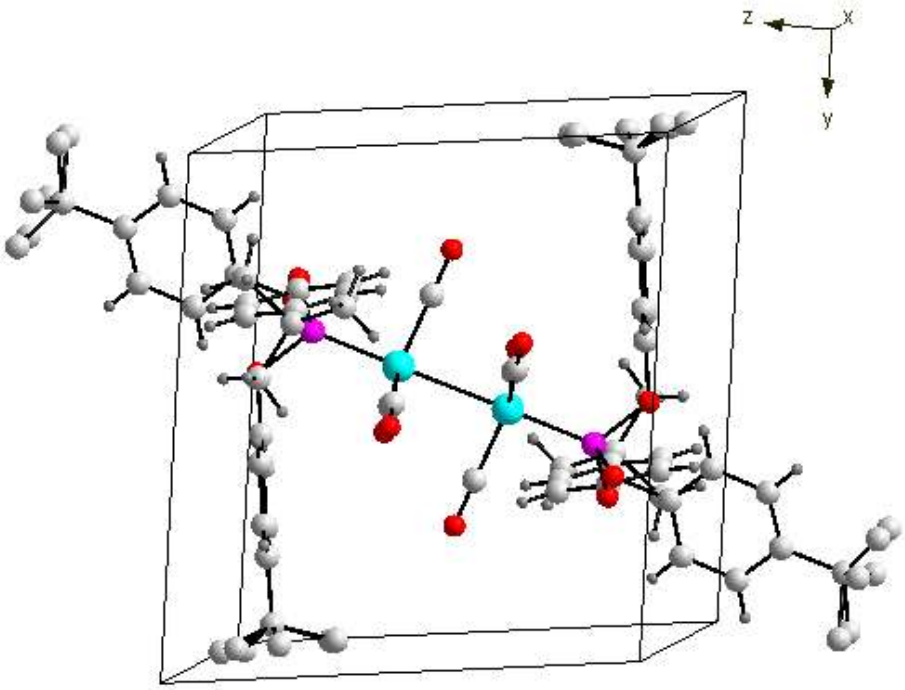

Figure 4.2: The partial projection of $[Co_2(CO)_6\{P(O\text{-}4\text{-}^tBuC_6H_4)_3\}_2]$ ***(1b).*** *Hydrogen atoms on the para-tertiary- butyl groups have been omitted for clarity.*

(2)

(1)

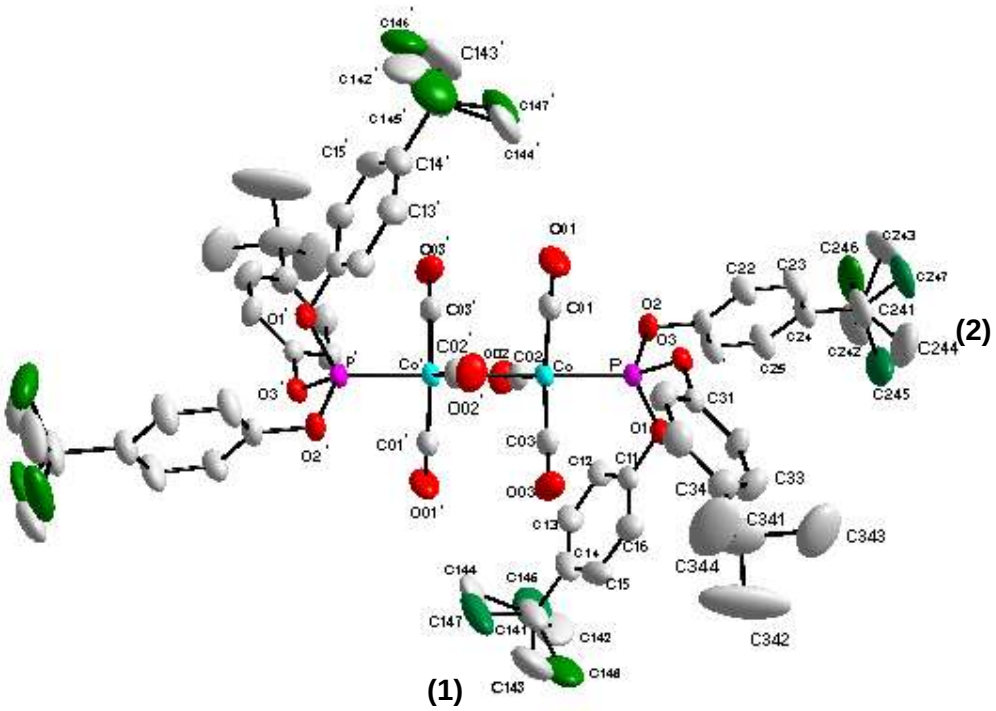

Figure 4.3: Molecular diagram of $[Co_2(CO)_6\{P(O\text{-}4\text{-}^tBuC_6H_4)_3\}_2]$ ***(1b)*** *showing the atom numbering system. The phenyl ring numbering is such that the first digit refers to the rings and number of the rings. The second digit refers to the C-atom in the ring. The disordered para-tertiary butyl groups are indicated by the green ellipsoids (1) and (2). H atoms are omitted for clarity. Thermal ellipsoids are drawn at a 30% probability for non hydrogen atoms. Primed atoms were generated by symmetry (1-x+1,-y+1,-z+1).*

The dinuclear arrangements which are formed by two fragments of $[–Co(CO)_3L]$ and represented in Figure 4.3 are comparable with similar structures in literature.[9,10] The structure has shown the substitution of bridging carbonyls which were present in the starting material $[Co_2(CO)_8]$ **(4)**. The molecular structure shows its dinuclear arrangement which is formed by two trigonal $[–Co(CO)_3\{P(O\text{-}4\text{-}^tBuC_6H_4)_3\}]$ fragments with the $P(O\text{-}4\text{-}^tBuC_6H_4)_3$ **(b)** ligands occupying *trans*–configurations with respect to the Co-Co bond (see Table 4.2). The molecule lies on a centre of symmetry bisecting the Co-Co bond. Phosphite ligands in the dimer have an effective solid state cone angle of 175.4° which agrees very well with the reported value given in literature.[10]

The Co centers displayed the expected distorted trigonal bipyramidal geometries associated with these[11] molecules; the Co-atom is displaced by 1.788 Å towards the apical phosphite ligand. The presence of the inversion center at the centre of Co-Co bond ensures that the carbonyl groups attached to the Co atoms adopt a fully staggered conformation. All the carbonyl groups are essentially linear [Co-C-O with equivalent angles the average is 179.04(14)°].The axial P-Co-Co angle indicates a small deviation from linearity with an angle of 179.38(6)° (see Table 4.2).

Table 4.2: Selected Interatomic Bond Distances (Å) and Angles (°) of $[Co_2(CO)_6\{P(O\text{-}4\text{-}^tBuC_6H_4)_3\}_2]$ ***(1b).***

Bond distances (Å)			
Co – C(01)	1.784(2)	P – O(3)	1.610(2)
Co – C(02)	1.786(2)	O(3) – C(31)	1.406(2)
Co – C(03)	1.788(2)	C(01) – O(01)	1.134(2)
Co – P	2.118(3)	C(02) – O(02)	1.135(1)
Co – Co	2.665(4)	O(1) – C(21)	1.418(3)
P–O(1)	1.604(2)	O(2) – C(21)	1.407(2)
P – O(2)	1.598(2)	C(03)-O(03)	1.134(2)
Bond angles (°)			
C(02)-Co-C(01)	119.4 (10)	P-O(1)-O(3)	99.85(10)
C(03)-Co-C(01)	118.9(10)	O(1)-P-O(2)	103.0(10)
C(02)-Co-C(03)	119.6(10)	O(2)-P-Co	114.5(8)
C(02)-Co-P	96.2(7)	O(1)-P-Co	119.8(8)
C(3)-Co-P	95.7(7)	O(3)-P-Co	117.7(8)
C(1)-Co-P	92.9(7)	O(1)-C(11)-P	123.9(11)
C(3)-Co-Co[a])	84.3(6)	O(2)-C(21)-P	122.0(1)
C(2)-Co-Co[a])	84.4(6)	O(3)-C(31)-P	119.9(11)
C(1)-Co-Co[a])	84.4(6)	C(01)-O(01)-Co	178.4(14)
P-Co-Co[a])	179.38(6)	C(02)-O(02)-Co	179.5(14)
P-O(2)-O(3)	98.71(10)	C(03)-O(03)-Co	179.2(14)
Symmetry code: [a] = 1 – x, 1 –y, 1 – z			

From Table 4.2 the P-O bond length have an average of 1.604(2) Å and the Co-C bond length average for all three is 1.786(2) Å. The Co-C bond lengths are slightly longer than the P-O bond lengths. The bond angle of C(02)-Co-P (96.2(7)º) is larger than C(3)-Co-P(95.7(7)º) and C(1)-Co-P (92.9(7)º) indicating that it is further away from phosphorus. All the bond angles of Co-O-C are within the range of 179.0(14)° indicating their linearity.

The bond angles of C(02)-Co-C(01), C(03)-Co-C(01) and C(02)-Co-C(03) are 119.4(10), 118.9(10) and 119.6(10)º respectively (trigonal pyramidal geometry around the cobalt centre). The angles are almost 120°. The smaller angle is for the two carbonyls occupying the one side of the trigonal plane.

There is a 0.5 statistical occupancy on the disordered carbons which is present on the *para*-tertiary butyl groups on rings 1 and 2, see Figure 4.3. The probable explanation for this disorder is that the tertiary butyl phenyl phosphites have spatial freedom which allows them to have possible rotation along both the P-O and O-C

bonds.[11,12] This has presented a considerable distortion on the phenyl rings (see Table 4.3). The *para*-tertiary-butyl substituents of the phosphite ligands had an affected the angles of the phenyl ring which show some deviations from the expected bond angle of the phenyl ring of 120°. This has presented a considerable distortion on the phenyl rings[11,12] (see Table 4.3). The phenyl ring angles range from 116 to 119° for the angles that include the *para*-tertiary butyl, the further the angle is it conforms to the angle of the phenyl ring of 120º.

Table: 4.3. Selected bond angles in the phenyl rings of $[Co_2(CO)_6\{P(O\text{-}4\text{-}^tBuC_6H_4)_3\}_2]$ ***(1b)*** *illustrating the deviations from the ideal geometry of 120°.*

Bond angles (º)			
C(23)-C(24)-C(25)	116.8(12)	C(16)-C(11)-C(12)	121.5(13)
C(25)-C(26)-C(21)	119.7(10)	C11-C12-C13	118.9(13)
C(26)-C(21)-C(22)	120.1(13)	C(35)-C(34)-C(33)	116.9(1)
C(21)-C(22)-C(23)	119.4(11)	C(34)-C(33)-C(32)	122.2(12)
C(31)-C(14)-C(33)	118.3(13)	C(33)-C(32)-C(31)	119.5(11)
C(15)-C(16)-C(11)	117.0(12)	C(31)-C(36)-C(35)	118.7(11)

Table 4.4: Selected torsion angles of $[Co_2(CO)_6\{P(O\text{-}4\text{-}^tBuC_6H_4)_3\}_2]$ ***(1b)***

Torsion angle (º)	
Co-P-O(3)-C(31)	-68.6(14)
Co-P-O(2)-C(21)	177.6(10)
Co-P-O(1)-C(11)	11.6(17)
P-O(2)-C(21)-C(26)	-96.4(15)
P-O(2)-C(21)-C(22)	87.6(16)
P-O(3)-C(31)-C(36)	90.8(15)
P-O(3)-C(31)-C(32)	91.3(16)
P-O(1)-C(11)-C(16)	106.1(15)
O(3)-P-O(1)-C(11)	141.7(12)
O(3)-P-O(2)-C(21)	56.5(14)

The torsion angles in Table 4.4 show that the structure is not bent along the P-Co-Co-P moiety. The tri(4-tertiaryphenyl)phosphite has two phenyl rings which fold inwards and the third phenyl ring folds outwards. The phenyl substituents which are on a phosphite moiety coordinated to a metal center tend to fold away; this is a general phenomenon with the phosphite ligands. [11,13] This phenomenon can be seen with Co-P-O(3)-C(31) being bent by -68.6(14), phenyl ring 3. Phenyl ring 3 shows that it is not flat it is slightly bent with P-O(2)-C(21)-C(26) equal to -96.4(15)º. The torsion angles of phenyl ring 3 indicate that the ring is almost flat where P-O(3)-C(31)-C(36) is 90.8(15)º and P-O(3)-C(31)-C(32) is 91.3(16)º.

4.5 Crystal structure of $[Co_2(CO)_6\{P(O\text{-}2\text{-}EtC_6H_4)_3\}_2]$ (1c)

The partial projection of the title compound **(1c)** in the unit cell is represented in Figure 4.5, while the molecular diagram showing the disorder on the phenyl rings and 2-ethyl groups of **1c** is presented in Figure 4.6. The molecular diagram showing the numbering scheme of **1c** is represented in Figure 4.6. Selected bond distances and angles of the complex are given in Tables 4.5. Supplementary data containing a complete list of atomic coordinated, anisotropic displacement parameters, bond distances and angles are given in the **Appendix**, Table **B1 – B4**.

4.5.1 Packing of the crystal structure (1c)

Figure 4.4 shows that the title compound crystallizes in the monoclinic space group P 2(1)/c, with four molecules per unit cell (see Table 4.1).

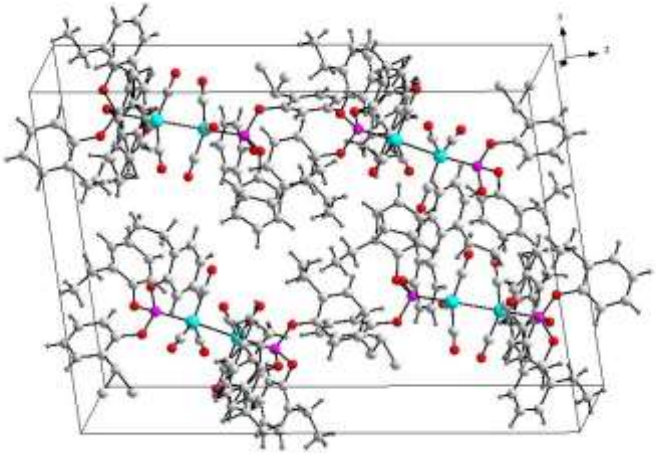

Figure 4.4: Partial projection of the unit cell of $[Co_2(CO)_6\{P(O\text{-}2\text{-}EtC_6H_4)_3\}_2]$ ***(1c)***

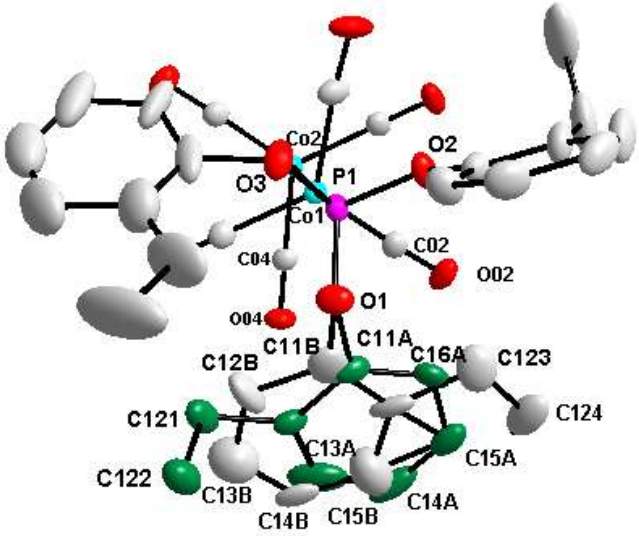

Figure 4.5: Molecular structure of $[Co_2(CO)_6\{P(O\text{-}2\text{-}EtC_6H_4)_3\}_2]$ ***(1c)*** *showing the disorder of the phenyl rings. The diamond sketch presents the disorder in the phenyl ring as green atoms. Thermal ellipsoids are drawn at a 30% probability for non-hydrogen atoms. There is a disorder on the carbons of the 2-ethyl moiety on ring 5, C522 and C523 represented as green atoms but is not shown in this structure.*

Figure 4.5 shows that the phenyl ring and the ethyl group of the coordinated ligand disorder into two (indicated by green and grey ellipsoid carbon atoms) with C(11A), C(12A), C(13A), C(14A), C(15A) and C(16A), 2-ethyl C(121) and C(122) (green ring) and C(11B), C(12B), C(13B), C(14B), C(15B) and C(16B), 2-ethyl C(123) and C(124) (grey ring). This is probably due to the vibrations of the carbons in an ellipsoid manner. All the carbons on the phenyl rings have 0.5 statistical occupational disorders on the carbon atoms. The phosphite ligands compared to phosphines do not have a rigid geometry and the degrees of freedom are larger thus they often show these types of disorders. The phosphite ligands do not seem to be rigid due to the rotation of the P–O and O–C bonds, whilst the phosphine ligands do not have these bonds and are therefore rigid. The structure has shown the exclusion of bridging carbonyls which were present in the starting material $[Co_2(CO)_8]$ **(4)**.

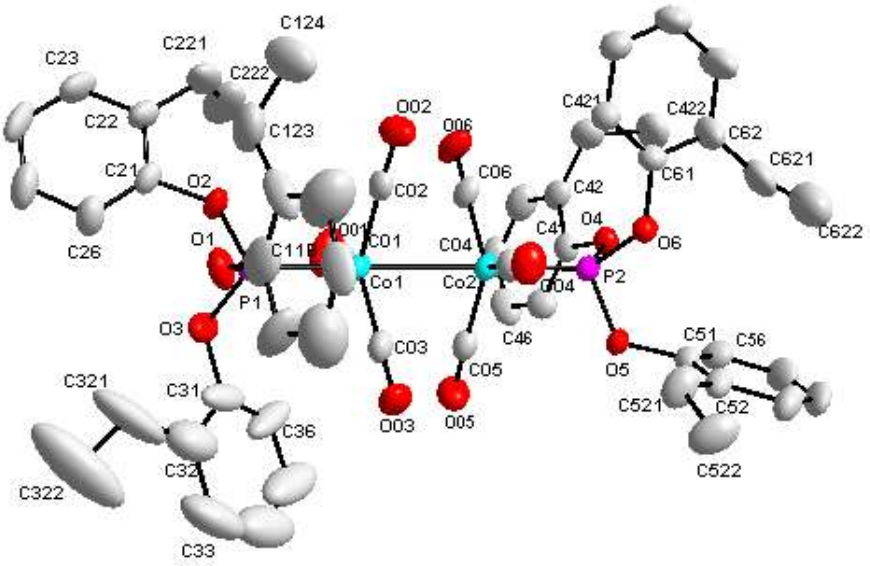

Figure 4.6: Crystal structure of $[Co_2(CO)_6\{P(O\text{-}2\text{-}EtC_6H_4)_3\}_2]$ ***(1c)*** *showing the atom numbering scheme. The phenyl ring numbering is such that the first digit refers to the ring number and the second digit refers to the C-atom in the ring. The H atoms are omitted for clarity. Thermal ellipsoids are drawn at a 30% probability for non-hydrogen atoms. The disorder of the phenyl ring and the ethyl moiety is not shown in this structure.*

Figure 4.6 shows a dinuclear arrangement formed by two trigonal fragments [-$Co(CO)_3L$], the phosphite ligands in *trans* positions with respect to the Co-Co bond (2.661(1) Å). The Co-Co bond length for this structure is slightly shorter than the one for **1b**, and can be attributed to the $P(O\text{-}4^tBuC_6H_4)_3$ **(b)** ligands on the para position. The Co atom displays trigonal bipyramidal geometry with the CO atoms. There is slight deviation from linearity of the [Co-C-O angles with an average of 176.9(1)°] the only one which is almost linear is Co(1)-C(3)-O(3) with an angle of 179.47º. Due to the disorder each phosphite ligand has two different cone angles. The molecule does not lie on an inversion centre, and the phosphite ligands have an effective solid state cone angle of 189.4° and 183.8° measured by using the angle of Co(1)-P(1), with an average of 186.4°. The other effective solid state cone angles were 173.3º and 179.9º measured by using the angles of Co(2)-P(2), with an average of 176.6º. A trigonal plane is defined by the Co and the three CO ligands which is common for these structures. The tris(2-ethylphenyl)phosphite has got two phenyl rings show bending inwards as an umbrella, whilst the third phenyl ring bends outwards.

Table 4.5. Selected bond angles in the phenyl rings of $[Co_2(CO)_6\{P(O\text{-}2\text{-}EtC_6H_4)_3\}_2]$ (1c) illustrating the deviations from the ideal geometry of 120º.

Bond angles (º) Disordered phenyl rings			
C(51)-C(52)-C(53)	115.3(2)	C(11B)-C(16B)-C915B)	116.2(1)
C(54)-C(55)-C(56)	119.8(2)	C(12B)-C(13B)-C(14B)	116.1(1)
C(12A)-C(11A)-C(16A)	124.7(11)	C(13B)-C(14B)-C(15B)	116.9(1)
C(11A)-C(12A)-C(13A)	113.6(2)	C(34)-C(33)-C(32)	129.5(2)
C(11A)-C(16A)-C(15A)	115.4(2)	C(13B)-C(12B)-C(11B)	117.5(2)
C(15A)-C(14A)-C(13A)	123.6(2)	C(31)-C(36)-C(35)	118.7(11)
C(14A)-C(15A)-C(16A)	120.3 (2)	C(12B)-C(11B)-C(16B)	122.9(19)
Phenyl rings without disorder			
C(41)-C(42)-C(43)	115.7(4)	C(45)-C(44)-C(43)	120.2(2)
C(45)-C(46)-C(44)	119.5(2)	C(52)-C(51)-C(56)	124.0(4)
C(46)-C(41)-C(42)	122.9(2)	C(45)-C(44)-C(43)	120.2(2)

Table 4.5 shows the deviations from the ideal bond angle of 120º from those of the phenyl rings. With $[Co_2(CO)_6\{P(O\text{-}2\text{-}EtC_6H_4)_3\}_2]$ **(1c)** three phenyl rings have been selected for the purpose of comparison of the different angles. Phenyl ring 1 with the disordered phenyl rings was selected, phenyl ring 5 with the disorder on the *ortho* ethyl substituents and phenyl ring 4 without any disorder. Comparison of the angle with the *ortho* ethyl phenyl ring 1A the bond angle is 113.59(2)º, for phenyl ring 1B it is 116.2(1)º and for the phenyl ring without a disorder it was found to be 115.7(4)º. The phenyl ring with the disorder of the *ortho* ethyl which is disordered is seen at C(51)-C(52)-C(53) with an angle of 115.3(2)º.

Phenyl ring 1A has the angle with the most deviation from the 120º ideal geometry of the phenyl rings with an angle of only 113.59(2)º. The contribution of the deviation from the general 120º of the phenyl rings can be attributed to the ortho ethyl substituents bringing in the deviation from conformity than the actual disorders of the phenyl rings. The angles which are opposite to the *ortho* ethyl are close to 120º. C(14A)-C(15A)-C(16A) has an angle of 120.3(2)º. C(12B)-C(11B)-C(16B) with an angle of 122.9(19)º.

Table 4.6: Selected Interatomic bond distances and angles (º) of $[Co_2(CO)_6\{P(O\text{-}2\text{-}EtC_6H_4)_3\}_2]$ (1c)

Bond distances (Å)			
Co(1) – C(01)	1.775(5)	P(1) – O(2)	1.578(3)
Co(1) – C(02)	1.789(5)	P(1) – O(3)	1.604(3)
Co(1)– C(03)	1.784(5)	P(2) – Co(2)	2.122(11)
Co(1) – P(1)	2.127(12)	O(01) – C(11A)	1.441(12)
Co(1) – Co(2)	2.661(7)	O(02) – C(21)	1.406(5)
Co(2) – P(2)	2.122(11)	O(03) – C(31)	1.419(6)
P(1) – O(1)	1.592(3)		
Bond angles (°)			
C(02)-Co -C(01)	113.2(1)	O(1)-P(1)-O(2)	105.6(1)
C(03)-Co-C(01)	124.8(1)	O(2)-P(1)-Co(1)	110.3(2)
C(02)-Co-C(03)	119.4(1)	O(1)-P(1)-Co(1)	119.7(1)
C(02)-Co-P(1)	98.2(1)	O(3)-P(1)-Co(1)	120.0(2)
C(03)-Co-P(1)	96.9(1)	O(1)-C(11A)-P(1)	123.0(1)
C(01)-Co-P(1)	90.9(1)	O(2)-C(21)-P(1)	133.2(2)
C(03)-Co-Co	84.9(1)	O(3)-C(31)-P(1)	121.5(2)

C(02)-Co-Co	84.0(1)	Co(1)-C(01)-O(01)	175.2(2)
C(01)-Co-Co	84.9(1)	Co(1)-C(03)-O(03)	179.5(2)
P-Co-Co	175.8(1)	Co(1)-C(02)-O(02)	175.1(2)
P-O(2)-O(3)	99.4(1)		

Table 4.6 gives selected bond distances and bond angles. Co-C bond distances give an average of 1.783(5) Å. The bond angles for C(02)-Co-C(01), C(03)-Co-C(01) and C(02)-Co-C(03) are 113.2(1), 124.8(1) and 119.4(1)º respectively. The angles for all the carbonyl groups which are trigonal bipyramidal are different.

4.6. The cobalt carbonyl phosphite dimers $[Co_2(CO)_6L_2]$ (1)

Dimers, **1b** and **1c** showed a 0.5 statistical occupancy on the carbons which were disordered. The *para*-tertiary-butyl group on the phenyl ring and ethyl group of the $[Co_2(CO)_6\{P(O\text{-}4\text{-}^tBuC_6H_4)_3\}_2]$ **(2a)** has a disorder (see Figure 4.3). This disorder is probably due to the vibration of the atoms in two positions. The disorders on the molecular diagrams of both dimers had a contribution on the effective solid state cone angles. A summary of selected bond distances, bond angles and cone angles of various dimers described in this study as well as literature examples are presented in Table 4.9.

Table 4.7: Structural correlations for complexes of the type $[Co_2(CO)_6\{L\}_2]$ ***(1)*** *(L = PX_3, X = alkyl, alkoxy or aroyl)*

	Distance in Å			Angle in (º)		Cone Angle (º)	Ref.
Ligand (L)	Co-Co	Co-P	Co-CO	P-Co-CO	P-Co-Co		
CO	2.522(1)	—	1.82(1)	—	—		12
$P(OPh)_3$	2.672(4)	2.122(4)	1.783(2)	95.0	177.3(2)	128	9
$P(O\text{-}2\text{-}EtC_6H_4)_3$	2.661(1)	2.122(0)	1.784(2)	96.1(1)	175.80	176.6	TW
$P(O\text{-}4\text{-}^tBuC_6H_4)_3$	2.665(8)	2.119(9)	1.780(4)	96.0(7)	179.30(7)	175.4	TW
$P(O\text{-}2,4\text{-}^tBuC_6H_4)_3$	2.706(5)	2.134(4)	1.776(7)	96.3(2)	174.95(4)	175	10
Phoban-C_2	2.707(3)	2.199(4)	1.765(13)	99.9(4)	174.4(13)	*	14
Phoban-C_5	2.688(9)	2.207(9)	1.775(3)	103.0(9)	170.5(3)	*	14
Phoban-C_3NMe_2	2.6885(8)	2.205(9)	1.778(4)	102.8(2)	171.3(4)	*	14
Phoban-Cy	2.653(10)	2.196(8)	1.783(2)	102.2(4)	173.6(15)	*	14

*The ranges of the Tolman cone angles for the phoban ligands were from 159 -165º

From the Table 4.7, P-Co-Co bond angle indicate that all the molecules of these structures deviate slightly from linearity with bond angles ranging from 174 to 179˚. The structures with the smaller cone angles have not deviated a lot from linearity because they have angles of 177.3(2) and 179.30(7)º for $P(OPh)_3$ **(a)** and $P(O\text{-}4\text{-}^tBuC_6H_4)_3$ **(b)** respectively. The P-Co-Co angles of the ligands with the larger cone angles $P(O\text{-}2\text{-}EtC_6H_4)_3$ **(c)** and $P(O\text{-}2,4\text{-}^tBu_2C_6H_3)_3$ **(d)** also have the same configuration with angles of 175.80 and 174.95(4)º respectively. The $P(O\text{-}2\text{-}EtC_6H_4)_3$ **(c)** had two different solid state cone angles because they had a disorder which affected the measuring of the cone angles.

The $[Co_2(CO)_6\{P(OPh)_3\}_2]$ **(1a)** with the triphenylphosphite ligand conforms to the folding of the phosphite as an umbrella.[12,11] All the ligands have folded in as an umbrella because there are no substituents on the phenyl rings. Co-P bond distances for $P(OPh)_3$ **(a),** $P(O\text{-}4\text{-}^tBuC_6H_4)_3$ **(b),** $P(O\text{-}2\text{-}EtC_6H_4)_3$ **(c)** and $P(O\text{-}2,4\text{-}^tBu_2C_6H_3)_3$ **(d)** range from 2.122(4), 2.119(9), 2.122(11) and 2.134(4) Å respectively. The $P(O\text{-}2,4\text{-}^tBu_2C_6H_3)_3$ **(d)** has a longer bond distance compared to the other ligands which can be attributed to the larger cone angle. This would mean that the steric bulk of the ligand pulls the phosphorus atom thus lengthening the bond length. The Co-Co bond distances vary between 2.661(1) to 2.706(5) Å, the trend seems to be that the substituents which are attached to the phenyl ring have an influence on the bond distance. The Co–Co bond distance of $P(OPh)_3$ **(a)** is longer than that of $P(O\text{-}4\text{-}^tBuC_6H_4)_3$ **(b)** and $P(O\text{-}2\text{-}EtC_6H_4)_3$ **(c)** because the phenyl rings of the triphenylphosphite ligand are bent inwards thus lengthening the bond of the Co-Co.

4.7 Crystal structure of $[HCo(CO)_2\{P(O\text{-}4\text{-}^tBuC_6H_4)_3\}_2]$ (3b)

The partial projection of the title compound **(3b)** in the unit cell is represented in Figure 4.6, while the molecular diagram showing the numbering scheme is represented in Figure 4.7. Selected bond distances and angles of the complex are given in Tables 4.6. Supplementary data containing a complete list of atomic coordinated, anisotropic displacement parameters, bond distances and angles are given in the **Appendix**, Table **C1 – C4**.

4.7.1 Packing of the crystal structure (3b)

The bisphosphite hydride complex crystallized in the triclinic space group $P\bar{1}$, with two molecules per unit cell (see Table 4.1).

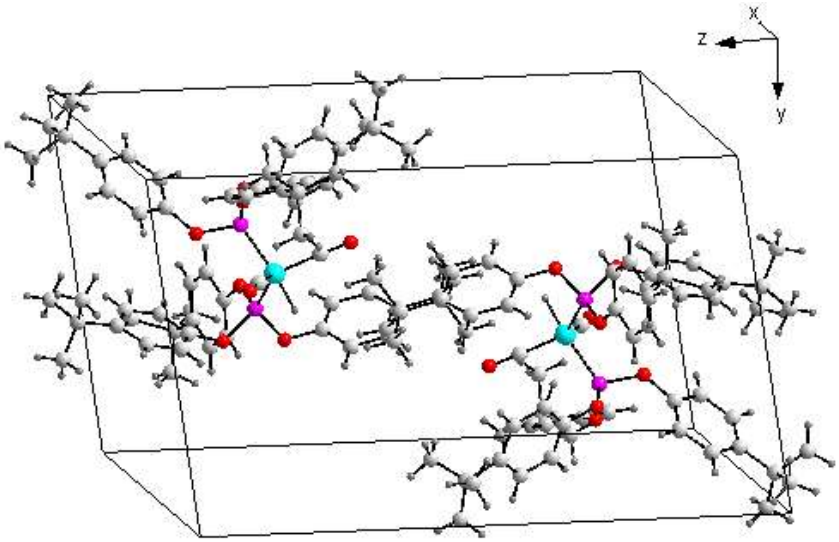

Figure 4.6: The partial projection unit cell of [HCo(CO)$_2${P(O-4-^{t}BuC$_6$H$_4$)$_3$}$_2$] ***(3b).***

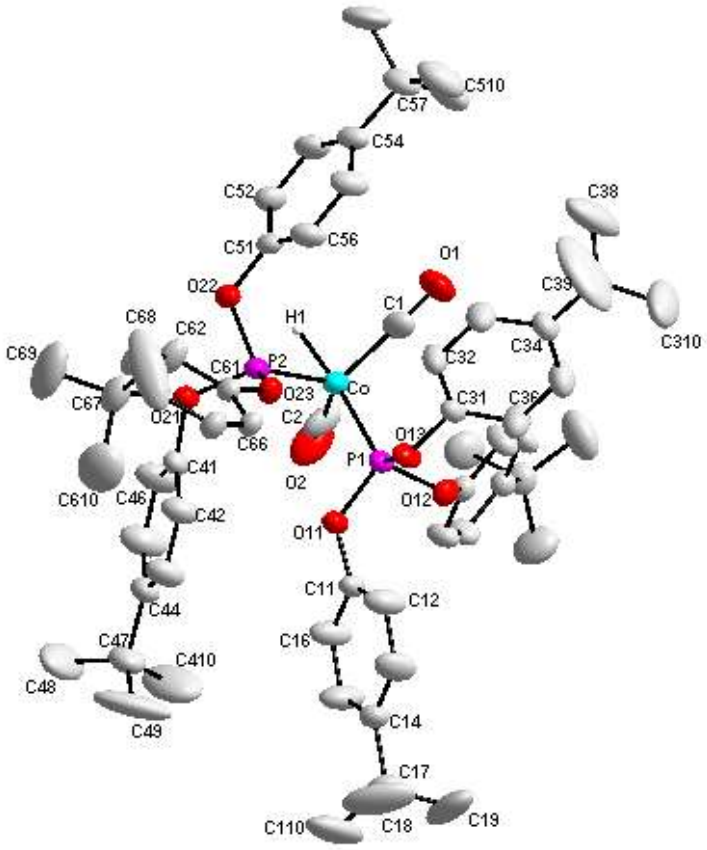

*Figure 4.7: Molecular diagram showing the atom numbering scheme of [HCo(CO)$_2${P(O-4-^{t}BuC$_6$H$_4$}$_3$] **(3b)**.The H atoms are omitted for clarity. Thermal ellipsoids are drawn at a 30% probability for non-hydrogen atoms.*

This structure of $[HCo(CO)_2\{P(O\text{-}4\text{-}^tBuC_6H_4\}_3)_2]$ **(3b)** represents a rare example of a hydride structure of cobalt phosphite carbonyl **3b** is stabilised by $P(O\text{-}4\text{-}^tBuC_6H_4)_3$ **(b)** ligands. The complex exhibits a severely distorted trigonal bipyramidal structure with one $P(O\text{-}4\text{-}^tBuC_6H_4)_3$ ligand and two carbonyls occupying the equatorial plane. The hydride and the other ligand $P(O\text{-}4\text{-}^tBuC_6H_4)_3$ **(b)** are in a *trans* orientation (H(1)-Co-P(1) = 172.1(28)º in the apical positions relative to the trigonal plane. An interesting aspect of this structure is that, one of the phosphite ligand is bonded *trans* to the hydride whereas the published triphenyl phosphite had the hydride bonded in a trans orientation with (H(1)-Co-C(1), more discussion on this concept is in Section 4.7.2. The Co-P bond lengths of 2.125(6) and 2.108(7) Å in **3b** are significantly shorter than the same bond lengths of 2.665(4) Å in $[Co_2(CO)_6\{P(O\text{-}4\text{-}^tBuC_6H_4)_3\}_2]$ **(1b)**. This indicates the *trans*-influence which is exerted by the Co-Co metal bond compare to the single Co in **3b**. The P-O bond distances of 1.610(2), 1.598(2) and 1.604(2) Å in 1b see Table 4.2 are slightly shorter than the same bond lengths of 2.125(6) and 2.108(7) Å in **3b** see Table 4.8. The Co-P(1) bond length of 2.125(6) Å *trans* to the Co-H moiety in **(3b)** is longer than the Co-P(2) bond length of 2.108(7) Å (see Table 4.7). This phenomenon can be attributed to the thermodynamic *trans*-influence of the hydride, and the pattern of bond angles subtended at the cobalt center. The *trans*-influence of the hydride is known to elongate the bond *trans* to it.[15] The hydride **(3b)** has a bond length for Co-H(1) of 1.472(5) Å, this type of bond shortening relative to the typical value of 1.55 Å for the first row transition metal hydrides is characteristic of X–ray crystallography.[15,16] The Co-C(2) bond in the hydride complex **(3b)** is comparable with the Co-CO bonds in **(1b)**, which range from 1.785(0) to 1.788(0) Å.

Table 4.8: Selected Interatomic bond Distances (Å) and angles (º) of $[HCo\{P(O\text{-}4\text{-}^tBuC_6H_4)_3\}_2]$ ***(3b)***

Bond distances (Å)			
Co – H(1)	1.472(5)	P(1) – O(12)	1.609(5)
Co – C(2)	1.723(5)	P(1) – O(1)	1.584(3)
Co – C(1)	1.758(4)	P(2)-O(21)	1,613(4)
Co – P(1)	2.125(6)	P(1) – O(3)	1.605(5)
Co – P(2)	2.108(7)	P(2) – Co(2)	2.128(7)
P(1) – O(11)	1.584(3)	O(01)-C(11A)	1.481(2)
P(1) – O(13)	1.605(5)	Co-C(1)	1.757(4)
P(2)-O(22)	1.618(4)	Co-C(1)	1.728(5)
Bond angles (°)			
Co-H(1)-C(2)	85.2(24)	P(1)-O(11)-Co	113.3(20)
H(1)-Co(1)-C(1)	84.7(21)	P(1)-O(11)-O(12)	102.9(24)
Co-H(1)-P(2)	73.1(25)	P(1)-O(13)-Co	121.9(30)
Co-H(1)-P(1)	172.1(28)	P(1)-O(12)-Co	118.6(23)

Co-C(2)-C(1)	117.9(20)	P(2)-O(23)-O(21)	102.7(27)
Co-C(2)-P(2)	118.2(28)	P(2)-O(23)-O(22)	103.4(27)
Co-C(2)-P(1)	97.7(25)	P(2)-O(23)-Co	114.2(23)
Co-C(1)-P(2)	116.6(21)	P(2)-O(21)-O(22)	91.4(19)
Co-C(1)-P(1)	97.7(25)	P(2)-O(21)-Co	122.9(23)
Co-P(2)-P(1)	99.1(19)	P(1)-Co-H(1)	172.1(28)
P(1)-O(11)-O(13)	99.3(23)	P(2)-Co-H(1)	73.1(24)

*Table 4.9: Selected bond angles in the phenyl rings of [HCo{P(O-4-^{t}BuC$_6$H$_4$)$_3$}$_2$] **(3b)** illustrating the deviations from the ideal geometry of 120º.*

Bond angles (º)	
C(16)-C(11)-C(12)	119.2(34)
C(12)-C(13)-C(14)	122.8(25)
C(14)-C(15)-C(16)	123.3(34)
C(15)-C(16)-C(11)	119.8(25)
C(26)-C(21)-C(22)	125.8(25)
C(22)-C(23)-C(24)	122.1(37)
C(24)-C(25)-C(26)	122.9(34)
C(25)-C(24)-C(23)	116.2(24)
C(35)-C(36)-C(31)	119.8(27)
C(35)-C(34)-C(33)	115.8(32)
C(34)-C(33)-C(32)	122.3(27)
C(34)-C(35)-C(36)	122.8(26)

The phenyl bond angles of the Cobalt phosphite carbonyl hydride [HCo{P(O-4-^{t}BuC$_6$H$_4$)$_3$}$_2$] **(3b)** show deviations from the ideal bond angle of 120º as indicated in Table 4.9. The angles which have oxygen attached to the central carbon C(16)-C(11)-C(12) (119.2(34)º and C(35)-C(36)-C(31) (119.8(25)º The same deviation is seen on the angle of the carbon attached to the 4-*tertiary* group C(35)-C(34)-C(33) (115.8(32)º and C25-C24-C23 (116.2(24)º). As the angles move away from the angles with the substituents they change and become larger such as C(14)-C(15)-C(16) (123.3(34)º) and C(24)-C(25)-C(26) (122.9(34)º)

4.7.2 Geometries related to the 5-coordinated structures (Hydrides)

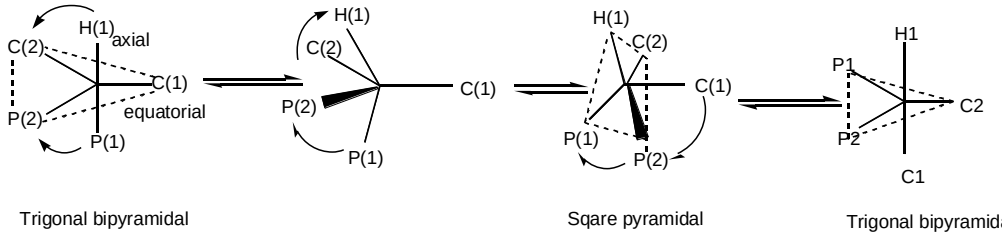

Figure 4.8 The Berry pseudorotation mechanism[17] for 5 coordinated structures

In Figure 4.8 the Berry *pseudo*rotation explains the geometry that can be seen for the five coordinated complexes. The Berry *pseud*orotation mechanism is a way in which the

trigonal bipyramidal molecules isomerise by exchanging the two axial ligands for two of the equatorial ones. It is an accepted mechanism for *pseudo*rotation. The two axial ligands close like a pair of scissors pushing their way in between two of the equatorial groups which scissor out to accommodate them. This will form the square based pyramid where the base is the four interchanging ligands and the tip is the pivot ligand.

Berry *pseudo*rotation shows the different possible geometries which are available for the hydride complexes. The trigonal bipyramidal structures have two distinct type of geometries, one is where the hydride is in the apical position with H(1) opposite to the

carbon atom and the other one has the H(1) opposite the phosphorus atom. The next geometry of these structures is the square pyramidal. In Section 4.7.2.1 a more in depth discussion will be done on the specific hydrides which have been isolated and their geometries.

There are known complexes that can adopt a number of coordination geometries without actually having a change of the ligand coordination mode.[18] Their geometry is similar to that of isomers, although the behaviour is completely different (see Figure 4.8 and 4.9). Powell suggested the term allogons[19] to describe the tetrahedral and square planar forms of dibromobis(benzyldiphenylphosphine)nickel(II) It is not common to isolate two allogons, although the allogons of $[HCo(CO)_2(PPh_3)_2]$ have been isolated. The structure which was isolated was obtained as a byproduct from the reaction. The geometry of both products was different, one was trigonal bipyramidal and the other was square pyramidal.[19] This can be used to explain the geometry of the hydrides (see Figure 4.8)

The square pyramidal structure has not been a usual geometry so far the hydrides are more trigonal bipyramidal.

4.7.2.1 Geometry of $[HCo(CO)_2\{P(O\text{-}4\text{-}^tBuC_6H_4)_3\}_2]$ (3b)

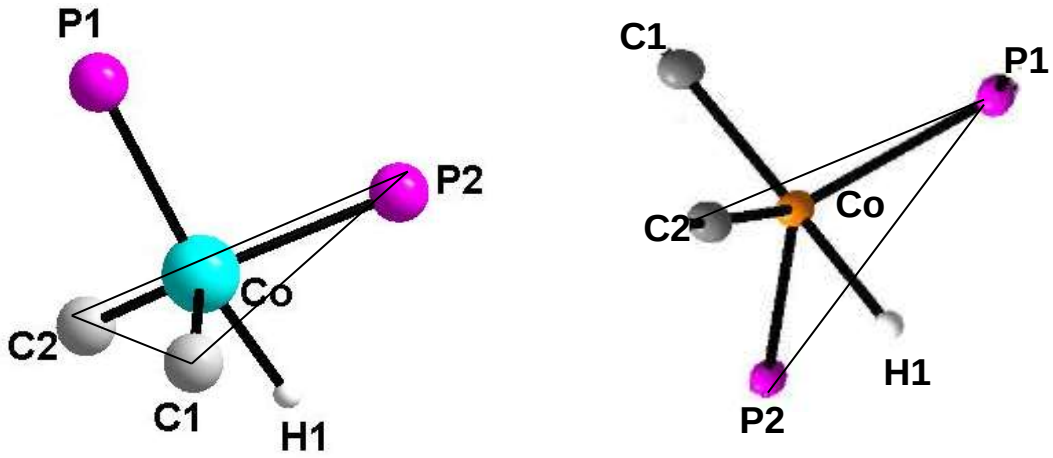

Figure 4.9: Core geometry of $[HCo(CO)_2\{P(O\text{-}4\text{-}^tBuC_6H_4)_3\}_2]$ ***(3b)*** *represented by* ***(A)*** *and the geometry of $[HCo(CO)_2\{P(OPh)_3\}_2]$.****(3a)*** *represented by* ***(B).***

Figure 4.9 is a representation of the geometry adopted by $[HCo(CO)_3\{P(O\text{-}4\text{-}^tBuC_6H_4)_3\}_2]$

(3b). the geometry of the hydride is trigonal bipyramidal. There were no allogons which

were isolated for this structure. The H(1)-Co-P(1) are in the apical position and P(2)-C(1)-C(2) are in the equatorial position. Figure 4.8 is an explanation how the 5 coordinated structures can change positions by rotating of the atoms. It shows how the hydride in Figure 4.9 can

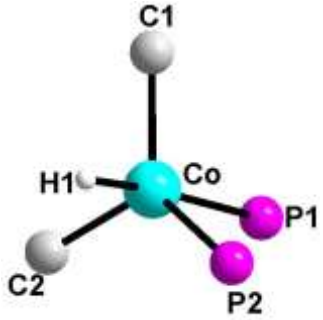

be rotated to a position were the hydride has H(1)-Co-C(1) in the apical position replacing the original H(1)-Co-P(1). This is away to explain the difference in geometry of the bisphosphite cobalt carbonyl hydrides.

Figure 4.10: Rotation of the hydride into the square pyramidal position

In solution there is presumably equilibrium between the allogons, although in this study the hydride **(3b**) had trigonal bipyramidal geometry and not the square planar. Figure 4.8 shows the square pyramidal geometry when the hydride is in equilibrium. In this structure the P(1) and the H(1) are still subtended and not flat as the square pyramidal geometry. This was used as a resemblance of how the geometry of the hydride would look like.

The structures of $[HCo(CO)_3L]$ **(2)** type species are known to be very important in as catalytic intermediates in hydroformylation reactions. The Heck and Breslow studies suggested that the aldehyde reduction occurs *via* the alkoxy intermediate.[20] Comparison of the geometry of $[HCo(CO)_2\{P(O\text{-}4\text{-}^tBuC_6H_4)_3\}_2]$ **(3b)** with known structures in literature will be discussed in Section 4.7.2.2.

4.7.2.2 Molecular structure of $[HCo(CO)_2\{P(O\text{-}4\text{-}^tBuC_6H_4)_3\}_2]$ (3b) in comparison to known structures

a)

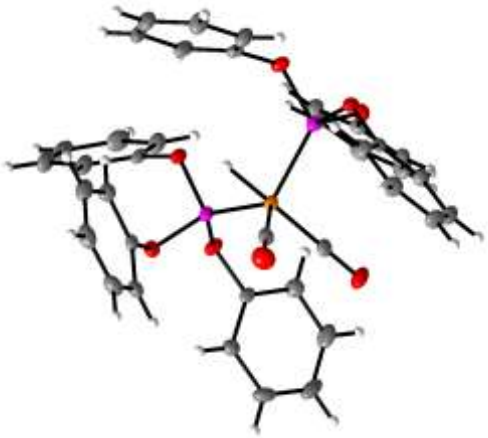

$[HCo(CO)_2\{P(OPh)_3\}_2]$ **(3a)**

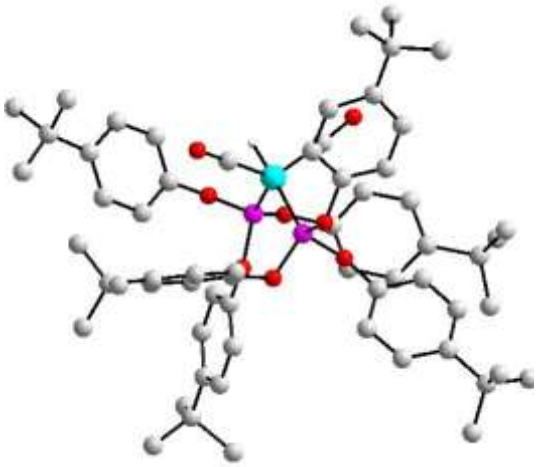

$[HCo(CO)_2\{P(O\text{-}4\text{-}^tBuC_6H_4)_3\}_2]$ **(3b)**

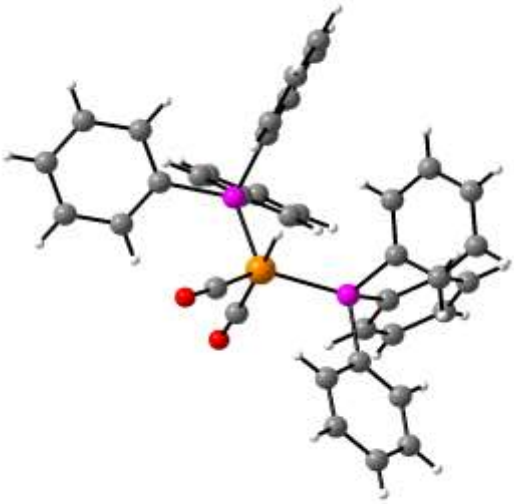

$[HCo(CO)_2\{(PPh)_3\}_2]$

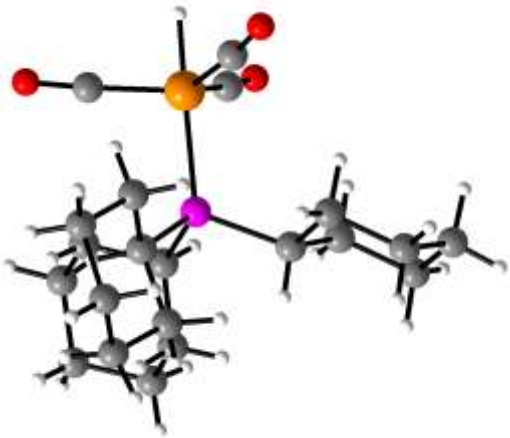

$[HCo(CO)_3\{PCy)_3\}]$

b)

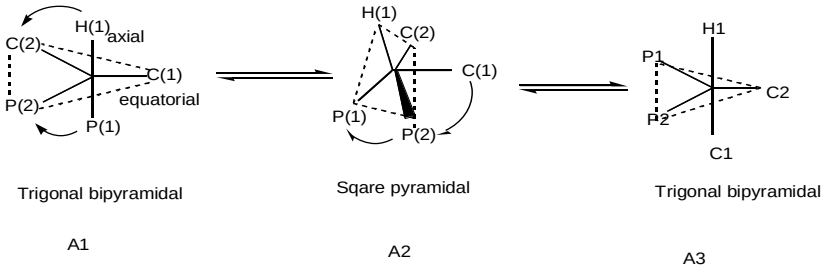

Figure 4.12: a) Crystal structures of known structures compared with the one from this study. b) Adopted geometries of these structures.

The crystal structures of the hydrides can adopt the following possible geometries which are listed in Figure 4.12(b) A1, A2 and A3. The two cobalt phosphite carbonyl hydride complexes $[HCo(CO)_2L]$ **(3)** have shown us two possible geometric adoptions. These have proved to be a rare combination. The $[HCo(CO)_2\{P(O\text{-}4\text{-}^tBuC_6H_4)_3\}_2]$ **(3b)** has a *trans* H(1)-Co-P(1) orientation in the apical position whereas $[HCo(CO)_2\{P(OPh)_3\}_2]$ **(3a)** has a *trans* H(1)-Co-C(1) orientation.[9] Despite the difference in orientation they are both trigonal bipyramidal which is quite interesting. The $[HCo(CO)_2\{P(OPh)_3\}_2]$ **(3a)** does not have steric bulk when compared to $[HCo(CO)_2\{P(O\text{-}4\text{-}^tBuC_6H_4)_3\}_2]$ **(3b)**.

The bisphosphite hydride $[HCo(CO)_2\{P(O\text{-}4\text{-}^tBuC_6H_4)_3\}_2]$ **(3b)** has H(1)-Co-P(1) = 172.1(28)º and $[HCo(CO)_2\{P(OPh)_3\}_2]$ **(3a)** has H(1)-Co-C(1) = 177.9(13)º. The difference in the angles could be due to having the phosphorus being connected to the phenyl ring. This would also show that the phenyl rings of the phosphites have a tendency of folding inwards. The *trans* H(1)-Co-C(1) orientation of **3a** is almost linear because there is no bulk on the carbon atom. The Co-C(1) bond *trans* to the Co-H moiety is significantly shortened (1.758(3) Å) compared to the Co-C(2) bond (1.775(3) Å)

The *trans* H(1)-Co-P(1) orientation of **3b** has Co-P(1) bond *trans* to the Co-H moiety is significantly lengthened (2.125(6) Å) compared to the Co-P(2) bond (2.108(7) Å). The *trans* influence affects the bond length of the Co-P compared to when the bond

is
Co-C.[15]

The only known published monophosphine hydride structure is $[HCo(CO)_3\{PCy)_3\}]$[21] shown in Figure 4.12(a). The structure has trigonal bipyramidal geometry with a *trans* H(1)-Co-P(1) orientation. The bond length of the Co-P bond length was lengthened to 2.235(7) Å. This structure's three carbonyls are in the equatorial position and PCy in the axial sites. This structure $[HCo(CO)_2\{(PPh)_3\}_2]$ was isolated as two allogons, it gave a byproduct which gave two geometries.[18] In this publication they obtained the more unusual geometry of the square pyramidal (see Figure 4.12(b) A2.The two structures have one of them as trigonal bipyramidal (TBP) and the other as square planar (SP). The TBP structure had the arrangement of the ligands placing the hydride and one carbonyl ligand in the axial position and the larger phosphine ligands occupying the equatorial positions. The complexes of the form $HM(P\text{-}P)_2$, where P-P represents a bidentate diphosphine. It is expected that this structure would adopt a square pyramidal geometry with the hydride in the axial position. Crystal structures of the structure show that in the solid state it adopts a distorted TBP geometry with the hydride in the equatorial plane e.g. $[HRh\{P(C_2F_5)_2CH_2CH_2P(C_2F_5)_2\}_2]$,[22] and $[HIr(dppe)_2]$,[23] dppe = bis(diphenylphosphinoethane). A point of interest regarding the different hydrides was that $[HCo(CO)_2\{P(OPh)_3\}_2]$ **(3a),** $[HCo(CO)_2\{P(O\text{-}4\text{-}^tBuC_6H_4)_3\}_2]$ **(3b)**, $[HCo(CO)_2\{(PPh)_3\}_2]$ and $[HCo(CO)_3\{PCy)_3\}]$ all crystallized in the same space group being triclinic even the $[HCo(CO)_2\{(PPh)_3\}_2]$ which was square pyramidal.

4.8 Conclusion

A variety of cobalt complexes have been successfully synthesized and characterized by X-ray crystallography. The dimers $[Co_2(CO)_6\{P(O\text{-}4\text{-}^tBuC_6H_4)_3\}_2]$ **(1b)** and $[Co_2(CO)_6\{P(O\text{-}2\text{-}EtC_6H_4)_3\}_2]$ **(1c)** were used as precursors in the hydroformylation reaction. The hydride $[HCo\{P(O\text{-}4\text{-}^tBuC_6H_4)_3\}_2]$ **(3b**) was also synthesized and successfully characterized by X-ray crystallography. The hydride forms by the splitting of the dimer, into two species during hydroformylation in the presence of syngas and gives a compound with one Co atom (see Figure 4.8).

The phenyl substituents which are coordinated to a metal centre on the phosphite ligands have a tendency of folding away[11,12] in an umbrella shape. The dimer structures of these complexes are similar being substituted by two phosphite ligands. The two phenyl rings bend inwards but the last phenyl ring bends outwards. They both have a trigonal plane which is defined by the Co and the three CO ligands. The

difference with this structure is that the disorder is on the phenyl ring. The P-O bond lengths are 1.604(2), 1.596(2) and 1.612(2) Å and are comparable with similar structures in the literature. The effective solid state cone angles are much larger than expected. Due to the disorders on the phosphite ligands the tris(2-ethylphenyl)phosphite has got more than one measurements. Depending on how the phenyl ring ethyl substituents made a contribution to the cone angle. In the study of the sterically demanding phosphite of P(O-2,4-^{t}Bu$_2$C$_6$H$_3$) **(d)** no bisphosphite hydride was observed during hydroformylation even at 100 equivalence of phosphite ligand this was attributed to the large cone angle of 175º.[9] The structure had substituents on the *para* and *ortho* position, the structures in this study had much larger cone angles.

The cone angles of 176.6 and 186.4º for [Co$_2$(CO)$_6${P(O-2-EtC$_6$H$_4$)$_3$}$_2$] **(1c)** are larger than the cone angle of 175º for [Co$_2$(CO)$_6${P(O-2,4-^{t}Bu$_2$C$_6$H$_3$)$_3$}$_2$] **(1d)** but the bisphosphite hydride was seen in both of these dimers and a crystal structure was obtained for **1b.** The dimer with the larger cone angle is [Co$_2$(CO)$_6${P(O-2-EtC$_6$H$_4$)$_3$}$_2$] **(1c)** with the phenyl ring disorder and having a substituents on the *ortho* position. The phenyl ethyl groups were pointing in different directions probably contributing to making the cone angle becoming larger. The [Co$_2$(CO)$_6${P(O-4-^{t}BuC$_6$H$_4$)$_3$}$_2$] **(1b)** had an effective cone angle of 175.4º which was contributed by the disorders on the *para*-tertiary-butyl group. The difference when compared to the triphenyl phosphite with a cone angle of 128º, the bisphosphite hydride formed but was not converted to the monophosphite hydride. The initial speculation was that with a large cone angle the bisphosphite hydride does not form. In this study the bisphosphite hydride does form with the large cone angles but is eventually converted to the monophosphite hydride which is the active catalyst in hydroformylation.

The cobalt phosphite carbonyl hydride[9] which was reported in literature had the hydride and one of the carbonyl group in a *trans* H(1)-Co-C(1) orientation with a bond angle of 177.9(13)º in the apical position relative to the equatorial plane. The hydride reported in this study **3a** is in a *trans* orientation with the phosphorus atom H(1)-Co-P(1) in the apical position relative to the equatorial plane with a bond angle of 172.19(28)º. Similar structures have been reported such as [HCo{P(OPh)$_3$}$_4$] reported with a similar orientation H(1)-Co(1)-P(1) with a bond angle of 177.6(11)°.[15] Hydride angles which are in the apical position are similar despite whether they are *trans* to carbon or phosphorus. The difference is that the Co-C(1) bond trans to the Co-H moiety in the hydride of the reported structure of P(OPh)$_3$ was shortened to 1.758 Å. Instead the hydrides for this study **3a** and the reported study of [HCo{P(OPh)$_3$}$_4$] both

having H(1)-Co-P(1) had the Co-P(1) bonds *trans* to the Co-H moiety lengthened to 2.125(6) and 2.119 Å respectively. The hydride was trigonal bipyramidal as explained in Section 4.6.3.2.

Table 4.10: Comparison of geometries of different hydride complexes

Complex	Geometry	Co-H (Å)	Reference
$[HCo(CO)_2\{P(O\text{-}4\text{-}^tBuC_6H_4)_3\}_2]$	(TBP)	1.472(5)	TW
$[HCo(CO)_2\{P(OC_6H_5)_3\}_2]$	(TBP)	1.45(3)	10
$[HCo(CO)_2(PPh)_3]$	(TBP)	1.379(3)	18
$[HCo(CO)_3\{PCy)_3\}]$	(TBP)	1.43(3)	21
$[HCo(CO)_2(PPh)_3]$	(SP)	1.45(4)	18

The hydrides Co-H bond distances do not differ significantly between the phosphites and the phosphines. There is no specific trend that can be followed. The hydrogen of the hydride can be *trans* the carbonyl with the bond opposite the hydride of Co-C being shorter. The hydride can also be *trans* the phosphorus and the bond of Co-P being lengthened. The geometries of the hydrides have shown the possibility of having a H(1)-Co-P(1) the only other known structure of the cobalt phosphite carbonyl hydride which has a H(1)-Co-C(1) for the triphenyl phosphite. It was interesting to notice that they both bonded on different atoms but the geometry was the same.

References

1 W. Friedrich, P. Knipping and M. Laue, *Sitzungsberichte derkyl Bayerische, Akademie der Wissenschaffen*. München, 1912, 303.

2 M.M. Woolfson, "*An Introduction to X-ray crystallography*", Cambridge University Press, 1970. W. Clegg, A.J. Blake R.O. Gold and P. Main, "*Crystal Structure Analysis, Principles and Practice*", International Union of Crystallography, Oxford University Press, Oxford, 2004.

3 S.C. van der Slot, J. Duran, J. Luten, P.C.J. Kamer and P.W.N.M. van Leeuwen, *Organometallics*, 2002, **21**, 3873.

4 L.J. Farrugia, *J. Appl. Cryst*., 1999, **32**, 837.

5 G.M. Sheldrick, SHELXL97, Programme for the refinement of crystal structures, University of Göttingen, Germany, 1997.

6 Bruker, *SAINT*-Plus. Version 7.12 (including XPREP), Bruker AXS Inc., Madison, Wisconsin, USA, 2004.

7 Bruker, *SAINT*-Plus. Version 7.12 (including XPREP), Bruker AXS Inc., Madison, Wisconsin, USA, 2004.

8 K. Bradenburg, Diamond (Ver. 2. 1e), Crystal Impact GbR, Bonn, Germany, 2001.

9 M. Haumann, R. Meijboom, J.R. Moss and A. Roodt, *J. Chem. Soc., Dalton Trans*., 2004, 1679.

10 R. Meijboom, M. Haumann, A. Roodt and L. Damoense, *Helv. Chim. Acta*, 2005, **88**, 676.

11 L. Kirsten. "*MSc Thesis*", RAU, May 2005.

12 G.G. Summer, H.P. Klug and L.E. Alexander, *Acta Cryst*., 1964, **17**, 732.

13 K.A. Bunten, L. Chen, A.L. Fernandez and A.J. Pöe, *Coord. Chem. Rev*., 2002, **23**, 41.

14 P.N. Bungu and S. Otto, *Dalton Trans*., 2007, 2876.

15 J.D. Crane and N. Young, *Acta Cryst*, 2004, **E260**, m487.

16 R.G. Teller and R. Bau, *Struct. Bonding (Berlin)*, 1981, **44**,1

17 http://en.wikipedia.org/wiki/Berry_mechanism 14/12/2007.

18 D. Zhao and L. Brammer, *Inorg. Chem*., 1994, **33**, 5897.

19 B.T. Killbourn and H.M.J. Powell, J. *Chem. Soc*., 1970, 1688.

20 a) R.F. Heck and D.S. Breslow, *Chem., Ind. (London)*, 1960, 467. b) R.F. Heck and D.S. Breslow, *J. Am. Chem. Soc*., 1961, **83**, 4023.

21 J.S. Leigh and K.H. Whitmire, *Acta Cryst*., 1989, C**45**, 210.

22 R.C. Schnabel and D.M. Roddick, *Organometallics*., 1993, **12**, 704.

23 B.K Teo, A.P. Ginsberg and J.C. Calabrese, *J. Am. Chem. Soc*., 1976, **98**, 3027.

Chapter 5

Spectroscopic studies

5.1 Introduction

High pressure infrared (HP-IR) spectroscopy has been used for over 30 years in the study of homogeneous transition metal catalyzed reactions and to identify catalytic intermediates. The method is used for studying reactions under drastic conditions (*i.e.*, high pressure and high temperature). These conditions require a careful choice of the construction material and the design of the spectroscopic cell. The procedure is ideal for reactions which make use of the gas and liquid phase reactants. The reactants in the hydroformylation reaction are both in the liquid and gas phase. The design must be able to allow efficient transfer of the reactants from the gas phase to the liquid phase, because the reactants are in both the gas as well as the liquid phase[1]. The transfer rate can be maximized by the following:

1) Maximizing the interfacial area between the phases and
2) Increasing the rate of transport of the molecules across the interface.

The rate of transfer between the phases can be increased by stirring the contents in the reactor. Both stirred-tank and packed-column reactors are used in industrial hydroformylation.[1] The reactions make use of gases such as CO (carbon monoxide), H_2 (hydrogen) or CO/H_2 (syngas). The technique is useful for complexes which have transition metal complexes as intermediates in the catalytic reaction. HP-IR is also an important tool in monitoring the depletion and formation of organic reactants. This can be observed in chapter 6 where 1-octene is added and absorptions are seen at 1822 and 1640 cm^{-1}. As the depletion of 1-octene is observed the formation of the aldehyde can be observed by the absorption at 1734 cm^{-1}. Cobalt can plate out on vessel walls, and rhodium (and many other transition metal catalysts) can also react with metal surfaces. The following are some catalytic reactions which make use of the HP-IR spectroscopy:

- Alkene hydroformylation
- Methanol carbonylation
- Alkene methoxycarbonylation
- Alcohol homologation

These *in situ* studies will provide information on the dominant metal species, or the catalytic resting states. Most of the intermediate species in the catalytic reactions are very active and short lived; this makes it difficult for them to be observed under working catalytic conditions.

5.2 Cell design

The cells that are used in HP-IR need to exhibit high mechanical strength as well as resistance towards corrosion by solvents and reagents. HP-IR cells can be categorized into two types, based on their optical configuration, namely transmission cells and reflectance cells. A transmission cell uses IR transparent windows of high mechanical strength (*e.g*. CaF_2, ZnS) between which the sample solution is contained, such that the IR beam from a spectrometer can pass directly through the sample. High pressure transmission cells are regarded as more robust of the liquid cells; they are routinely used in many laboratories for the measurement of solution IR spectra under ambient conditions. In the reflectance cell the IR beam is directed through an IR-transmitting crystal which has a surface which is in contact with the sample solution. The system is arranged in such a way that one or more internal reflections of the IR beam occur at the interface of the crystal and sample.

5.2.1 Transmittance cells

The transmittance cells in HP-IR spectroscopy can be divided into two categories, namely (1) where the contents of the high pressure vessel are observed directly through the IR transparent windows (2) where the reaction solution is circulated from the autoclave to an auxiliary observation cell.

5.2.2 Amsterdam flow cell

This is a cell design developed by the group of van Leeuwen in Amsterdam, with the aim of monitoring relatively fast catalytic reactions[2,3] The design of the HP-IR spectroscopic cell is shown in Figure 5.1. The rotation of the stirrer blades is used to force the solution from the lower chamber of the reaction vessel through the spectroscopic cell and back into the upper chamber. The total volume of the autoclave is 50 cm^3, the volume of the liquid in the circulation loop is only 0.35 cm^3 and circulation velocities of 1.4-7.7 $cm^3\ s^{-1}$ can be achieved (with a 0.4 mm window spacing) Typical operating conditions with 2200 rpm stirring the reaction solution would reach the center of the IR BEAM 56 ms after leaving the main vessel, but at

a maximum stirring rate it could be lowered to 33 ms. During a catalytic reaction the total volume is kept low at 15 cm^3 this is to ensure efficient mixing between the upper and lower chamber of the main autoclave unit. The cell has been used together with rapid FTIR scanning, enabling the study of species which are present during the hydroformylation reaction using phosphite modified rhodium catalysis. It has also been employed in the investigation of elementary reaction steps in the hydroformylation mechanism, such as CO ligand dissociation and exchange between rhodium hydrides and H_2.[4,2]

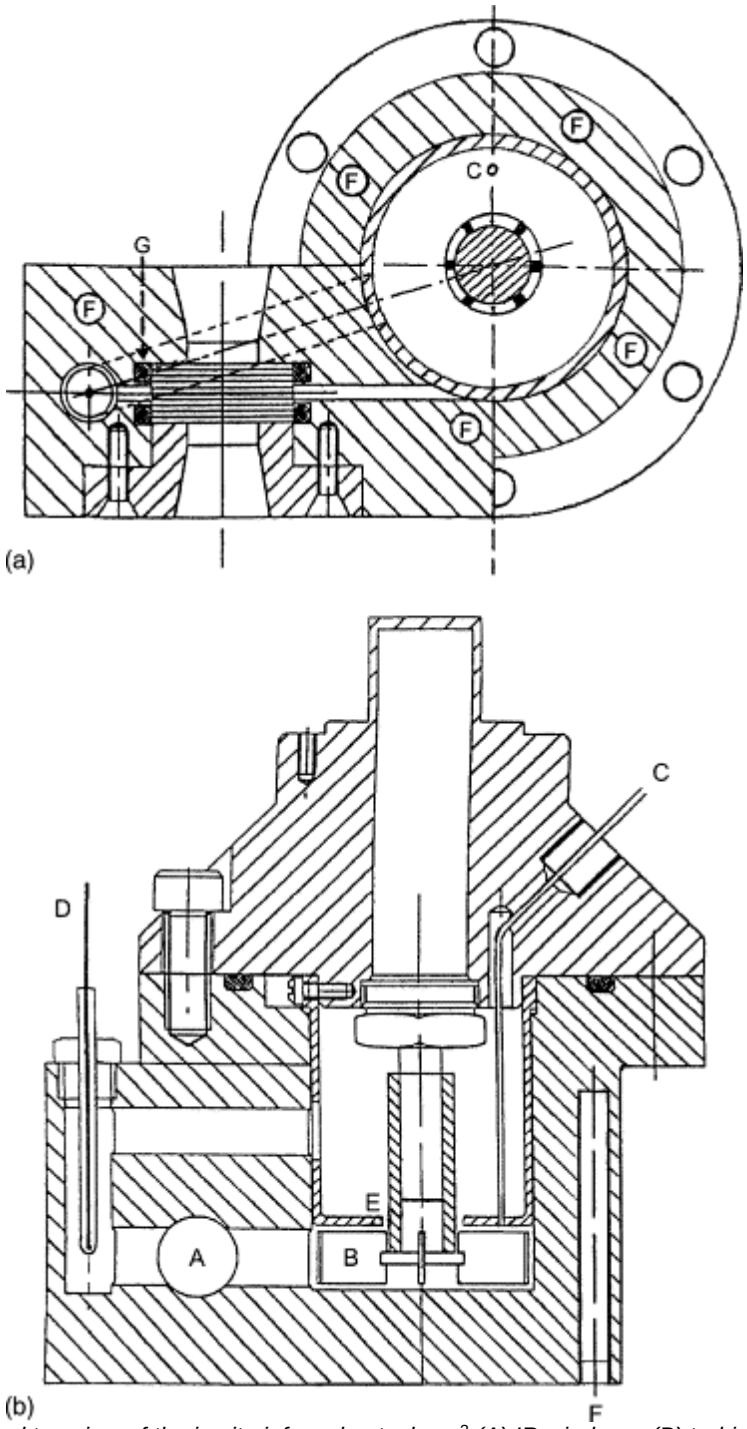

Figure 5.1 Side-and top view of the in situ infrared autoclave:[3] *(A) IR windows; (B) turbine rotor; (C) reagent addition; (D) thermocouple; (E) opening between upper and lower chamber; (F) electrical heaters; (G) Kalrez® O-rings.*

5.3 Chemistry based on synthesis gas

'Synthesis gas' (syngas) is a mixture of hydrogen and carbon monoxide gas.

The increase in the interest of using syn gas is as a result of having petroleum as a major industrial feedstock. Synthesis gas is already used in the making of linear aldehydes, alcohols, and their derivatives using hydroformylation. It is also used in the synthesis of methanol and from methanol the synthesis of acetic acid making use of the 'Monsanto[5] process' and with the modification of acetic acid, acetic anhydride is formed. In the presence of certain homogeneous transition-metal catalysts, alkenes react with synthesis gas CO/H_2 in a ratio 1:1 or 1:2 to produce aldehydes. In the presence of the dimeric species the hydrogen in syn gas splits it into two to generate the hydride species, which is the active catalyst.

$$\underset{\textbf{(1)}}{[Co_2(CO)_6L_2]} \xrightarrow[140\ ^\circ C]{H_2,\ CO} \underset{\textbf{(2)}}{2[HCo(CO)_3L]}$$

*Scheme 5.1: In situ HP-IR; Preformation of the monophosphite cobalt carbonyl hydride **2** from the dimeric species **1** in the presence of syngas under reaction conditions.*

5.4 Conclusion

The HP-IR has proven to be very useful because it could operate at these high pressures and temperatures. The technique has also enabled the identification of significant metal complexes in a catalytic reaction. It has also made it possible for the identification of the selectivity of these catalytic reactions. The cobalt phosphite reactions indicated that the temperature of the catalytic reaction was important in the formation of the cobalt phosphite catalyst. At 120ºC the catalyst had just started forming. Without the temperature reaching 140ºC the catalytic reaction did not proceed as expected. The reactant intermediates could also be identified, which meant that the reaction could be monitored. If anything went wrong it could be identified by the type of spectra that was seen. The HP-IR spectroscopy has proved to be a very important tool in homogeneous catalysis.

References

1 B.C. Gates., "*Catalytic Chemistry*", John Wiley and Sons, Inc. 1992.

2 P.C.J. Kamer, A. van Rooy, G.C. Schoemaker and P.W.N.M. van Leeuwen, *Coord. Chem. Rev.,* 2004, **248**, 2409.

3 S.C. van der Slot, P.C.J. Kamer, P.W.N.M. van Leeuwen, J.A. Iggo and B.T. Heaton, *Organometallics.,* 2001, **20**, 430.

4 S.C. van der Slot, J. Duran, J. Luten, P.C.J. Kamer and P.W.N.M. van Leeuwen, *Organometallics*., 2002, **21**, 3873.

5 C.M. Thomas and G. Sűss-Fink., *Coord. Chem. Rev*., 2003, **243**, 125.

Chapter 6
HP–IR spectroscopic investigations on aromatic cobalt phosphite: stability studies

6.1 HP–IR Spectroscopy

A brief introduction on HP-IR spectroscopy has been given in Chapter 5. This chapter will concentrate on the HP-IR experiments. The experiments will give reaction processes as they were being observed during hydroformylation. The experiments try to have a follow up and an understanding of the events occurring during hydroformylation. All details will be explained in this Chapter as the experiments are performed.

6.2 Introduction

In order to develop and optimize the capability of novel homogeneous catalyst systems it is essential that the nature of the interaction between metal complexes and organic reactants, substrates as well as potential feedstock poisons, be understood. A key part of this understanding lies in knowing how catalysts can be designed and how particular metal-ligand systems can activate hydrocarbon based feedstock (both functionalized and unfunctionalized) in a beneficial manner. The initial aim and objectives of this study was to understand the intimate relationship between phosphite modified cobalt complexes as catalyst models in hydroformylation reactions, with special emphasis on reaction mechanism and solution behavior. Due to the catalyst behaviour during hydroformylation by having a decrease in the spectra of the monophosphite cobalt carbonyl hydride $[HCo(CO)_3L]$ **(2)**, this indicated the importance of studying the stability of the hydride during hydroformylation. The study focused on cobalt complexes using aromatic phosphites as ligands in the hydroformylation of 1-octene.

Hydroformylation reactions which involve cobalt phosphite modified catalysts have a number of side reactions that can occur. The side reactions that can occur due to the phosphite ligands are hydrolysis, alcoholysis and *trans*–esterification.[1] Phosphine ligands compared to phosphite ligands tend to have more hydrogenation during hydroformylation.

This chapter concentrates on the hydroformylation of 1-octene using the different phosphite ligand systems $P(OPh)_3$ **(a)**, $P(O\text{-}4\text{-}^tBuC_6H_4)_3$ **(b)** and $P(O\text{-}2\text{-}EtC_6H_4)_3$ **(c).** The hydroformylation activity of the different cobalt carbonyl phosphite complexes will be described, particularly trying to establish the influence the different ligands have on the reaction rate of the catalytic cycle. Since phosphites have similar electronic properties, we will try to establish the influence the steric bulk of the phosphites have on the hydroformylation reaction. Stability involves thermal stability, hydrolysis, alcoholysis and stability towards the aldehydes.[2] The stability runs of all these hydrides in the absence of 1-octene were observed. The hydrides were used in the hydroformylation of 1-octene to determine the influence the hydride has on the reaction in regards to the formation of the aldehyde. The cobalt phosphite catalysts were preformed then tested in the hydroformylation reaction with 1-octene.

6.3 Process parameters

The following are the process parameters that were taken into consideration in order to have an effective and efficient catalytic hydroformylation cycle.

6.3.1 Temperature

A variety of reaction conditions were conducted before a decision was made to use the specific conditions used in this study. Hydroformylation reaction was attempted at [Co]/[L] = 8, [Co] = 1500 ppm, syngas H_2/CO ratio = 2:1 and a temperature of 120°C. The hydroformylation reaction was tried several times and was unsuccessful. It was realized that the reactor could only reach a temperature of 120ºC and could not reach the maximum temperature of 140ºC. When the reactor reached the maximum hydroformylation temperature of 140ºC, it was only then that the hydroformylation reaction proceeded consistently. The reason for this happening was that at 120ºC the monophosphite hydride was beginning to be formed and at 140ºC it was completely formed. In previous experiments using $P(OPh)_3$ **(a)** and $P(O\text{-}2,4\text{-}^tBu_2C_6H_3)_3$ **(d)** ligands it was discovered that the hydride starts forming at 120°C and is completely formed at 140°C.[3,4] It confirms why the hydroformylation reaction at the lower temperatures was not successful. All the hydroformylation reactions in this study were performed at 140ºC for all the ligands. At this temperature hydroformylation activity could be observed.

6.3.2 Syngas ratio and pressure

Syngas H_2/CO ratio of 2:1 and a pressure of 50 bar was used in the experiments[4] of $P(OPh)_3$ **(a)** and $P(O\text{-}2,4\text{-}^tBu_2C_6H_3)_3$ **(d)**. Under industrial hydroformylation conditions using modified cobalt catalysts, the aldehydes which were formed were converted to the corresponding aldehydes.[5] In the publication of $P(OPh)_3$ **(a)** and $P(O\text{-}2,4\text{-}^tBu_2C_6H_3)_3$ **(d)** it was reported that the aldehyde as well as the alkene were not hydrogenated. This was indicated by the small amount of hexanols that had formed (< 1%) and pentane (< 0.2 %) when using $[P(OPh)_3]/[Co] > 4$.[4] The overall linearity of the formation of the aldehydes was reasonably good when it was compared to other modified cobalt systems.[6,7,8] From the previous experiments it was observed that phosphites, unlike phosphines, did not produce a significant amount of hydrogenation products. It was therefore decided to use syngas H_2/CO of a 1:1 ratio. In the previous experiments the syngas pressure used was 50 bar. The pressure used for all the experiments was 50 bar. A minimum pressure of 25 bar can be used before cobalt plating occurs in complexes that use cobalt as a metal. The catalysts in homogeneous catalysis have a variety of ways[1] in which they can decompose: metal deposition occurs, which is the plating of the metal, the ligand can also decompose, there could also be reactions with impurities, the dimer can also be formed, and the metal center can also react with the ligand. When using a 1:1 ratio of H_2/CO the reaction rate is essentially independent of pressure[2] due to the opposing orders of H_2 and CO.

$$\frac{\delta(\text{Aldehyde})}{\delta t} = k[\text{alkene}][H_2][CO]^{-1}]$$

Pressure variation studies performed using $P(O\text{-}2,4\text{-}^tBuC_6H_4)_3$ **(d)** as a ligand revealed that at pressures between 50 - 60 bar no unmodified hydride[3] was formed.

6.3.3 Ligand to metal ratio

In previous experiments for $P(OPh)_3$ (a), (cone angle 128°) and $P(O\text{-}2,4\text{-}^tBu_2C_6H_3)_3$ (d), (cone angle 175º) it was discovered that the lowest [phosphite]/[Co] ratio required to prevent the formation of $[HCo(CO)_4]$ (5) was 4:1. At this ratio the bisphoshite hydride $[HCo(CO)_2\{P(OPh)_3\}_2]$ **(3a)** was formed. This hydride was found to be inactive in hydroformylation. All the experiments with $P(O\text{-}2,4\text{-}^tBu_2C_6H_3)_3$ **(d)** as ligand conducted with a minimum [phosphite]/[Co] ratio of 4:1 did not form the bisphosphite hydride. Even at a hundred equivalence no bisphosphite hydride was

formed when using P(O-2,4-^{t}Bu$_2$C$_6$H$_3$)$_3$ **(d)** as a ligand, this proved that the larger cone angle phosphite did prevent the formation of the bisphosphite hydride. This also initiated using intermediate ligands between 128º and 175º. This reason for the variation on the cone angles was to try and establish the smallest cone angle that would be able to prevent the formation of bisphosphite hydride [HCo(CO)$_2$L$_2$] **(3)**. It was also discovered that using a high [phosphite]/[Co] ratio formed the bisphosphite cobalt carbonyl hydride [HCO(CO)$_2$L$_2$] **(3)** which is presumed to be inactive in hydroformylation.[4]

For the stability runs using [HCo(CO)$_3${P(O-2,4-^{t}Bu$_2$C$_6$H$_3$)$_3$}] **(2d)**, it was observed that at a [L]/[M] ratio of 8:1 with a temperature of 140°C slight hydride decomposition was observed. When the [L]/[M] ratio was increased to 12:1 this resulted in a virtually stable system. From previous experiments which were performed by using the less bulky ligand[3] P(OPh)$_3$ **(a)** it was discovered that the bisphosphite hydride species occurred at higher ligand to metal ratios of 12:1. These hydride species proved to be inactive as hydroformylation catalysts[4] when compared to the monophosphite hydride complexes. Due to all the considerations it was then decided to use a [phosphite]/[Co] of 8:1. The decision was also based on the fact that the ligands being used are intermediate having cone angles between 128° and 175°.

A [L]/[Co] of 4 was sufficient to prevent the formation of the unmodified hydride [HCo(CO)$_4$] **(5)**, although under these conditions the bisphosphite hydride was formed but was immediately converted to the monophosphite hydride.[4] The [L]/[Co] in this study was 8, this would not exclude the possibility of having a conversion of the bisphosphite hydride to the monophosphite hydride. A semi batch process was used where the addition of 1-octene is done after an hour through the cannula after the formation of the hydride. The formation of the monophosphite hydride [HCo(CO)$_3$L] **(2)** was studied using L = P(OPh)$_3$ **(a)**, P(O-4-^{t}BuC$_6$H$_4$)$_3$ **(b)** or P(O-2-EtC$_6$H$_4$)$_3$ **(c)** at a ligand/metal ratio of 8, the cobalt concentration was kept constant at 1500 ppm throughout all of the experiments.

6.3.4 Cobalt concentration

The initial experiments for this study were performed at a [Co] = 1800 ppm. It was ultimately decided to use a [Co] = 1500 ppm so that the results can be correlated with the previous experiments which were performed for P(OPh)$_3$ **(a)** and P(O-2,4-^{t}Bu$_2$C$_6$H$_3$)$_3$ **(d)**. According to the results of the study of the sterically demanding

hydride no bisphosphite cobalt hydride was observed under the conditions were the cobalt concentration was 1000, 1400 and 1800 ppm.

6.3.5 1–alkene

Cobalt is a preferred metal for the hydroformylation of long chain alkenes. In the experiments for $P(OPh)_3$ **(a)** and $P(O\text{-}2,4\text{-}^tBu_2C_6H_3)_3$ **(d)**, 1-pentene was used as the alkene of choice. For this study 1-octene was used in order to try and understand the effect the different alkenes have on hydroformylation reactions. 1-octene is not volatile when compared to 1-pentene which is highly volatile and was therefore not used. The cobalt catalysts are preferred for the hydroformylation of long chain linear alkenes.[9]

6.3.6 Reaction solvent

In the experiments for $P(OPh)_3$ **(a)** and $P(O\text{-}2,4\text{-}^tBu_2C_6H_3)_3$ **(d)**, octane was used as a solvent. For this study octane could not be used as a solvent, because 1-octene was used as the 1-alkene. To exclude the possibility of having octane in solution it was decided to use dodecane. This would exclude the possibility of not being able to enable identification of the octane as a product that is from the reaction and not the solvent.

6.4 Experimental procedure

All the HP-IR experiments were carried out in a HP-IR autoclave with a control-box which was used to control and indicate the temperature while the pressure was controlled by a high pressure regulator. The HP-IR cell was obtained on loan from Sasol and a brief description is given in the previous Chapter. All spectra were collected with a resolution of 4 cm^{-1} with 32 scans.

All the experiments were performed under reaction conditions of syngas H_2/CO ratio 1:1, pressure of 50 bar. The solvent (dodecane, 12 ml) in the autoclave reactor was purged three times with syngas. Thereafter a background of the solvent was taken at room temperature. The cell was removed after venting, opened and the reagents added to the solvent. Choice of

6.4.1 HP–IR hydroformylation procedure

The same procedure for all experiments of HP-IR reactions was followed; therefore one representative procedure will be described.

Reaction conditions were as follows:

[Co] = 1500 ppm, [L]/[Co] = 8, pressure of 50 bar at a temperature of 140°C. $[Co_2(CO)_6\{P(O\text{-}4\text{-}^tBuC_6H_4)_3\}_2]$ **(1b)**; (0.142 g, 0.114 mmol) was dissolved in dodecane (12 ml) from the reactor and mixed with 8 eq of $P(O\text{-}4\text{-}^tBuC_6H_4)_3$ **(b)**; (0.765 g, 1.598 mmol). The solution was placed in the reactor. The solution was purged with syngas three times. The initial spectrum was recorded after stirring for about one minute at 25ºC and 50 bar. The formation of the hydride was monitored by taking spectra at temperature intervals from 25; 55; 90; 105; 10; 125; 135; until the temperature reaches 140ºC. At this stage the catalyst had been completely formed and 70 eq of 1-octene (2.51 ml, 15.988 mmol) was introduced into the reactor *via* cannula. The 1-octene was flushed with syngas and transferred into the solution in the reactor. The solution was stirred for a minute and spectra taken. The 1-octene absorbance was observed at 1640 and 1822 cm^{-1}. Spectra were taken after every 15 minutes over a period of 4 hours. At this stage the spectra shows a synchronized decrease of the 1-octene absorbance at 1639 and 1822 cm^{-1} and an increase of the formation of nonanal aldehyde at an absorbance of 1734 cm^{-1}.

6.5 Results and discussion

6.5.1 *In situ* HP–IR cobalt phosphite catalyst preforming

The preformed hydride $[HCo(CO)_3L]$ **(2)** is an important intermediate step in the hydroformylation reaction of 1-octene. The ν_{CO} absorbance at 1975, 1974 and 1984 cm^{-1} were used as indicators for the dimeric species $[Co_2(CO)_6\{P(OPh)_3\}_2]$ **(1a)**, $[Co_2(CO)_6\{P(O\text{-}4\text{-}^tBuC_6H_4)_3\}_2]$ **(1b)** and $[Co_2(CO)_6\{P(O\text{-}2\text{-}EtC_6H_4)_3\}_2]$ **(1c)** respectively (see Figure 6.1 and Chapter 3). The formation of all three monosubstituted hydrides **2a**, **2b** and **2c** were observed at 55ºC, 115ºC and 90ºC respectively in dodecane. At 140°C these hydrides had completely formed and showed absorbance peaks at 2071, 2021 and 2000 cm^{-1} (for **2a**), 2071, 2017 and 2002 cm^{-1} (for **2b**) and 2072, 2020 and 2000 cm^{-1} (for **2c**). Table 6.1 shows the formation of all the different hydrides under hydroformylation conditions and disappearance of the dimer and compared to those in literature.

Table 6.1: Results of High-Pressure IR Studies on the Formation of Monophosphite hydride in Dodecane.

Ligand (L)	Entry	L:M	Pressure (bar)	[a]T_{MH} (ºC)	[b]T_{BH} (ºC)	[c]T_{Dimer} (ºC)	[d]T_{UH} (ºC)	Solvent	Ref.
$P(OPh)_3$ **(a)**	1	8	50	55	125	135	105	dodecane	TW
$P(O\text{-}4\text{-}^tBuC_6H_4)_3$ **(b)**	2	8	50	115	115	125	n.d	dodecane	TW
$P(O\text{-}2\text{-}EtC_6H_4)_3$ **(c)**	3	8	50	90	105	135	55	dodecane	TW
$P(OPh)_3$ **(a)**	4	8	50	122	120	140	n.d	octane	4
$P(O\text{-}2,4\text{-}^tBu_2C_6H_4)_3$ **(d)**	5	8	50	105	none	125	n.d	octane	3

[a]Temperature where the monophosphite hydride first appeared; [b]Temperature where the bisphosphite hydride first appeared; [c]Temperature where the dimer disappeared; [d] Temperature where the unmodified hydride first appeared.

Table 6.1 gives the results obtained for the disappearance of the dimeric species during preformation of the hydrides compared with those in literature. The dimers had disappeared after reaching 135ºC for $P(OPh)_3$ **(a**) and $P(O\text{-}2\text{-}EtC_6H_4)_3$ **(c)**, for $P(O\text{-}4\text{-}^tBuC_6H_4)_3$ **(b)** it disappeared at 125ºC. The monophosphite hydride is stable in solution because it is seen appearing before the bisphoshite hydride but at 140ºC it is still in solution. The bisphosphite hydride has completely disappears at 140ºC and only the monophosphite carbonyl phosphite is in solution. The cone angles of $P(O\text{-}2\text{-}EtC_6H_4)_3$ **(c)**, for $P(O\text{-}4\text{-}^tBuC_6H_4)_3$ **(b)** are larger and have the bisphosphite hydride forming but at 140ºC it has completely disappeared.

The dimer disappearance for the ligands ranges between 125 to 135ºC and has completely disappeared at 140ºC. All these species including the ones in literature entry 4 and 5 show the importance of temperature on the formation of the monophosphite hydride $[HCo(CO)_3L]$ **(2)**.

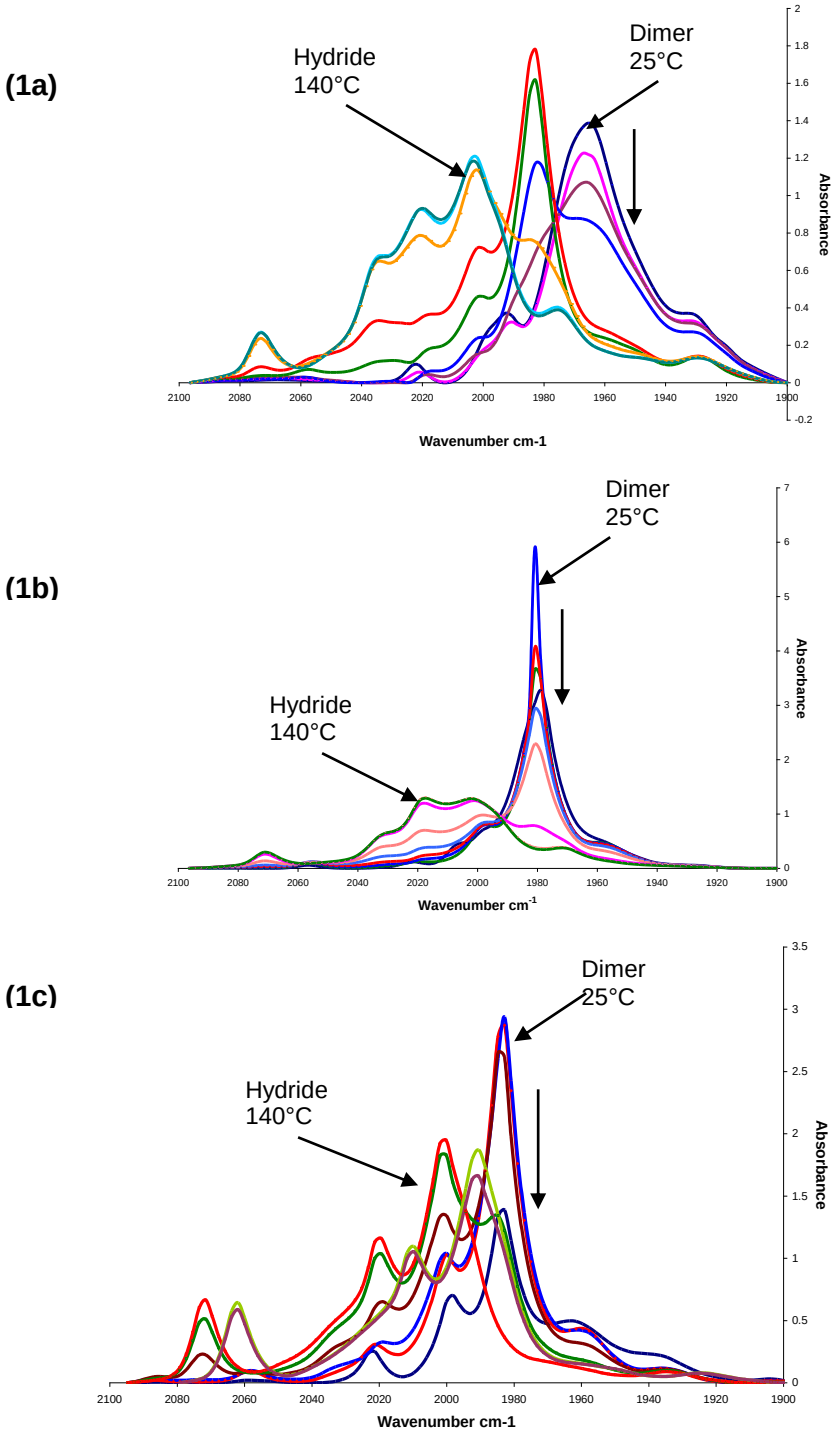

Figure 6.1: The hydrides ***(1a):*** *$[HCo(CO)_3\{P(OPh)_3\}]$* ***(2a)****,* ***(1b)****: $[HCo(CO)_3\{P(O\text{-}4\text{-}^tBuC_6H_4)_3\}]$* ***(2b)*** *and* ***(1c):*** *$[HCo(CO)_3P(O\text{-}2\text{-}EtC_6H_4)_3]$* ***(2c)*** *were formed In situ and used in the hydroformylation of 1-octene the was monitored using a rapid scan IR technique (32 scans) see Figure 6.2. These hydrides were formed in dodecane, [L]/[M] = 8; [Co] = 1500 ppm at 50 bar syngas 1:1 ratio: 25, 55, 90, 105, 115, 125, 135 and 140 ºC.*

These monophosphite cobalt carbonyl hydrides **2a**, **2b** and **2c** were used in the hydroformylation of 1-octene and will be discussed in the following section see Figure 6.2 (a), (b) and (c).

6.5.1.1 *In situ* HP–IR hydroformylation reactions

Figure 6.2 **(a)**, **(b)** and **(c)** shows the HP-IR spectra of the hydroformylation reaction using $P(OPh)_3$ **(a)**, $P(O\text{-}4\text{-}^tBuC_6H_4)_3$ **(b)** and $P(O\text{-}2\text{-}EtC_6H_4)_3$ **(c)** as ligands in the presence of 1-octene. For the hydroformylation reaction of 1-octene (see Figure 6.2) where $P(OPh)_3$ **(a)**, spectra were taken after every 10 minutes over a period of 4 hours, $P(O\text{-}4\text{-}^tBuC_6H_4)_3$ **(b)**, spectra were taken every 30 minutes over a period of 5 hours and $P(O\text{-}2\text{-}EtC_6H_4)_3$ **(c)**, spectra were taken every 15 minutes over a period of 4 hours representing the hydroformylation activity of the different systems using the different ligands as indicated.

Cleavage of the dinuclear complex to produce the hydride species with the formation of hydridocarbonyls of the type $[HM(CO)_3L]$ was only obtained under high CO/H_2 pressure and temperatures. The results indicate that the hydroformylation for $P(O\text{-}2\text{-}EtC_6H_4)_3$ **(c)** Figure 6.2**(c)** and 6.5**(c)** with the hydride which was preformed with 1-octene added immediately after preformation and with the cobalt carbonyl phosphite hydride which aged in solution before being used for hydroformylation of 1-octene are comparable. This would indicate that the hydride formed with the ligand with the larger cone angle is more stable compared to those of the smaller cone angles. The activity of the hydride of $P(OPh)_3$ **(a)** and $P(O\text{-}4\text{-}^tBuC_6H_4)_3$ **(b)** gave much lower conversion with the hydride which was allowed to stay longer in solution. It would not *exclude* the fact that the hydrides of these two ligands were destroyed significantly over a period of time much more than the hydride of $P(O\text{-}2\text{-}EtC_6H_4)_3$ **(c)**. When the hydride was left in solution for a couple of hours before addition of the 1-alkene, the hydride was aged although there was some active hydride in the solution. $P(OPh)_3$ (a) is the only one with a small cone angle of 128º and $P(O\text{-}4\text{-}^tBuC_6H_4)_3$ **(b)** has a cone angle of 175.4º.

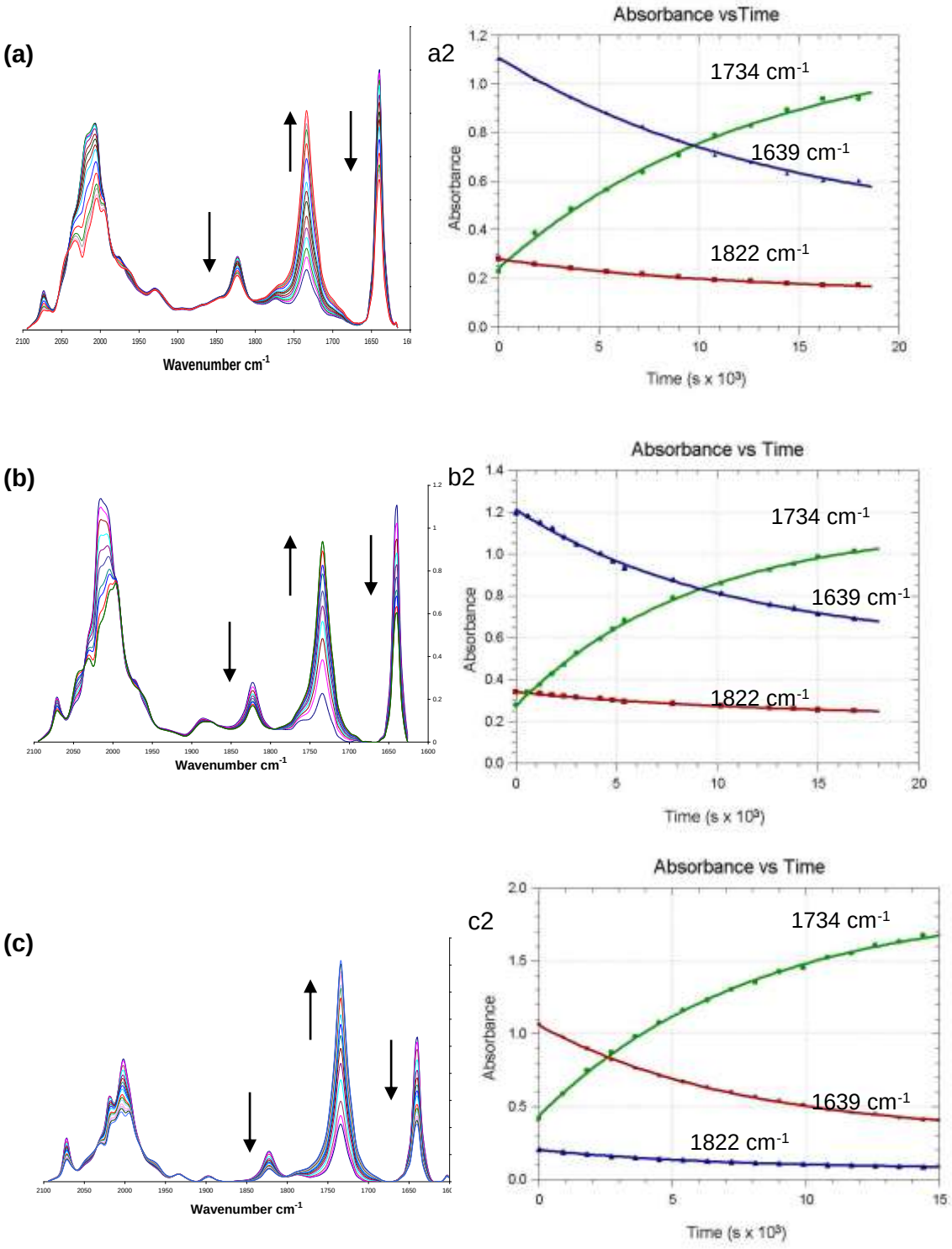

Figure 6.2: HP-IR spectrum of hydroformylation of 1-octene using $P(OPh)_3$ ***(a),*** *$P(O\text{-}4\text{-}^tBuC_6H_4)_3$* ***(b),*** *and $P(O\text{-}2\text{-}EtC_6H_4)_3$* ***(c)*** *as ligands, a2, b2 and c2 are the corresponding kinetic plots of the hydroformylation see Table 6.2. The hydroformylation of 1-octene was at 140° in dodecane. [Co] = 1500 ppm, [L]/[Co] 8:1, pressure = 50 bar Syngas H_2/CO = 1:1. [1-octene]/[Co] = 70.*

Kinetics

According to the spectra there is an indication of hydroformylation activity see Figure 6.2 **(a)**, **(b)** and **(c)**. There is a clear indication that all the different ligands **a**, **b** and **c** had a decrease in the absorbance of 1-octene indicated by 1639 and 1822 cm^{-1}. There is a subsequent increase of the absorbance of the aldehyde at 1739 cm^{-1}. The same behaviour was observed in the previous study of $P(OPh)_3$ **(a)**, and $P(O\text{-}2,4\text{-}^tBu_2C_6H_3)_3$ **(d)**, in the hydroformylation of 1-pentene.[3,4] The hydride formed by using $P(O\text{-}2,4\text{-}^tBu_2C_6H_3)_3$ **(d)** as a ligand was very stable and there was no change in the spectra of the hydride in the area (1900 -2100 cm^{-1}). When $P(OPh)_3$ **(a)**, $P(O\text{-}4\text{-}^tBuC_6H_4)_3$ **(b)**, and $P(O\text{-}2\text{-}EtC_6H_4)_3$ **(c)** were used as ligands, a change in absorbance (a decrease) was observed in the carbonyl region of the hydride. This led to the further studying of the hydride and its activity in hydroformylation.

Following the decrease of the alkene absorption at 1639 cm^{-1} over time revealed linear rate dependence with the concentration of 1-octene. Assuming the absorption in the mixture to be linear with concentration, the observed rate constant for 1-octene conversion was obtained according to the *pseudo* first order rate law (equation 6.1).[2,3,4] (see Appendix D).

$$\frac{\delta[\text{1-octene}]}{\delta t} = k_{obs}[\text{1-octene}] = k_{obs}[\text{aldehyde}] \qquad \textbf{(6.1)}$$

The results of these HP-IR hydroformylation experiments are compiled in Table 6.2. The results are derived from the kinetic plots from Figure 6.2a2, b2 and 2c.

Table 6.2: Observed rate constants of the formation of the aldehyde and depletion of the 1-alkene for the different ligands.

Ligand	1734 cm^{-1} k_{obs} s^{-1}, x10^4	1639 cm^{-1} k_{obs} s^{-1}, x10^4	1822 cm^{-1} $k_{obs}s^{-1}$, x10^4	Alkene	Reference:
$P(OPh)_3$ **(a)**	1.13(4)	0.95(5)	0.8(3)	1-octene	TW
$P(O\text{-}4\text{-}^tBuC_6H_4)_3$ **(b)**	0.79(6)	0.71(8)	0.9(4)	1-octene	TW
$P(O\text{-}2\text{-}EtC_6H_4)_3$ **(c)**	1.31(3)	1.36(6)	1.6(3)	1-octene	TW
$P(O\text{-}2,4\text{-}^tBu_2C_6H_3)_3$ **(d)**	7.3(4)	—	—	1-pentene	3
$P(OPh)_3$ **(a)**	1.7	—	—	1-pentene	3

The absorption at 1822 cm^{-1} is unique for terminal alkenes. Therefore, the k_{obs} value obtained for the absorption at 1822 cm^{-1} is the value for the consumption of 1-octene in the system. The 1-octene can be hydroformylated to the desired aldehyde, isomerised to internal octenes and hydrogenated to octane. GC analysis of end-of-

run samples could not verify known percentage of products which were formed and to be able to verify if there were any side reactions. The k_{obs} value obtained for the absorption at 1734 cm^{-1} accounts for aldehyde synthesised in the system, which is a combination of both the linear and branched aldehydes. The results in Table 6.2 for the observed rate constant for the formation of the aldehyde indicate the following trend $P(O\text{-}2\text{-}EtC_6H_4)_3$ > $P(OPh)_3$ > $P(O\text{-}4\text{-}^tBuC_6H_4)_3$ reaction rate. The k_{obs} value obtained for the 1639 cm^{-1} and the values obtained for the 1822 cm^{-1} and 1734 cm^{-1} absorptions are all similar, within experimental error and given in Table 6.2. From the observation that the k_{obs} values for the three absorptions are within experimental error, for each phosphite, we can conclude that no *significant* isomerisation of the 1-octene occurred. In addition, significant hydrogenation of either the 1-octene or the aldehyde product is unlikely as this would result in differences in the calculated k_{obs} values.

Table 6.3: Values of A_∞ and conversion:

Ligand	A_∞, 1639 cm^{-1}	% Conversion A_∞/A_0
$P(OPh)_3$ **(a)**	0.56	54
$P(O\text{-}4\text{-}^tBuC_6H_4)_3$ **(b)**	0.38	66
$P(O\text{-}2\text{-}EtC_6H_4)_3$ **(c)**	0.31	71

It can be seen from table 6.3 that there was significant conversion of the 1-octene to the aldehyde taken from Figure 6.2 (a), (b) and (c) of the hydroformylation of 1-octene. The percentage conversion indicates that the ligand with a larger cone angle **1c** had a better conversion. There is a definite trend $P(OPh)_3$ **(a)** < $P(O\text{-}4\text{-}^tBuC_6H_4)_3$ **(b)** < $P(O\text{-}2\text{-}EtC_6H_4)_3$ **(c)**. The reactions did not reach completion. The percentage conversion from 1-octene to the formation of the aldehyde is 54% for $P(OPh)_3$ **(a),** 66% for $P(O\text{-}4\text{-}^tBuC_6H_4)_3$ **(b)** and 71% for $P(O\text{-}2\text{-}EtC_6H_4)_3$ **(c).**

Figure 6.3 shows the changes in the carbonyl region during hydroformylation of 1-octene in the hydride region (1900 – 2100 cm^{-1}).

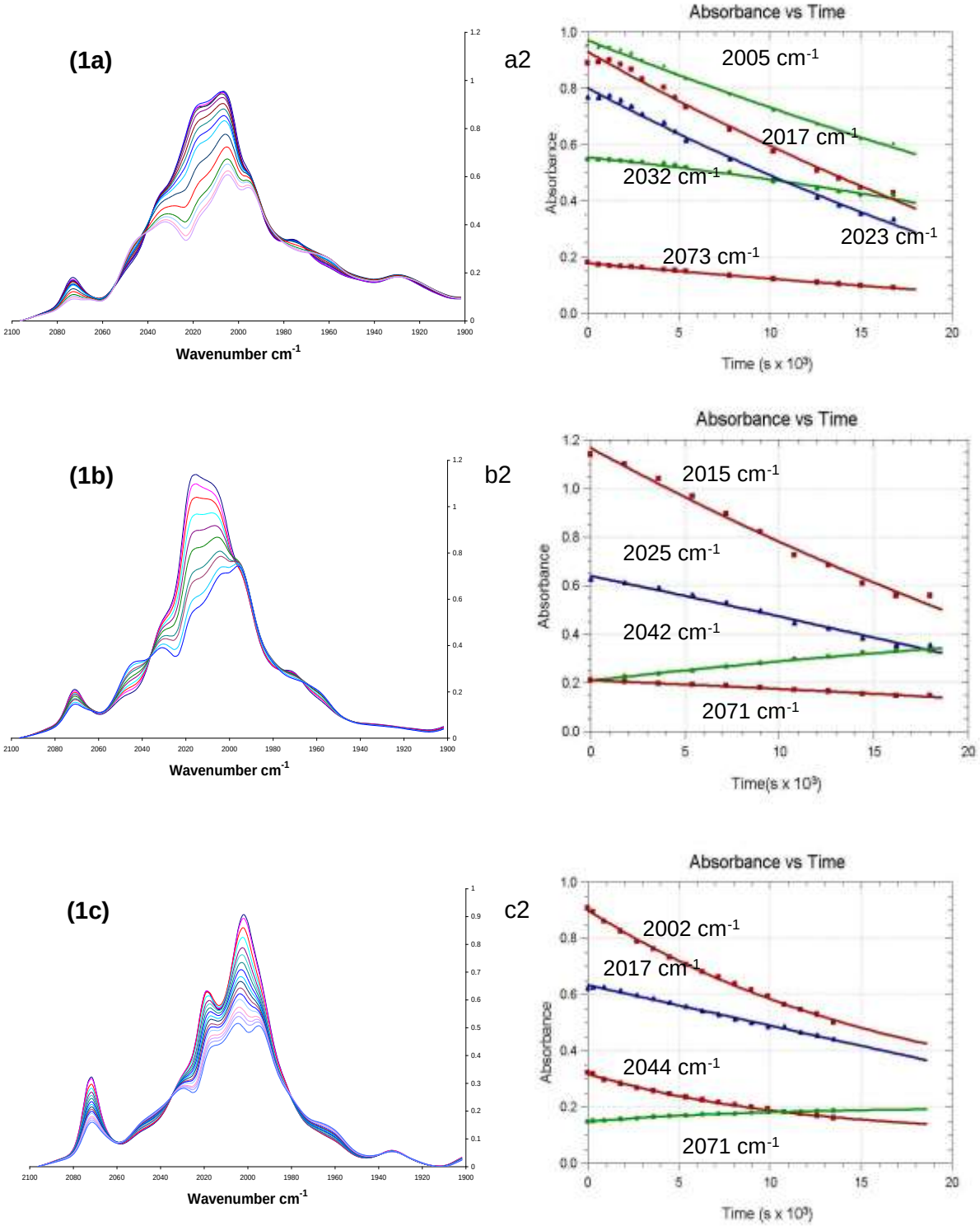

Figure 6.3: Changes in IR spectra of $[HCo(CO)_3\{P(OPh)_3\}]$ ***(1a)*** *, $[HCo(CO)_3\{P(O\text{-}4\text{-}^tBuC_6H_4)_3\}]$* ***(1b)*** *and $[HCo(CO)_3\{P(O\text{-}2\text{-}EtC_6H_4)_3\}]$* ***(1c)*** *during the hydroformylation of 1-octene see same spectra as in Figure 6.2(a), (b) and (c)****,*** *a2, b2 and c2 are the corresponding kinetic plots of the changes in the carbonyl region where the hydrides absorb (1900 – 2100* cm^{-1}) see k_{obs} results in Table 6.3.

In Figure 6.3, **(1a)**, **(1b)** and **(1c)** are the spectra representing the hydrides **2a**, **2b** and **2c** respectively in the carbonyl region during the hydroformylation of 1-octene; the results were fitted on a kinetic plot assuming a first order rate constant. The kinetic plots gave some values of the rate of formation which were negative. This would not exclude the formation of cobalt carbonyl species during hydroformylation. When compared to the values of the rate of formation results from hydroformylation, those in the hydride absorption carbonyl region were much lower. Therefore it can not be excluded that the hydroformylation reaction was much faster than the rate of what was happening in the carbonyl region where the hydride absorbs.

6.6 Qualitative observation

The unmodified hydride exhibits a strong absorbance at 2034 cm^{-1}, since the absorbance is close to the 2022 cm^{-1} band of the modified hydride can appear either as a shoulder or peak at large concentrations. The small peak at 2053 cm^{-1}, however, suggests that small amounts of unmodified hydride do in fact form under these conditions. In Figure 6.2**(a)**, 6.2**(b)** and 6.2**(c)** shown is the HP-IR spectra of the hydroformylation reaction using $P(OPh)_3$ **(a)**, $P(O\text{-}4\text{-}^tBuC_6H_4)_3$ **(b)** and $P(O\text{-}2\text{-}EtC_6H_4)_3$ **(c)** as ligands in the presence of 1-octene.The hydroformylation of 1-octene was studied for the different ligands using similar reaction conditions. For the hydroformylation reaction of 1-octene where $P(OPh)_3$ **(a)**, spectra was taken after every 10 minutes over a period of 4 hours, $P(O\text{-}4\text{-}^tBuC_6H_4)_3$ **(b)**, spectra was taken every 30 minutes over a period of 5 hrs and $P(O\text{-}2\text{-}EtC_6H_4)_3$ **(c)**, spectra was taken every 15 minutes over a period of 4 hours representing the hydroformylation activity of the different systems using the different ligands as indicated. Repeated scans indicated that the monophosphite cobalt modified hydride was indeed an active hydroformylation catalyst for all the phosphites in the carbonyl region. Hydroformylation activity was observed by observing an increase of the absorption at 1734 cm^{-1}, indicative of aldehyde formation, was observed see Figure 6.2 **(a)**, **(b)** and **(c)**. A decrease in the absorptions at 1639 cm^{-1} and 1822 cm^{-1}, indicative of depletion of 1-alkene, was observed concurrently with the increase of the 1734 cm^{-1} absorbance. During the hydroformylation reaction, the IR spectrum where the cobalt phosphite hydride absorbs in the region 1900 to 2100 cm^{-1}, a change in the spectra was observed for all the hydrides. No other absorptions in the carbonyl region (other than aldehyde absorption) were observed, Figure 6.2.(a), 6.2.(b), 6.2.(c) shows the overlay of selected IR spectra of typical runs of the hydroformylation of 1-octene and

Figure 6.2.a2, 6.2.b2, 6.2.c2 shows the kinetic plots of the increase of the formation of the aldehyde at 1734 cm^{-1} absorption and the depletion of the 1-octene at 1639 and 1822 cm^{-1} absorptions over time. There was no indication of side reactions or products. No bridging carbonyls were observed to form.

6.6.1 Changes in carbonyl region

From the above described experiments we observed some changes in the region where the cobalt carbonyl hydrides absorb (1900 – 2100 cm^{-1}). It was reported previously that there are changes in the carbonyl region of the $P(OPh)_3$ **(a)** systems[4] indicating a shift from the mono-phosphite species to the bis-phosphite. In contrast, previously reported experiments using $P(O\text{-}2,4\text{-}^tBu_2C_6H_3)_3$ **(d)**,[3] showed no changes in the same region. During the process of hydroformylation the hydride in the carbonyl region was not stable. Repeated scans showed a shift of the spectra of the hydride.

The changes in the carbonyl region are depicted in Figure 6.2.**(2a)**, 6.2.**(2b)** and 6.2.**(2c)** along with a first-order fit of these changes at various wavenumbers (6.2.a2, b2 and.c2). A first order behaviour is not necessarily what is being observed here. From the results in Table 6.2 it is clear that changes in the carbonyl region are approximately an order of magnitude slower than the observed hydroformylation reaction.

We concluded above that no significant internalisation or hydrogenation occurred, however a minor amount of these reactions would not induce a large effect on the observed rate constants of hydroformylation. This does not imply that these reactions do not occur at all! The changes in the carbonyl region are an order of magnitude slower, so it is possible that, when these side reactions occur at this rate, we observe the reaction of these products with the cobalt species. Minor amounts of internal alkenes can be formed. Hydroformylation of internal alkenes is significantly slower than hydroformylation of terminal alkenes,[10] and cannot be discarded as reason for the changes in the carbonyl region. The negative k_{obs} values, which were obtained, could indicate the possibility of the acyl and alkyl carbonyl species being formed. A number of different reactions could occur with the cobalt-hydride species as the follows:

1. mono-to-bis phosphite hydride

Conversion of the cobalt precursor to an active catalyst is an important part of the hydroformylation reaction.[11]

The peak assignments to the different cobalt hydride species were based on literature values.[3,4] It was observed that with a [L]/[Co] of 4 it was sufficient to prevent the formation of the unmodified hydride [$HCo(CO)_4$], although under these conditions the bisphosphite hydride with absorbance at 2034, 1990 and 1872 cm^{-1} was formed but was immediately converted to the monophosphite hydride at the absorbance of 2071, 2021 and 2001 cm^{-1} as was indicated by the decrease at 2034 cm^{-1}. The monophosphite hydride of [$HCo(CO)_3\{P(O\text{-}2,4\text{-}^tBu_2C_6H_4)_3\}$] **(2d)** having strong IR absorbance at 2071, 2021 and 200 cm^{-1}, it formed independent of Co concentration or ligand excess. No unmodified hydride or bisphosphite hydride was observed during these experiments.[3]

During synthesis of the monophosphite hydride the absorbance of [$HCo(CO)_3\{P(OPh)_3\}$] **(2a)**, [$HCo(CO)_3\{P(O\text{-}4\text{-}^tBuC_6H_4)_3\}$] **(2b)** and [$HCo(CO)_3\{P(O\text{-}2\text{-}EtC_6H_4)_3\}$] **(2c)** were observed at 2071, 2017 and 2002 cm^{-1} and 2074, 2023 and 2001 cm^{-1} respectively. The bisphosphite hydride had IR absorbance at 2034, 1995 and 1975 cm^{-1} and 2034, 1995 and 1970 cm^{-1} respectively see section 3.5(a - d). The cobalt monophosphite hydrides [$HCo(CO)_3\{P(OPh)_3\}$] **(2a)**, [$HCo(CO)_3\{P(O\text{-}4\text{-}^tBuC_6H_4)_3\}$] **(2b)** and [$HCo(CO)_3\{P(O\text{-}2\text{-}EtC_6H_4)_3\}$] **(2c)** indicated by absorbance at 2071, 2021 and 2000 cm^{-1}; 2071, 2017 and 2002 cm^{-1} and 2072, 2020 and 2000 cm^{-1} respectively were preformed by HP-IR spectroscopy. The monosubstituted hydrides started forming at 55ºC, 115ºC and 90ºC in dodecane, they had completely formed by the time the temperature reached 140ºC (see Fig. 6.1). In Table 6.1 is a summary of the results which were obtained during the preformation of the hydrides. The bisphosphite hydride for [$HCo(CO)_2\{P(OPh)_3\}_2$] **(3a)**, [$HCo(CO)_2\{P(O\text{-}4\text{-}^tBuC_6H_4)_3\}_2$] **(3b)** and [$HCo(CO)_2\{P(O\text{-}2\text{-}EtC_6H_4)_3\}_2$] **(3c)** at the temperature of 125, 105 and 115ºC was observed. It was immediately converted to the monophosphite hydride and had completely disappeared at 140ºC see Scheme 6.1. The ν_{CO} absorbance at 1975, 1980 and 1984 cm^{-1} were used as indicators for the dimeric species [$Co_2(CO)_6\{P(OPh)_3\}_2$] **(a)**, [$Co_2(CO)_6\{P(O\text{-}4\text{-}^tBuC_6H_4)_3\}_2$] **(b)** and [$Co_2(CO)_6\{P(O\text{-}2\text{-}EtC_6H_4)_3\}_2$] **(c)** which had completely disappeared at 140ºC.

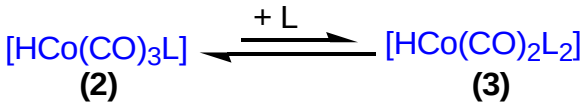

Scheme 6.1: Representation of equilibrium between the monophosphite and bisphosphite hydride

In section 6.7 the catalytic cycle explains the equilibrium between the monophosphite **(3)** hydride and the bisphosphite hydride **(2).** The monophosphite hydride and the bisphosphite hydride were seen during the hydroformylation reaction. According to the Heck and Breslow[12,13] catalytic cycle the monophosphite hydride formation is the most important step. The monophosphite hydride is the active catalyst in the hydroformylation cycle.[3,4] The monophosphite cobalt carbonyl hydride $[HCo(CO)_3L]$ **(2)** is active catalyst which converts 1-octene to the aldehyde.

2. Reaction of the hydride with 1-alkene

Intra molecular insertion of a hydride to an alkene is an obligatory step in the hydroformylation catalytic cycle. The microscopic reverse, β-hydride elimination is the most important mechanism for metal alkyl decomposition and for metal-catalyzed alkene isomerisation. The hydride, the metal and the alkene must all become coplanar; the addition is cis and has a four-centered transition state with the centroid of the alkene. The catalysts function in a catalytic cycle of reactions that consumes the reactants and regenerates the catalytic species is to be active in the production of selective products. The first step in a catalytic cycle is the coordination of the alkene to the cobalt phosphite hydride.[14] The coordination of the 1-alkene to the hydride can be rationalized by using the Heck and Breslow mechanism.[12] The addition of 1-octene to the reaction with an absorbance at 1639 and 1822 cm^{-1} was observed. The absorbance of the 1-octene decreased in a synchronized manner as the aldehyde was being formed at 1740 cm^{-1}. The actual π-complex could not be observed but the synchronized decrease of 1-alkene and the increase of the aldehyde formation revealed that the reaction was happening. Figure 6.2 **(a)**, **(b)**, and **(c)** also show the catalytic performance of the catalyst. The hydroformylation reaction would only occur if the alkene was coordinated to the hydride.

3. Reaction of the hydride with aldehyde

Aldehyde production occurs *via* a reaction sequence involving a monohydride precursor that ultimately yields a metal acyl intermediate which in turn eliminates the aldehyde after addition of H_2. Examples of cobalt acyl and alkyl resting states have

been isolated.[15] According to the Heck and Breslow catalytic cycle the hydride in the does not take part in the catalytic cycle. After the addition of hydrogen to the acyl species the aldehyde is formed and the regeneration of the monophosphite hydride which is returned to the catalytic cycle.

4. Reaction of the hydride with internal alkenes

The 1-alkenes have a much higher activity than the internal alkenes. The reaction may be a thousand times faster. Reactions of internal alkenes in hydroformylation have slower rates of reactions.[10] The k_{obs} values for the decrease of the 1-octene was similar with the other k_{obs} values for the synthesis of the aldehyde, this would not *exclude* the fact that no internal alkenes were formed. The k_{obs} values were all within experimental values. If the hydride had any reaction with the internal alkenes the conversion of 1-octene to the aldehyde would be lower.

5. Reaction of the hydride with alcohols

The hydrogenation of the aldehyde could be excluded because from the previous study of the $P(OPh)_3$ **(a)** the formation of alcohols was insignificant. Also from the same reasoning as the internal alkenes no hydrogenation is a possibility. With no hydrogenation the hydride can not react with the alcohols.

6. Decomposition in the hydroformylation reaction

Homogeneous catalysis can have different types of decompositions. There can be metal decomposition, ligand decomposition, reaction with impurities, dimer formation and reaction of the metal center with the ligand.[1] Metal deposition in homogeneous hydroformylation reactions has been the main reason for the deactivation of the catalyst. Metal plating is easier to observe than the ligand decomposition. Metal plating is the main reason for the loss of the cobalt phosphite hydride. If there is any cobalt plating the reaction will not proceed because the hydroformylation reaction depends on the monophosphite hydride $[HCo(CO)_3L]$ **(2)** for the reaction to be able to complete the catalytic cycle. With the hydroformylation of all these phosphite ligands which were used **(a)**, **(b)** and **(c)** no cobalt plating was observed.

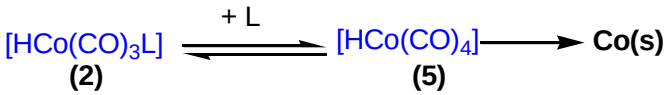

*Scheme 6.2: Representation of equilibrium between the monophosphite **(2)** and unmodified hydride **(5)** and eventually the deposition of the cobalt metal*

Catalytic processes rely a lot on the presence of the ligand for their selectivity and activity. If the ligand is lost by decomposition the catalytic reason will not be able to continue. There are a variety of side reactions that can occur, during hydrogenation the alkene can be hydrogenated to the alkane and this would prevent the reaction from continuing If decomposition is due to the formation of the dimer and there is an equilibrium the reaction will still proceed there will only be a reduction in the amount of hydride present. None of these reactions were observed during hydroformylation.

7. Alkyl and acyl species.

Alkyl and acyl species have been isolated under hydroformylation conditions. Although they are generally not seen easily because their reactions are fast and they do not have arresting state. Table 6.4 gives a few examples from some publications.

Table 6.4: Alkyl and acyl complexes

Complex	Alkyl IR ν_{CO} (cm^{-1})	Acyl IR νCO (cm^{-1})	Reference
$[CH_3CH_2CH_2Co(CO)_3(PBu_3)]$	2027(w), 1970(w), 1948(vs)		16
$[CH_3CH_2CH_2C(O)Co(CO)_3(PBu_3)]$		2041(w), 1971(s), 1950(vs), 1680(m)	16
$[(CH_3)_2CHC(O)Co(CO)_3(PBu_3)]$		1968(s), 1949(vs), 1678(m)	16
$[CH_3C(O)Co(CO)_3PPh_3]$		1680(w)	17
$[CH_3C(O)Co(CO)_3PPh_3]$ terminal		2048, 1979, 1958	17

^{vs}very strong, ^{s}strong, ^{m}medium, ^{w}weak

From Table 6.4, there is weak absorption spectrum at 2041. According to Figure 6.3 there is a weak IR spectrum for **b** and **c** at 2042 cm^{-1} indicating the presence of the acyl species. This peak can not be seen for $P(OPh)_3$. These experiments have shown that the alky and acyl species are intermediates in the hydroformylation catalytic cycle. The peak at 2042 cm^{-1} did not come out as strong peaks. The acyl species is not arresting state and is quickly converted to the aldehyde after addition of H_2 and regeneration of the hydride occurs.

In order to exclude some of the above explanations for the decreasing spectra in the hydride absorption carbonyl region, we repeated the experiment *without* 1-octene.

The experiment was performed in order to gain additional insight into the behaviour of the system and to exclude some of the above mentioned possibilities.

6.7 Stability runs of the modified hydride species

In order to obtain more information on the catalytic activity of the modified hydrides, were performed a number of hydride stability runs at syngas H_2/CO = 1 with a pressure of 50 bar and temperature of 140ºC. The ligand to cobalt ratio was kept constant at 8 for all the reactions in the study. These experiments were performed in paraffin (dodecane) as a solvent. In these experiments, the cobalt concentration was 1500 ppm, to enable correlation with previous experiments. After preformation of the modified hydride at the desired temperature and a starting temperature of approximately 25ºC, the hydride was allowed to form at 140ºC.

After preformation of the monophosphite hydride [$HCo(CO)_3L$] **(2)** the, 1-octene was not added as for the hydroformylation reaction. The hydride was allowed to age in solution as reported in Figure 6.4. The hydrides were allowed to be in the reactor for 1 hour for [$HCo(CO)_3\{P(OPh)_3\}$] **(2a)**, 1 hours [$HCo(CO)_3\{P(O\text{-}4\text{-}^tBuC_6H_4)_3\}$] **(2b)** and 2 hours for [$HCo(CO)_3\{P(O\text{-}2\text{-}EtC_6H_4)_3\}$] **(2c)** all at 140ºC, spectra were taken after every ten minutes see (Figure 6.4).

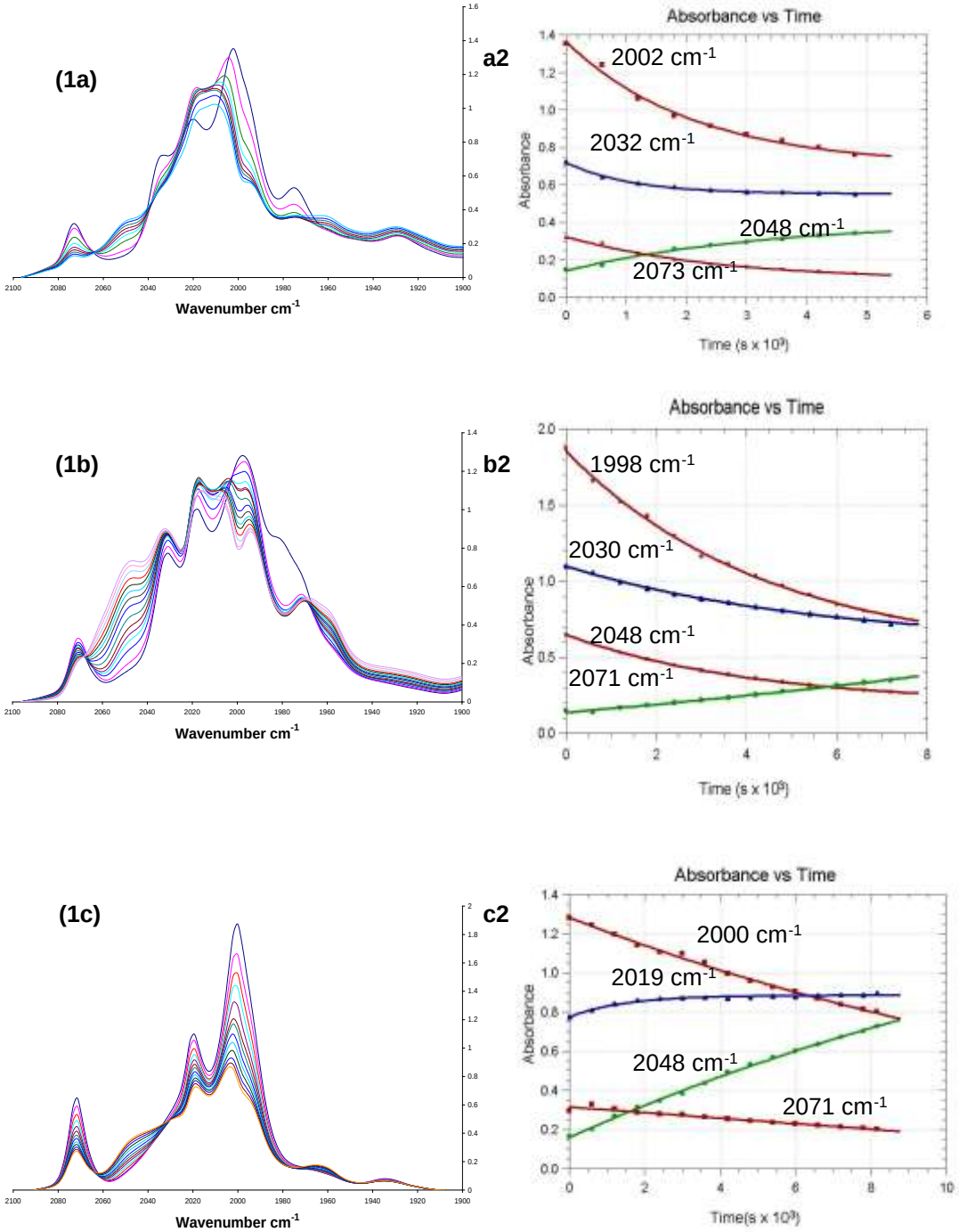

Figure 6.4: HP-IR spectrum of the hydrides without 1-octene of $[HCo(CO)_3\{P(OPh)_3\}]$ ***(1a)*** *for 1 hour, $[HCo(CO)_3\{P(O\text{-}4\text{-}^tBuC_6H_4)_3\}]$* ***(1b)*** *for 1 hour and $[HCo(CO)_3\{P(O\text{-}2\text{-}EtC_6H_4)_3\}]$* ***(1c)*** *for 2 hours at 140 °C, spectra was taken after every 10 minutes; a2, b2 and c2 are the kinetic plot of hydrides. [Co] = 1500 ppm, [L]/[Co] 8:1, pressure = 50 bar Syngas H_2/CO = 1:1.*

In Figure 6.4, $[HCo(CO)_3\{P(OPh)_3\}]$ **(1a)**, $[HCo(CO)_3\{P(O\text{-}4\text{-}^tBuC_6H_4)_3\}]$ **(1b)** and $[HCo(CO)_3\{P(O\text{-}2\text{-}EtC_6H_4)_3\}]$ **(1c)** the monophosphite hydride had completely formed at 140ºC. After its formation it was allowed to stir for a further 1 hour for $P(OPh)_3$ **(a)**, and $P(O\text{-}4\text{-}^tBuC_6H_4)_3$ **(b)** and 2 hours for $P(O\text{-}2\text{-}EtC_6H_4)_3$ **(c)** at 140ºC. The absorbance spectra were taken after every 10 minutes for all the species. The data was fitted to a first order rate constant to be able to obtain the kinetic plots. The reason for doing this was to try and observe the changes in the carbonyl region. As can be observed from the changes in the carbonyl region in Figure 6.2 and Figure 6.3, the only spectra which do not show any significant change are for the $P(O\text{-}2\text{-}EtC_6H_4)_3$ **(c).** The hydroformylation activity of monophosphite hydride kept in solution at 140ºC and 50 bar syngas over varying periods between 1 hr and 2 hrs was observed in this experiment. This was done in order to study the hydroformylation with the decomposed catalysts from the stability runs.

6.8 Kinetics

Table 6.5: Results from the hydroformylation of hydride in stability run and without stability run.

Ligand	[a]k_{obs} s^{-1}, 1734 cm^{-1} (10^4)	[b]k_{obs} s^{-1}, 1734 cm^{-1} (10^4)
$P(OPh)_3$ **(a)**	1.13(4)	3.7(6)
$P(O\text{-}4\text{-}^tBuC_6H_4)_3$ **(b)**	0.79(6)	0.30(4)
$P(O\text{-}2\text{-}EtC_6H_4)_3$ **(c)**	1.31(3)	1.85(8)

[a]Results from hydroformylation: see figure 6.2, **(a)**, **(b)** and **(c);** [b]Results from hydroformylation: see figure 6.5, **(a)**, **(b)** and **(c)**

From the results of hydroformylation it can be seen from Table 6.5 that the results are comparable within experimental error. The results obtained from the hydroformylation when the hydrides which were allowed to stay longer in solution $P(O\text{-}2\text{-}EtC_6H_4)_3$ **(c)** as a ligand with a larger cone angle of 189.9°**,** gave a better conversion of the 1-octene to the aldehyde compared to $P(OPh)_3$ **(a)** and $P(O\text{-}4\text{-}^tBuC_6H_4)_3$ **(b).** The experiment indicated that the hydride used for testing the stability was not destroyed completely in the process.

The absorption bands for the formation of the monophosphite hydride[4] for $P(OPh_3)_3$ **(a)** for the previous experiment appeared at ν_{CO} 2071, 2021 and 2000 cm^{-1}. The results obtained from Table 6.5 are similar and within experimental error, this would indicate that the same species are responsible for the hydroformylation reaction. The hydride species were responsible for the hydroformylation activity represented in Figure 6.2, **(a)**, **(b)** and **(c)** as well as figure

6.5, **(a)**, **(b)** and **(c)**. The k_{obs} results obtained for the hydride allowed to age before addition of 1-octene was the same species as the one preformed and immediately reacted with 1-octene. There was indication of low activity which was shown by the hydride due to the destruction of the hydride during the time it was allowed to be in the reactor without 1-octene. This would indicate the reason for the low conversion from alkene to the aldehyde for the hydride. It would also indicate that there is a low concentration of the active hydride responsible for the hydroformylation. The internal octenes would have made the reaction much slower than what it was. The k_{obs} values obtained indicate a reasonably fast reaction with reasonable conversions from 1-octene to the formation of the aldehyde.

*Table 6.6: Results of High-Pressure IR studies of the hydride in the hydroformylation of 1-octene (Figure 6.3) and stability studies of the hydride in the absence of 1-octene (Figure 6.4) for the different ligands **a**, **b** and **c**.*

1) Ligand		$P(OPh)_3$ **(a)**			
Results from Table 3.1		**Figure 6.3**		**Figure 6.4**	
$[HCo(CO)_3L]$ **(2)** ν_{CO}, cm^{-1}	$[HCo(CO)_2L_2]$ **(3)** ν_{CO}, cm^{-1}	Wavenumber ν_{CO}, cm^{-1}	k_{obs}, s^{-1} 10^4	Wavenumber ν_{CO}, cm^{-1}	k_{obs}, s^{-1} 10^4
	1971				
	1996				
1997		2005	0.1(1)	2002	4.7(4)
		2017	0.9(9)		
2021		2023	0.2(1)		
	2034	2032	-0.3(3)	2032	3 (1)
				2048	9(2)
2073		2073	0.2(5)	2073	3(1)

2) Ligand		$P(O\text{-}4\text{-}^tBuC_6H_4)_3$ **(b)**			
		Figure 6.3		**Figure 6.4**	
$[HCo(CO)_3L]$ **(2)** ν_{CO}, cm^{-1}	$[HCo(CO)_2L_2]$ **(3)** ν_{CO}, cm^{-1}	Wavenumber ν_{CO}, cm^{-1}	k_{obs}, s^{-1} 10^4	Wavenumber ν_{CO}, cm^{-1}	k_{obs}, $s^{-1}10^4$
	1975				
	1995				
2002				1998	0.06(2)
2017		2015	0.06(6)		
	2034	2025	-0.2(1)	2030	7(1)
		2042	0.1(3)	2048	-4.6(4)
2071		2071	-0.4(5)	2071	0.004(533)

3) Ligand		$P(O\text{-}2EtC_6H_4)_3$ **(c)**			
		Figure 6.3		**Figure 6.4**	
$[HCo(CO)_3L]$ **(2)** ν_{CO}, cm^{-1}	$[HCo(CO)_2L_2]$ **(3)** ν_{CO}, cm^{-1}	Wavenumber ν_{CO}, cm^{-1}	k_{obs}, s^{-1} 10^4	Wavenumber ν_{CO}, cm^{-1}	k_{obs}, $s^{-1}10^4$
	1970				
	1998				
2001		2002	0.57(5)	2000	0.023(8)
2023		2017	-0.016(92)		
	2034			2030	0 018(12)
		2044	10.9(5)	2048	-0.05(4)
2074		2071	9(1)	2071	0.024(2)

Table 6.6 results will be tabulated as follows:

1. From the results of the synthesis of the bisphosphite cobalt $[HCo(CO)_2L_2]$ **(2)** (see Section 3.5.2 for **3b** and 3.5.4 for **3c** and for $P(OPh)_3$ **(a)** taken from the synthetic procedure in literature[4]. The IR spectrum is given in Table 6.6 column 1 and 2.

2. Results from Figure 6.3**(1a)**, **(1b)** and **(1c)** for the preformation of the monophosphite cobalt carbonyl hydride $[HCo(CO)_3L]$ **(2)**. The IR absorbance is recorded; see Table 6.6 in the appropriate heading as listed.

3. The individual monophosphite cobalt carbonyl hydrides $[HCo(CO)_3L]$ **(2), 2a, 2b** and **2c** are used in the hydroformylation of 1-octene as seen in Figure 6.2 (a), (b) and (c). The IR spectra and the k_{obs} results are also given in Table 6.6.

4. After the hydroformylation of 1-octene the spectra of the different monophosphite cobalt carbonyl hydrides **2a**, **2b** and **2c** are blown up and given in Figure 6.3 (1a), (1b) and (1c) with the respective kinetic plots given by a2, b2 and c2.

5. In order to get a clear understanding of what is happening to the monophosphite cobalt carbonyl hydride $[HCo(CO)_3L]$ **(2)** because of the decrease in the spectrum. A further test was done in which the hydride was preformed and obtaining the same results as for the first preformation of the hydride. As seen from Table 6.4(1a), (1b) and (1c) the monophosphite carbonyl hydrides **2a**, **2b** and **2c** were allowed to age over a period of 1hr for **2a** and **2b**, **2c** was 2hrs. The kinetic plots are given in a2, b2 and c2 with the k_{obs} results give in Table 6.5.

From these results we can try to establish if the same species are formed from both reactions. The monophosphite cobalt carbonyl hydrides **2a**, **2b** and **2c** formed in Figure 6.4(1a), (1b) and (1c) are all used in the hydroformylation of 1-octene in Figure 6.5(a1), (b1) and (c1).

From the results in Table 6.6 the 2073, 2071 cm^{-1} in the Table represents the formation of the same species for **2a**, **2b** and **2c**. In both Figure 6.3 and 6.4 for all species the peak absorbance of the monophosphite cobalt carbonyl species at 2073 cm^{-1} for $P(OPh)_3$ **(a)** and 2071 cm^{-1} for both $P(O\text{-}4\text{-}^tBuC_6H_4)_3$ **(b)** and $P(O\text{-}2\text{-}EtC_6H_4)_3$ **(c)**. The k_{obs} the ageing of the hydrides is happening much faster in Figure 6.4 than what is happening in Figure 6.3. In both instances the species are the same.

From the spectra of 2034 cm^{-1} in Table 6.6 the $P(OPh)_3$ **(a)** forms more of the bisphosphite cobalt carbonyl hydride $[HCo(CO)_2L_2]$ **(3)** under all circumstances in both Figure 6.3 and Figure 6.4. This confirms the results obtained in the literature on $P(OPh)_3$ **(a)** when it was used as a ligand.[4] $P(O\text{-}4\text{-}^tBuC_6H_4)_3$ **(b)** as triphenylphosphite is forming more bisphosphite cobalt carbonyl hydride $[HCo(CO)_2L_2]$ **(3)** in both Figure 6.3 and 6.4. $P(O\text{-}2\text{-}EtC_6H_4)_3$ **(c)** is the only ligand which does not form the bisphosphite cobalt carbonyl hydride $[HCo(CO)_2L_2]$ **(3)** in Figure 6.3, the bisphosphite hydride is only formed in Figure 6.4.

The spectra at 2000 cm^{-1} in Table 6.6 indicates an equilibrium between the monophosphite hydride $[HCo(CO)_3L]$ **(2)** and the bisphosphite hydride $[HCo(CO)_2L_2]$ **(3)** for $P(OPh)_3$ **(a)** and $P(O\text{-}2\text{-}EtC_6H_4)_3$ **(c)** in Figure 6.3 and 6.4, equilibrium for $P(O\text{-}4\text{-}^tBuC_6H_4)_3$ **(b)** exists in Figure 6.4 only. Eventually there is an indication that more of the monophosphite hydride $[HCo(CO)_3L]$ **(2)** is being formed in 6.3 than in 6.4. Figure 6.4 indicates that the same species is formed although the amount which becomes available after ageing is minimal. Table 6.5 also shows IR spectra of other species which have formed both $P(O\text{-}4\text{-}^tBuC_6H_4)_3$ **(b)** and $P(O\text{-}2\text{-}EtC_6H_4)_3$ **(c)** spectra are within the same range for Figure 6.3 and 6.4 at 2042 and 2048 cm^{-1}. $P(OPh)_3$ **(a)** has the spectra for 6.3 at 2017 cm^{-1} and the spectra for 6.4 at 2048 cm^{-1}. The k_{obs} for the kinetics of the spectra indicate that what is happening in Figure 6.3 is happening at a slower rate than what is happening to the hydride in Figure 6.4 for all the ligands **a**, **b** and **c**. Figure 6.4 a2, b2 and c2 from the kinetic plots a shoulder peak was seen at 2048 cm^{-1} for all the ligands **a**, **b** and **c**. As seen from Table 6.4 the IR absorbance at 2048 cm^{-1} is for the terminal absorbance for the acyl species. Although the absorbance was not strong this indicates the presence of the acyl species in solution.

6.9 Addition of 1-octene to the hydrides from the stability runs

After the hydrides of the different phosphites were subjected to the stability runs (see Figure 6.4, **(2a)**, **(2b)** and **(2c)**, 1-octene was added to the system and the pressure was increased to the predetermined pressure. The predetermined pressure was maintained for the duration of the hydroformylation experiment. All reaction conditions were maintained as those for the hydroformylation for the hydride reacted with 1-octene see Figure 6.2, **(a)**, **(b)** and **(c)**. [1-octene]/[Co] = 70 for these reactions see Figure 6.4, **(a)**, **(b)** and **(c).**

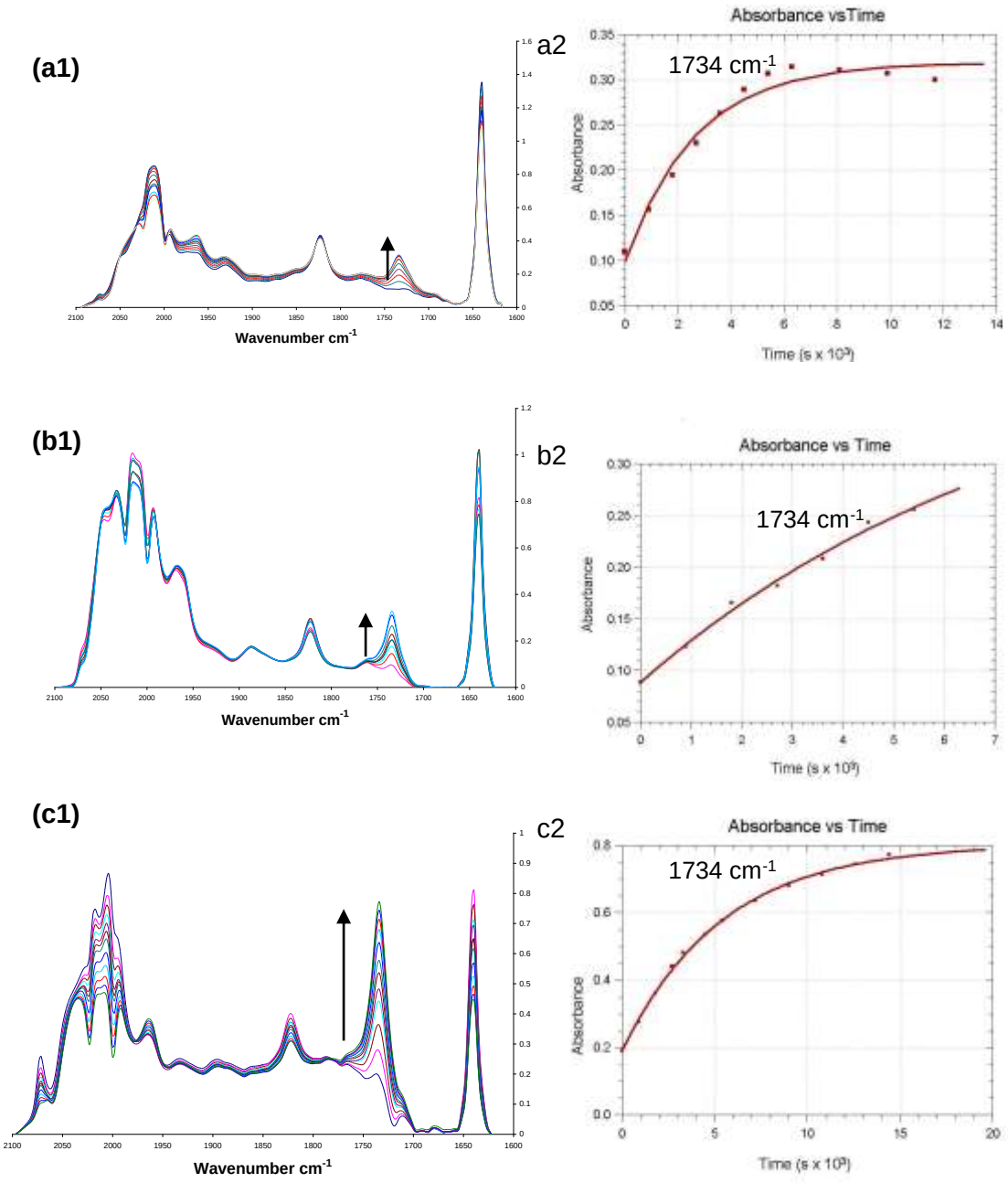

Figure 6.5: HP-IR spectrum of hydroformylation of 1-octene using $P(OPh)_3$ ***(a1)****, $P(O\text{-}4\text{-}^tBuC_6H_4)_3$* ***(b1)*** *and $P(O\text{-}2\text{-}EtC_6H_4)_3$* ***(c1)*** *with the hydride from the stability runs; a2, b2 and c2 are the corresponding kinetic plots of aldehyde formation at 1734 cm^{-1}. Hydroformylation of 1-octene was done at 140° in dodecane. [Co] = 1500 ppm, [L]/[Co] 8:1, pressure = 50 bar Syngas [H_2]/[CO] = 1. [1-octene]/[Co] = 70.*

The HP-IR spectra of hydroformylation runs using aged complexes in the presence of 1-octene are shown in Figure 6.5 **(a1)** $P(OPh)_3$, **(b1)** $P(O\text{-}4\text{-}^tBuC_6H_4)_3$ and **(c1)** $P(O\text{-}2\text{-}EtC_6H_4)_3$. The corresponding kinetic plots are represented in Figure 6.5 a2, b2 and c2. A significant amount of hydroformylation is occurring with the formation of the aldehyde at an absorbance of 1734 cm^{-1}. The rate of hydroformylation is comparable and it can be concluded that the same species is responsible for the

hydroformylation. From the conversion when looking at the kinetic plots of the formation of the aldehyde in Figure 6.5 a2, b2 and c2 that the concentration of the active catalyst is lower. In this case the active catalyst is lower than the initial runs of hydroformylation see Figure 6.2.

$P(OPh)_3$ **(a)**, $P(O\text{-}4\text{-}^tBuC_6H_4)_3$ **(b)** and $P(O\text{-}2\text{-}EtC_6H_4)_3$ **(c)** shows the hydroformylation activity of the monophosphite hydride, after the hydride was subjected to stability runs. The corresponding kinetic plots represented in Figure 6.4 a2, b2 and c2 show a low conversion of the 1-octene to the aldehyde. There is some formation of the aldehyde that can be observed. Some hydroformylation was observed although the rate of conversion was very low. According to the k_{obs} values which are within experimental error there is some production of the aldehyde during the hydroformylation reaction. The conversion of the 1-octene to the aldehyde was very low. This indicates that there is some hydride left after the hydride was allowed to decompose. The hydride which is still left in solution is not good enough to give a full conversion although it is still active in the hydroformylation reaction.

In Figure 6.5 **(a)**, **(b)** and **(c),** some of the 1-octene was converted to the aldehyde, even though the hydride was destroyed by allowing it to be in solution longer before the addition of 1-octene. More aldehyde was formed when using the tris(2-ethylphenyl)phosphite as a ligand. With tris(4-tertiaryphenyl)phosphite and triphenylphosphite as a ligand the conversion of 1-octene to aldehyde when using the hydride used in stability runs the rate of conversion was low. This experiment has proved that there is some active catalyst available for hydroformylation although the conversion from alkene to aldehyde is very low. This would indicate that the catalyst activity has been affected.

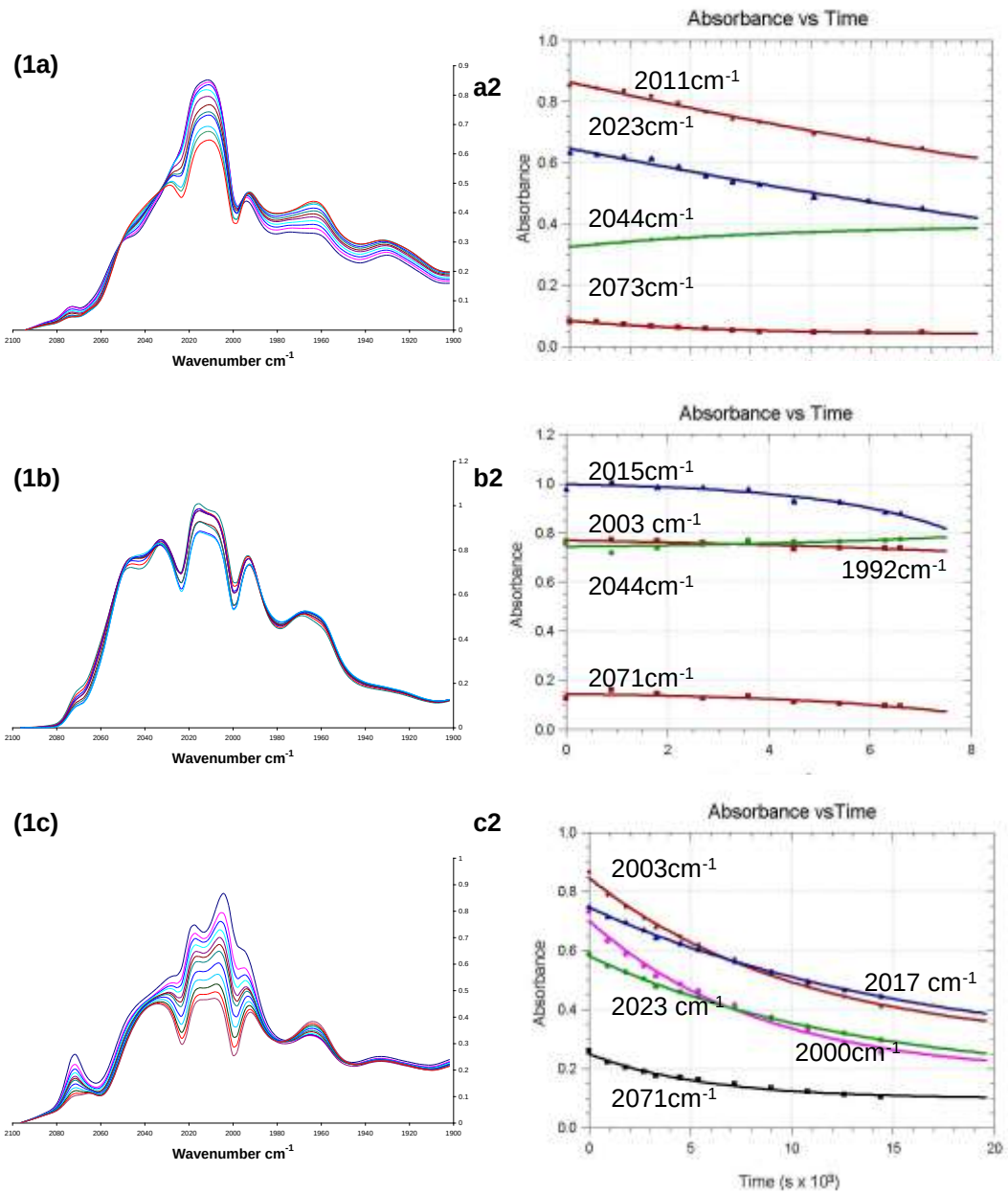

Figure 6.6: Changes in the spectra of the hydride in carbonyl region for $[HCo(CO)_3P(OPh)_3]$ ***(1a)****, $[HCo(CO)_3P(O\text{-}4\text{-}^tBuC_6H_4)_3]$* ***(1b)*** *and $[HCo(CO)_3P(O\text{-}2\text{-}EtC_6H_4)_3]$* ***(1c)****; a2, b2 and c2 are the corresponding kinetic plots of the changes in the carbonyl region. The hydride in the presence of 1-octene after it was subjected to stability runs.*

After having allowed the different phosphite hydrides to react further without 1-octene it can be seen from Figure 6.6, **(1a)**, **(1b)** and **(1c)** the effect this had on the spectra of the monophosphite cobalt carbonyl hydride $[HCo(CO)_3L]$ **(2)**. When we compared it to the spectra of the hydride which was from hydroformylation in the presence of 1-octene, both the spectra for 6.2**(a)**: $P(OPh)_3$ and 6.2**(b)**: $P(O\text{-}4\text{-}^tBuC_6H_4)_3$ **(b)** were completely different. The spectra of 6.2**(c)**: $P(O\text{-}2\text{-}EtC_6H_4)_3$ **(c)** and 6.4.**(c)**: $P(O\text{-}2\text{-}EtC_6H_4)_3$ **(c)** are nearly similar see Table 6.5.

6.10 Conclusion

Phosphites have made a contribution in the catalytic cycle of hydroformylation. The cobalt phosphite catalysts are active catalysts in hydroformylation with the monophosphite cobalt hydride $[HCO(CO)_3L]$ **(2)** as the active catalyst. The bisphosphite catalyst was inactive in hydroformylation from a previous publication.[3,4]

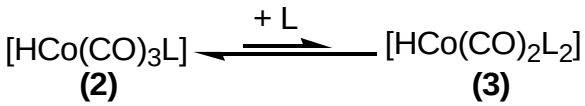

*Scheme 6.3: Schematic representation of the equilibrium between the monophosphite **(2)** and bisphosphite **(3)** hydrides.*

During hydroformylation the hydride formed from the dimer and an excess of the ligand. The unmodified hydride, monophosphite and bisphosphite all formed during the process. An equilibrium between the monophosphite and bisphosphite hydride existed during the process (see Scheme 6.3).

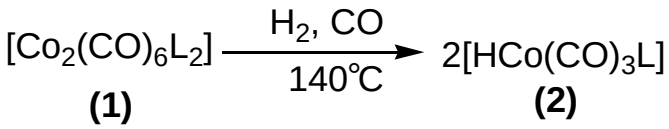

Scheme 6.4: Schematic representation of formation of hydride

Scheme 6.4, is the representation of the formation of the modified cobalt catalyst hydride under HP-IR spectroscopy. The dimer splits into two in the presence of syngas and an excess of ligand. The monophosphite hydride is then formed.

The hydroformylation of 1-octene in the presence of cobalt phosphite carbonyls of $[Co_2(CO)_6L_2]$ **(1)** with variations of ligands as $P(OPh)_3$ **(a),** $P(O\text{-}4\text{-}^tBuC_6H_4)_3$ **(b)** and $P(O\text{-}2\text{-}EtC_6H_4)_3$ **(c)** as catalyst precursors has been studied by following the infrared spectral changes under optimum reaction conditions in a high pressure spectroscopic cell. The results of the hydroformylation are consistent with the Heck and Breslow mechanism and those obtained during the hydroformylation of 1-pentene using[3,4] $P(OPh)_3$ **(a),** $P(O\text{-}2,4\text{-}^tBu_2C_6H_4)_3$ **(d)** as catalyst precursors. The dimers were used as precursors in the hydroformylation of 1-octene. HP-IR studies revealed that under reaction conditions the monophosphite hydride was the dominant species being formed and was an active hydride species in the

hydroformylation reaction. The bisphosphite hydride and the unmodified hydride formed but had eventually disappeared at 140ºC.

In the hydroformylation reactions it is important to be able to identify the type of hydride that is being formed. With the knowledge of the type of hydride that has formed the type of results obtained can then be rationalised. In Table 6.1 is a list of the different hydrides that formed at the different temperatures. In a publication using the unmodified hydride [$HCo(CO)_4$] **(5)** and 1-octene**,** the results reported a formation of 1-nonanal (75%) as the major product and small amounts of other side products (< 2%).[18]

These experiments have shown the importance of the stability of the cobalt phosphite catalyst in hydroformylation reactions. The hydride selectivity and activity are also important in the hydroformylation reaction. It is also evident that the monophosphite hydride is the active catalyst in the hydroformylation reactions as was previously reported. The experiments that were performed indicated the importance of temperature for the hydroformylation reaction. At 120ºC the hydride has just started to form and at 140ºC it is completely formed. The complete formation of the hydride was at 140ºC when $P(OPh)_3$ **(a)** and $P(O\text{-}4\text{-}^tBuC_6H_4)_3$ **(b)** were used as ligands, having the same cone angle. As soon as the ligand was changed to $P(O\text{-}2\text{-}EtC_6H_4)_3$ **(c)** the hydride had fully formed at 135ºC the temperature had decreased. The results from previous experiments using $P(OPh)_3$**(a)** as a ligand and pentene with a 2:1 syngas ratio reported complete formation of the monophosphite hydride at 120ºC in both toluene and paraffin.[4] What was happening in the carbonyl region where the hydride absorbs between (1900 – 2100 cm^{-1}) is not due to the side reactions that could have occurred during the hydroformylation or due to the addition of 1-octene to the reaction.

In the hydroformylation reaction it is important that the cobalt catalyst is preformed. The alkene is then added to enable the formation of the aldehyde.The reaction has also indicated that this reaction was catalytic. There has been debate as to whether the reactions are stoichiometric or catalytic. In the reactions the hydride was not stable, but the aldehyde formation was observed. These experiments confirmed that elevated temperatures were required in order to form the hydrides. The hydride was starting to form at 120ºC and was fully formed at 140ºC. This proved to be a very important factor because the hydroformylation reactions did not occur at temperatures below 140ºC.

In Figure 6.1 is the infrared spectrum of the preformation of the cobalt phosphite catalyst of the different ligands. The formation of the hydride was formed from the dimeric species as precursors. The hydrides $[HCo(CO)_3\{P(OPh)_3\}]$ **(2a)**, $[HCo(CO)_3\{P(O\text{-}4\text{-}^tBuC_6H_4)_3\}]$ **(2b)** and $[HCo(CO)_3P(O\text{-}2\text{-}EtC_6H_4)_3]$ **(2c)** were formed under hydroformylation conditions. All the hydrides were seen during hydroformylation. The formation of the hydrides and disappearance of the ligands is listed in Table 6.5

6.11 Hydroformylation catalytic cycle

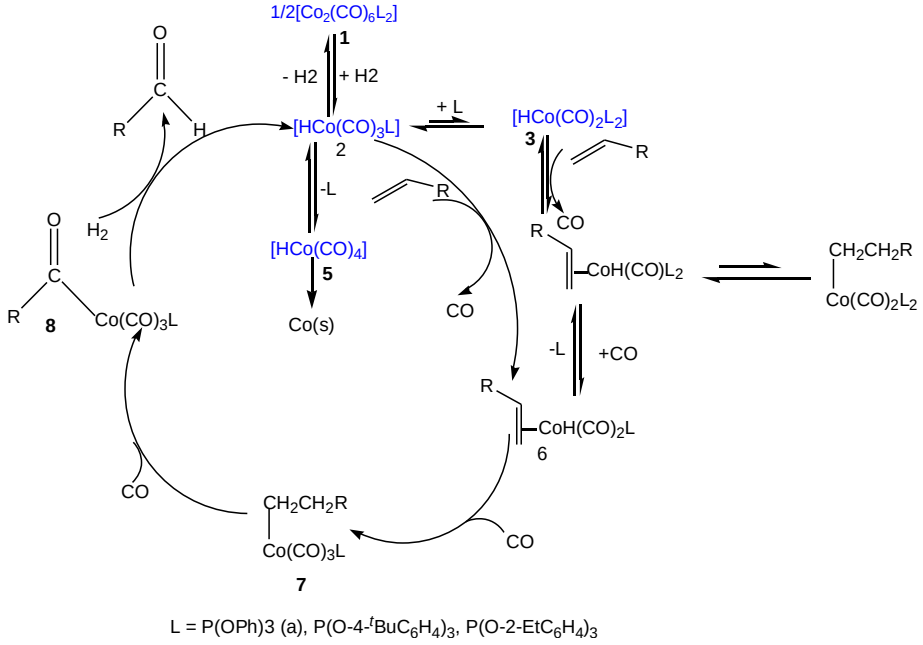

Scheme 6.1: Schematic representation of the cobalt phosphite catalysed hydroformylation reaction

The Heck and Breslow hydroformylation catalytic cycle was used to explain the results. The dimeric cobalt species were used with an excess of dimer with L as any of the phosphite ligands **a**, **b** or **c**. In the presence of syngas H_2/CO, the $[Co_2(CO)_6L_2]$ **(1)** is split into two to give the monophosphite cobalt carbonyl hydride $[HCo(CO)_3L]$ **(2)** in the presence of syngas. The bisphosphite $[HCo(CO)_2L_2]$ **(3)** is in equilibrium with the monophosphite hydride $[HCo(CO)_3L]$ **(2).** The bisphosphite hydride was immediately converted to the monophosphite hydride. The monophosphite is the predominant species $[HCo(CO)_3L]$ **(2)** which coordinates to 1-octene to give the π complex **6.** The alkyl species (7) is formed by migration of the hydrogen adding on *anti*-Markovnikov or Markovnikov to give the linear or branched alky species **7.** Addition of CO produces the acyl species **8**. With the addition of hydrogen the

aldehyde is formed and regeneration of the hydride. The complexes coloured in blue are seen in the carbonyl region. The reactant and product, 1-octene and the aldehyde absorbance can also be seen in the carbonyl region. There is a further equilibrium between the unmodified hydride [$HCo(CO)_4$] **(5)**. The unmodified hydride can cause cobalt plating of the hydride. The unmodified hydride can be coordinated to the alkene and loss of the CO and go back to the catalytic cycle. Even though the systems studied are different, the values obtained for the k_{obs} are reasonably comparable and a similar trend in the values is observed. From this we can conclude that the nature of the phosphite is not a significant factor on the reaction rate. Under the reported reaction conditions (see Table 6.2), this would not *exclude* the possibility that there has not been complete conversion of the alkene to the aldehyde.

No isomerisation to the internal alkene is suspected because the reaction was not very slow. Cobalt plating of the metal in the reactions was also not observed.

References

1 P.W.N.M. van Leeuwen, *Appl. Catal. A: Gen*., 2001, **212**, 61.

2 http://chemistry.lsu/stanley/webpub/4571-chapt16-hydroformylation, 29/11/07

3 R. Meijboom, M. Haumann, A. Roodt and L. Damoense, *Helv. Chemica Acta*. 2005, **88**, 676.

4 M. Haumann, R. Meijboom, J. Ross and A. Roodt, *Dalton Trans*., 2004, 1679.

5 C.D. Frohning and C.W. Kohlpaintner, in "*Applied Homogeneous Catalysis with Organometallic Compounds*", B. Cornils and W.A. Herrmann., Eds.; VCH: 1996, Vol. 1, p.75.

6 L. H. Slaugh and R. D. Mullineaux, *J. Organomet. Chem*., 1968, **13**, 469.

7 J. P. Steynberg,, K. Govender and P. J. Steynberg, *World Pat*., 2002014248, 2002.

8 C. Crause, L. Bennie, L. Damoense, C. L. Dwyer, C. Grove, N. Grimmer, W. Janse van Rensberg, M. M. Kirk, K. M. Mokheseng, S. Otto and P. J. Steynberg, *Dalton Trans*., 2003, 2036.

9 B.C. Gates, "Catalytic Chemistry", John Wiley and Sons, Inc. 1999, p.93.

10 R. Whyman, *J. Organomet. Chem*., 1974, **81**, 97.

11 C. Dwyer, H. Assumption, J. Coetzee, C. Crause, L. Damoense and M. Kirk, *Coord. Chem. Rev*., 2004, **248**, 653.

12 R.F. Heck and D.S. Breslow, *Chem. Ind. (London)*., 1960, 467. b) R.F. Heck and D.S. Breslow, *J. Am. Chem. Soc*., 1961, **83**, 4023.

13 C. Crause, L. Bennie, L. Damoense, C.L. Dwyer, C. Grove, W. Janse van Rensburg, M.M. Kirk, K.M. Mokheseng, S. Otto and P.J. Steynberg, *Dalton Trans*., 2003, 2036.

14 D.F. Shriver and P.W. Atkins, "*Inorganic Chemistry*", Oxford University Press, 1999, 3rd edition, p.593.

15 (a) R.F. Heck, *J. Am. Chem. Soc*., 1963, **85**, 651. (b) R.F. Heck and D.S. Breslow, *J. Am. Chem Soc*., 1962, **84**, 2499.

16 L. Rosi, A. Salvini, M. Bianchi, P. Frediani and F. Piacenti, *J. Organomet. Chem*., 1997, **535**, 147.

17 S.M. Massick, J.G. Rabor, S. Elbers, J. Marhenke, S. Bernhard, J.R. Schoonover and P.C. Ford, *Inorg. Chem*., 2000, **39**, 3098.

18 M.F. Mirbach, *J. Organomet. Chem*., 1984, **265**, 205.

Chapter 7

Evaluation of the study

7.1 Introduction

The relevance and success of this MSc. Study is briefly discussed in Section 7.2 and future research aspects are outlined in Section 7.3. The chemical relevance and results of this study are briefly discussed according to the pre-set aims which were established in **Chapter 1**.

7.2 Scientific relevance of this study

Previously in our group a study on the hydroformylation of 1-pentene using $P(OPh)_3$ **(a)** with a cone angle 128° and $P(O\text{-}2.4\text{-}t\text{-}Bu_2C_6H_3)_3$ **(d)** with a cone angle of 175° was investigated.[1,2] This research revealed that the triphenylphosphite formed the bisphosphite hydride. The bisphosphite hydride was inactive in the hydroformylation of 1-pentene and tris(2,4-di-tertiaryphenyl)phosphite was used as a ligand to form the monophosphite hydride. This was attributed to different cone angles between the ligands **a** and **b**. The monophosphite cobalt carbonyl hydride $[HCo(CO)_3L]$ **(2)** proved to be the active catalyst in hydroformylation of 1-pentene.

This MSc. study was motivated by the results obtained as indicated above. It was then decided to use a variety of phosphite ligands with intermediate cone angles between 128 and 175°. The reason for the variations of the ligand was to try and establish the smallest cone angle which would prevent the formation of the bisphosphite hydride.

The dimeric compounds $[Co_2(CO)_6\{P(O\text{-}4\text{-}^tBuC_6H_4)_3\}_2]$ **(1b)**, $[Co_2(CO)_6\{P(O\text{-}2\text{-}EtC_6H_4)_3\}_2]$ **(1c)**, $[Co_2(CO)_6\{P(O\text{-}4\text{-}^tBuC_6H_4)_3\}_2]$ **(1b)**, $[Co_2(CO)_6\{P(OPh)_3\}_2]$ **(1a)** $[Co_2(CO)_6\{P(O\text{-}2\text{-}EtC_6H_4)_3\}_2]$ **(1c)** as well as the hydride $[HCo(CO)_2\{P(O\text{-}4\text{-}^tBuC_6H_4)_3\}_2]$ **(3b)** were successfully synthesized and only crystals of **(1b**, **1c** and **3b** suitable for X-ray data collection were obtained. The structural results showed that the dimeric species have cone angles of 175.4 (for **1b**), 128 (for **1a**) and 176.6° (for **1c**).

The dimers were used as precursors for the formation of the monophosphite hydride in the hydroformylation of 1-octene. Cleavage of the dinuclear complex to produce

the hydride species with the formation of hydridocarbonyls of the type HM(CO)3L] was only obtained under high CO/H_2 pressure and temperatures. The hydroformylation of 1-octene in the presence of cobalt phosphite carbonyls of $[Co_2(CO)_6L_2]$ **(1)** with variations of ligands as $P(OPh)_3$ **(a),** $P(O\text{-}4\text{-}^tBuC_6H_4)_3$ **(b)** and $P(O\text{-}2\text{-}EtC_6H_4)_3$ **(c)** as catalyst precursors has been studied by following the infrared spectral changes under optimum reaction conditions in a high pressure spectroscopic cell. During the hydroformylation process, the IR spectra showed an absorbance change in the carbonyl region between 1900 – 2100 cm^{-1} (Figure 6.3). This change in absorbance was the indicated the possibility of the decomposition of the hydride. Kinetic results in Table 6.2 for the synchronized decrease of 1-octene (at 1822 and1639 cm^{-1}) and increase of aldehyde (at 1734 cm^{-1}) show that the rate of reactions are within the same experimental error.

The results obtained, in Table 6.3, also showed that the reaction did not go to completion, and only 54, 66 and 71% conversion of 1-octene to aldehyde formation was observed. The cobalt phosphite hydrides are important in the selectivity, stability and conversion rate of reaction. It was therefore important to understand the stability of the hydride. The hydride stability and conversion rate were studied in the hydroformylation of 1-octene in the presence and absence of 1-octene. With the experiment when $P(O\text{-}2,4\text{-}^tBu_2C_6H_3)_3$ **(d)** was used as a ligand the hydride was stable and none of these changes in the carbonyl region were observed. That was the reason why there was concern on trying to establish what could be happening in this region.

7.3 Future research

Further investigations which will be useful in the understanding of the hydroformylation reaction will be tabulated below.

- Synthesize the hydride of the $[HCo(CO)_2\{P(O\text{-}2\text{-}EtC_6H_4)_3\}_2]$ **(3c)** and try to obtain crystals of the hydride.
- HP-NMR experiments in order to correlate the results with previous experiments.
- Batch autoclave results in order to be able to see the selectivity of the products formed.
- Perform the HP-IR and do GC runs in order prove the selectivity of the products formed.
- Perform solution behaviour on the ligands by using different solvents.
- Study the selectivity and conversion rate with the different phosphite ligands.

- Comparison of equilibria as a function of phosphite cone angle.
- Try to establish the hydride equilibrium stages and establish if there are any side reactions which could be occurring.
- With the different hydrides study how the different allotopes can be in equilibrium whilst in solution
- Study the deactivation and regeneration of the catalyst
- Study the behaviour of hydroformylation in the presence of a terminal alkene and an internal alkene
- Try to establish all the intermediate reactants in the catalytic cycle.

References

[1] M. Haumann, R. Meijboom, J.R. Moss and A. Roodt, *Dalton Trans.*, 2004, 1679.

[2] R. Meijboom, M. Haumann, A. Roodt and L. Damoense, *Helv. Chim. Acta*., 2005, **88**, 676.

Appendix

Table **A1**: Crystal data and structure refinement for 5bm2ar1. $[Co_2(CO)_6\{P(O\text{-}4\text{-}^tBuC_6H_4)_3\}_2]$ **(1a)**

Identification code	5bm2ar1
Empirical formula	$C_{66}\ H_{78}\ Co_2\ O_{12}\ P_2$
Formula weight	1243.15
Temperature	293(2) K
Wavelength	0.71073 Å
Crystal system, space group	Triclinic, $P\bar{1}$
Unit cell dimensions	a = 12.180(19) Å α = 77.552(3)°.
	b = 12.460(2) Å β = 65.628(3)°
	c = 12.990(2) Å γ = 80.463(3)°
Volume ($Å^3$)	1746.9(5)
Z, Calculated density (Mg/m^3)	1, 1.107
Absorption coefficient (mm^{-1})	0.572
F(000)	576
Crystal size (mm)	0.54 x 0.36 x 0.34
θ range for data collection (°)	2.22 to 26.37.
Limiting indices	$-13 \le h \le 15$,
	$-15 \le k \le 15$,
	$-16 \le l \le 15$
Reflections collected / unique	10624 / 7052
	[R(int) = 0.0782]
Completeness to θ = 26.37	98.5 %
Absorption correction	None
Max. and min. transmission	0.8293 and 0.7477
Refinement method	Full-matrix least-squares on F^2
Data / restraints / parameters	7052 / 120 / 427
Goodness-of-fit on F^2	1.009
Final R indices [I>2θ(I)]	R1 = 0.0571, *wR2* = 0.1582
R indices (all data)	R1 = 0.0769, *wR2* = 0.1758
Largest diff. peak and hole ($e.A^{-3}$)	0.847 and -0.652

Table **A2**: Atomic coordinates (x 10^4) and equivalent isotropic displacement parameters (Å^2 x 10^3) for 5bm2ar1.U(eq) is defined as one third of the trace of the orthogonalized Uij tensor.

	X	y	z	U(eq)
Co	4480(1)	4510(1)	6083(1)	47(1)
P	3650(1)	3716(1)	7798(1)	46(1)
O(1)	2657(2)	4400(2)	8741(2)	62(1)
O(2)	4574(2)	3158(2)	8382(2)	59(1)
O(3)	2926(2)	2659(2)	8026(2)	55(1)
C(01)	5144(4)	3234(3)	5575(3)	70(1)
C(02)	5370(3)	5326(3)	6356(3)	61(1)
C(03)	3102(3)	5121(3)	5942(3)	63(1)
O(01)	5537(4)	2416(3)	5271(3)	119(1)
O(02)	5937(3)	5843(3)	6537(3)	90(1)
O(03)	2225(3)	5495(3)	5851(2)	93(1)
C(11)	2433(3)	5554(3)	8568(3)	61(1)
C(12)	3229(4)	6199(3)	8611(3)	73(1)
C(13)	3002(5)	7331(4)	8438(4)	92(1)
C(14)	2040	7833	8241	96(2)
C(15)	1239(5)	7191(4)	8214(4)	100(2)
C(16)	1417(4)	6009(4)	8401(3)	79(1)
C(141)	1811(8)	9119(5)	8009(5)	146(3)
C(142)	1770(30)	9580(7)	9018(16)	164(15)
C(143)	720(20)	9441(9)	7740(40)	194(17)
C(144)	2980(20)	9537(8)	6930(20)	155(13)
C(145)	2401(18)	9608(6)	8642(16)	181(7)
C(146)	419(10)	9449(7)	8532(16)	206(8)
C(147)	2310(20)	9493(6)	6751(7)	217(9)
C(21)	4172(3)	2625(3)	9540(2)	55(1)
C(22)	3966(4)	1545(3)	9804(3)	77(1)
C(23)	3610(5)	1026(3)	10935(3)	87(1)
C(24)	3461(4)	1585(3)	11800(3)	72(1)
C(25)	3692(5)	2657(3)	11494(3)	87(1)
C(26)	4068(4)	3189(3)	10358(3)	79(1)
C(241)	3001(6)	1011(4)	13067(4)	107(2)
C(242)	3246(16)	1640(8)	13791(6)	145(6)
C(243)	3624(14)	-190(6)	13136(6)	137(5)
C(244)	1615(8)	896(16)	13477(8)	174(8)

C(245)	1920(20)	1743(14)	13784(8)	159(11)
C(246)	4030(17)	960(20)	13529(12)	156(11)
C(247)	2690(20)	-124(11)	13171(8)	131(9)
C(31)	1841(3)	2797(2)	7852(2)	50(1)
C(32)	776(3)	2974(3)	8743(3)	68(1)
C(33)	-289(4)	3103(4)	8593(4)	85(1)
C(34)	-319(4)	3040(4)	7552(4)	77(1)
C(35)	778(4)	2839(4)	6673(3)	79(1)
C(36)	1859(3)	2718(3)	6811(3)	66(1)
C(341)	-1521(6)	3190(6)	7422(6)	131(2)
C(342)	-2388(8)	4100(9)	8020(10)	222(5)
C(343)	-2340(6)	2232(8)	8326(7)	164(3)
C(344)	-1451(7)	2925(9)	6359(7)	188(4)

Table **A3** Bond lengths [Å] for 5bm2ar1. $[Co_2(CO)_6\{P(O\text{-}4\text{-}^tBuC_6H_4)_3\}_2]$ **(1a)**

Co-C(01)	1.789(4)	C(13)-C(14)	1.328(5)
Co-C(02)	1.782(4)	C(14)-C(15)	1.375(6)
Co-C(03)	1.789(4)	C(14)-C(141)	1.565(6)
Co-P	2.1182(8)	C(15)-C(16)	1.435(6)
Co-Co#1	2.6652(8)	C(141)-C(147)	1.484(10)
P-O(2)	1.596(2)	C(141)-C(143)	1.478(17)
P-O(1)	1.604(2)	C(141)-C(142)	1.522(17)
P-O(3)	1.612(2)	C(141)-C(145)	1.554(13)
O(1)-C(11)	1.404(4)	C(141)-C(146)	1.564(13)
O(2)-C(21)	1.418(3)	C(141)-C(144)	1.600(16)
O(3)-C(31)	1.408(4)	C(142)-C(145)	0.72(3)
C(01)-O(01)	1.131(4)	C(142)-C(146)	2.04(3)
C(02)-O(02)	1.137(4)	C(143)-C(146)	0.94(3)
C(03)-O(03)	1.134(4)	C(143)-C(147)	1.84(3)
C(11)-C(16)	1.354(5)	C(144)-C(147)	0.95(3)
C(11)-C(12)	1.383(5)	C(144)-C(145)	2.06(3)
C(12)-C(13)	1.380(5)	C(21)-C(26)	1.350(5)
C(21)-C(22)	1.354(5)	C(31)-C(36)	1.368(4)
C(22)-C(23)	1.387(5)	C(32)-C(33)	1.368(5)
C(23)-C(24)	1.380(5)	C(33)-C(34)	1.387(5)
C(24)-C(25)	1.351(5)	C(34)-C(35)	1.381(6)
C(24)-C(241)	1.549(5)	C(34)-C(341)	1.518(6)
C(25)-C(26)	1.396(5)	C(35)-C(36)	1.380(5)
C(241)-C(242)	1.489(9)	C(341)-C(344)	1.455(9)
C(241)-C(247)	1.488(12)	C(341)-C(342)	1.520(10)
C(241)-C(245)	1.546(13)	C(341)-C(343)	1.620(10)
C(241)-C(244)	1.568(10)	C(241)-C(243)	1.565(9)
C(241)-C(246)	1.585(13)	C(242)-C(245)	1.60(2)
C(243)-C(247)	1.109(19)	C(243)-C(246)	1.82(2)
C(244)-C(245)	1.36(2)	C(244)-C(247)	1.651(19
C(31)-C(32)	1.359(5)		

Table **A3:** Bond angles [º] for 5bm2ar1. $[Co_2(CO)_6\{P(O\text{-}4\text{-}^tBuC_6H_4)_3\}_2]$ **(1a)**

C(01)-Co-C(02)	119.41(18)	C(01)-Co-C(03)	119.03(18)
C(02)-Co-C(03)	119.42(17)	C(03)-Co-P 95.	73(10)
C(01)-Co-Co#1	86.69(11)	C(02)-Co-Co#1	84.50(10)
C(03)-Co-Co#1	84.19(10)	P-Co-Co#1	179.38(3)
O(2)-P-O(1)	103.11(12)	O(2)-P-O(3)	98.82(11)
O(1)-P-O(3)	99.85(12)	O(2)-P-Co	114.38(8)
O(1)-P-Co	119.79(9)	O(3)-P-Co	117.70(8)
C(11)-O(1)-P	124.20(19)	C(21)-O(2)-P	121.90(19)
C(31)-O(3)-P	119.91(18)	O(01)-C(01)-Co	178.2(4)
O(02)-C(02)-Co	179.5(3)	O(03)-C(03)-Co	179.1(4)
C(16)-C(11)-C(12)	121.4(4)	C(16)-C(11)-O(1)	119.1(4)
C(12)-C(11)-O(1)	119.4(3)	C(11)-C(12)-C(13)	119.0(4)
C(14)-C(13)-C(12)	122.7(4)	C(13)-C(14)-C(15)	118.3(3)
C(13)-C(14)-C(141)	122.3(4)	C(15)-C(14)-C(141)	119.4(4)
C(14)-C(15)-C(16)	121.7(4)	C(11)-C(16)-C(15)	116.9(4)
C(147)-C(141)-C(143)	76.6(13)	C(147)-C(141)-C(142)	133.5(10)
C(143)-C(141)-C(142)	114.4(9)	C(147)-C(141)-C(14)	108.2(4)
C(143)-C(141)-C(14)	110.4(8)	C(142)-C(141)-C(14)	108.9(6)
C(147)-C(141)-C(145)	113.3(9)	C(143)-C(141)-C(145)	134.4(10)
C(142)-C(141)-C(145)	27.0(12)	C(14)-C(141)-C(145)	108.0(6)
C(147)-C(141)-C(146)	110.3(8)	C(143)-C(141)-C(146)	35.7(13)
C(142)-C(141)-C(146)	82.5(12)	C(14)-C(141)-C(146)	109.0(6)
C(145)-C(141)-C(146)	107.8(6)	C(147)-C(141)-C(144)	5.5(11)
C(143)-C(141)-C(144)	110.1(10)	C(142)-C(141)-C(144)	106.8(10)
C(14)-C(141)-C(144)	105.8(6)	C(145)-C(141)-C(144)	81.5(13)
C(146)-C(141)-C(144)	138.5(8)	C(145)-C(142)-C(141)	78.9(15)
C(145)-C(142)-C(146)	125.2(19)	C(141)-C(142)-C(146)	49.6(8)
C(146)-C(143)-C(141)	77.2(15)	C(146)-C(143)-C(147)	125.9(16)
C(141)-C(143)-C(147)	51.9(8)	C(147)-C(144)-C(141)	65.6(10)
C(147)-C(144)-C(145)	109.7(14)	C(141)-C(144)-C(145)	48.3(7)
C(142)-C(145)-C(141)	74.1(16)	C(142)-C(145)-C(144)	121.1(19)
C(141)-C(145)-C(144)	50.2(7)	C(143)-C(146)-C(141)	67.1(10)
C(143)-C(146)-C(142)	110.6(14)	C(141)-C(146)-C(142)	47.9(7)
C(144)-C(147)-C(141)	78.9(13)	C(144)-C(147)-C(143)	127.3(16)
C(141)-C(147)-C(143)	51.5(8)	C(26)-C(21)-C(22)	120.7(3)
C(26)-C(21)-O(2)	119.2(3)	C(22)-C(21)-O(2)	120.0(3)

C(21)-C(22)-C(23)	119.4(3)	C(24)-C(23)-C(22)	121.5(3)
C(25)-C(24)-C(23)	117.1(3)	C(25)-C(24)-C(241)	121.8(3)
C(23)-C(24)-C(241)	121.0(3)	C(24)-C(25)-C(26)	122.2(3)
C(21)-C(26)-C(25)	119.1(3)	C(242)-C(241)-C(247)	136.5(6)
C(242)-C(241)-C(24)	111.1(4)	C(247)-C(241)-C(24)	110.6(5)
C(242)-C(241)-C(245)	63.7(9)	C(247)-C(241)-C(245)	112.8(8)
C(24)-C(241)-C(245)	108.5(5)	C(242)-C(241)-C(244)	111.9(6)
C(247)-C(241)-C(244)	65.3(8)	C(24)-C(241)-C(244)	107.6(5)
C(245)-C(241)-C(244)	51.7(9)	C(242)-C(241)-C(243)	110.6(6)
C(247)-C(241)-C(243)	42.5(8)	C(24)-C(241)-C(243)	109.1(5)
C(245)-C(241)-C(243)	141.0(5)	C(244)-C(241)-C(243)	106.3(6)
C(242)-C(241)-C(246)	44.0(8)	C(247)-C(241)-C(246)	109.8(8)
C(24)-C(241)-C(246)	108.7(5)	C(245)-C(241)-C(246)	106.3(7)
C(244)-C(241)-C(246)	142.3(6)	C(243)-C(241)-C(246)	70.6(9)
C(246)-C(242)-C(241)	72.4(8)	C(246)-C(242)-C(245)	129.8(11)
C(241)-C(242)-C(245)	59.9(6)	C(247)-C(243)-C(241)	65.0(7)
C(247)-C(243)-C(246)	116.2(11)	C(241)-C(243)-C(246)	55.2(6)
C(245)-C(244)-C(241)	63.3(7)	C(245)-C(244)-C(247)	113.9(9)
C(241)-C(244)-C(247)	55.0(5)	C(244)-C(245)-C(241)	65.0(7)
C(244)-C(245)-C(242)	117.4(9)	C(241)-C(245)-C(242)	56.4(7)
C(242)-C(246)-C(241)	63.5(7)	C(242)-C(246)-C(243)	113.2(9)
C(241)-C(246)-C(243)	54.2(5)	C(243)-C(247)-C(241)	72.4(9)
C(243)-C(247)-C(244)	129.5(11)	C(241)-C(247)-C(244)	59.7(6)
C(32)-C(31)-C(36)	120.7(3)	C(32)-C(31)-O(3)	118.9(3)
C(36)-C(31)-O(3)	120.3(3)	C(33)-C(32)-C(31)	119.8(3)
C(32)-C(33)-C(34)	121.7(4)	C(35)-C(34)-C(33)	116.8(4)
C(35)-C(34)-C(341)	123.2(4)	C(33)-C(34)-C(341)	120.0(4)
C(34)-C(35)-C(36)	122.0(3)	C(31)-C(36)-C(35)	118.9(3)
C(344)-C(341)-C(342)	123.7(6)	C(344)-C(341)-C(34)	114.5(5)
C(342)-C(341)-C(34)	113.3(5)	C(344)-C(341)-C(343)	99.6(6)
C(342)-C(341)-C(343)	92.6(7)	C(34)-C(341)-C(343)	107.8(5)

Symmetry transformations used to generate equivalent atoms: 1-x+1,-y+1,-z+1

Table **A4:** Anisotropic displacement parameters ($Å^2$ x 10^3) for 5bm2ar1. The anisotropic displacement factor exponent takes the form:

$-2\pi^2 [h^2 a^{*2} U11 + ... + 2 h k a^* b^* U12]$

	U11	U22	U33	U23	U13	U12
Co	58(1)	47(1)	32(1)	2(1)	16(1)	8(1)
P	53(1)	46(1)	35(1)	2(1)	-15(1)	8(1)
O(1)	74(2)	53(1)	41(1)	-1(1)	-7(1)	8(1)
O(2)	58(1)	73(2)	39(1)	10(1)	-21(1)	13(1)
O(3)	60(1)	47(1)	54(1)	6(1)	-23(1)	11(1)
C(01)	84(3)	62(2)	47(2)	0(2)	-14(2)	7(2)
C(02)	69(2)	67(2)	43(2)	0(1)	-19(2)	13(2)
C(03)	71(2)	70(2)	40(2)	3(1)	-21(2)	5(2)
O(01)	170(3)	59(2)	88(2)	-17(2)	-17(2)	16(2)
O(02)	94(2)	109(2)	79(2)	-19(2)	-36(2)	34(2)
O(03)	75(2)	127(3)	64(2)	-3(2)	-31(1)	16(2)
C(11)	73(2)	57(2)	38(2)	-6(1)	-10(1)	2(2)
C(12)	88(3)	60(2)	62(2)	-14(2)	-17(2)	8(2)
C(13)	114(4)	63(3)	79(3)	-16(2)	-18(2)	4(2)
C(14)	131(4)	61(3)	65(2)-	10(2)	-12(3)	2(3)
C(15)	108(4)	105(4)	59(2)	-13(2)	-25(2)	43(3)
C(16)	78(3)	91(3)	57(2)	-13(2)	-22(2)	10(2)
C(141)	213(7)	77(3)	86(4)	-7(3)	-20(4)	39(4)
C(142)	200(30)	58(12)	170(20)	-48(12)	-8(17)	26(13)
C(143)	200(30)	130(20)	230(30)	21(18)	-100(20)	49(17)
C(144)	146(19)	75(13)	170(20)	56(13)	-30(15)	14(11)
C(145)	283(18)	91(8)	170(12)	-40(7)	-74(12)	35(8)
C(146)	270(16)	113(8)	171(13)	-44(7)	-55(10)	97(9)
C(147)	380(20)	78(6)	89(7)	12(5)	-23(10)	32(9)
C(21)	61(2)	62(2)	38(1)	6(1)	-22(1)	9(1)
C(22)	125(3)	57(2)	48(2)	-5(2)	-35(2)	5(2)
C(23)	157(4)	51(2)	56(2)	6(2)	-45(2)	26(2)
C(24)	109(3)	63(2)	47(2)	7(2)	-36(2	22(2)
C(25)	151(4)	71(2)	51(2)	2(2)	-49(2)	33(3)
C(26)	130(4)	63(2)	57(2)	13(2)	-48(2)	38(2)
C(241)	185(6)	86(3)	51(2)	19(2)	-46(3)	47(3)
C(242)	276(17)	20(8)	44(4)	9(4)	-68(7)	43(10)
C(243)	248(14)	83(6)	72(5)	19(4)	-78(7)	9(7)

C(244)	146(10)	229(18)	89(7)	34(9)	-3(6)	-60(10)
C(245)	210(20)	119(14)	64(9)	-13(8)	28(11)	-22(14)
C(246)	179(18)	200(20)	112(13)	74(13)	-102(13)	-81(15)
C(247)	200(20)	101(12)	81(10)	45(8)	-52(12)	-59(13)
C(31)	55(2)	44(2)	47(2)	2(1)	-17(1)	-13(1)
C(32)	61(2)	95(3)	45(2)	-4(2)	-14(2)	-21(2)
C(33)	61(2)	121(4)	69(2)	-20(2)	-18(2)	-12(2)
C(34)	70(2)	91(3)	76(3)	-8(2)	-36(2)	-10(2)
C(35)	98(3)	90(3)	60(2)	-6(2)	-41(2)	-23(2)
C(36)	68(2)	76(2)	54(2)	-14(2)	-18(2)	-15(2)
C(341)	107(4)	169(6)	153(6)	-52(5)	-87(4)	22(4)
C(342)	169(7)	216(9)	341(14)	-81(9)	-174(9)	66(7)
C(343)	94(4)	223(9)	182(7)	-4(6)	-57(5)	-60(5)
C(344)	135(6)	318(12)	153(7)	-8(7)	-101(5)	47(7)

Table **B1**: Crystal data and structure refinement for 5fbm2_om $[Co_2(CO)_6\{P(O\text{-}2\text{-}EtC_6H_4)_3\}_2]$ **(1b)**

Identification code	5fbm2_0m
Empirical formula	$C_{54}\ H_{54}Co_2O_{12}\ P_2$
Formula weight	1074.83
Temperature	293 K
Wavelength	0.71073 Å
Crystal system, space group	Monoclinic, P2(1)/c
Unit cell dimensions	a = 18.5777(5) Å ,α = 90.00°
	b = 10.5387(2) Å ,β = 96.62 (10)
	c = 26.4248(6) Å ,γ = 90°
Volume(Å^3)	5139.1(2)
Z, Calculated density (Mg/m^3)	4, 1.408
Absorption coefficient (mm^{-1})	0.770
F(000)	2266
Crystal size (mm)	0.29 x 0.20 x 0.05
θ range for data collection (°)	2.21 - 25.68
Limiting indices	-22≤*h*≤22
	-12≤*k*≤12
	-32≤*l*≤32
Reflections collected / unique	63289 / 9754 [R(int) = 0.0640]
Completeness to θ = 25	68 99.9 %
Absorption correction	none
Refinement method	Full-matrix least-squares on F^2
Data / restraints / parameters	9754 / 176 / 719
Goodness-of-fit on F^2	0.981
Final R indices [I>2sigma(I)]	R1 = 0.0553, *wR2* = 0.1306
R indices (all data)	R1 = 0.0866, *wR2* = 0.1515
Largest diff. peak and hole	0.833 and -0.596 e.Å^{-3}

Table **B2**: Atomic coordinates (x 10^4) and equivalent isotropic displacement parameters (Å^2 x 10^3) for 5fbm2_0m. U(eq) is defined as one third of the trace of the orthogonalized Uij tensor.

	x	y	z	U(eq)
Co(1)	2159(1)	-307(1)	8141(1)	30(1)
Co(2)	2520(1)	442(1)	7242(1)	28(1)
P(1)	1889(1)	-770(1)	8879(1)	30(1)
P(2)	2768(1)	890(1)	6498(1)	28(1)
C(01)	2501(3)	1191(4)	8361(2)	45(1)
C(02)	2854(2)	-1468(4)	8103(2)	34(1)
C(03)	1282(3)	-567(4)	7805(2)	38(1
C(04)	2259(2)	-1123(4)	7045(2)	35(1)
C(05)	1830(3)	1615(4)	7264(2)	39(1)
C(06)	3408(3)	746(4)	7555(2)	37(1)
O(01)	2753(2)	2116(3)	8530(1)	69(1)
O(02)	3320(2)	-2156(3)	8068(1)	51(1)
O(03)	721(2)	743(3)	7589(1)	50(1)
O(04)	2107(2)	-2123(3)	6902(1)	49(1)
O(05)	1377(2)	2348(3)	7267(1)	56(1)
O(06)	3978(2)	930(3)	7750(1)	52(1)
O(1)	1571(2)	-2138(3)	8982(1)	46(1)
O(2)	2570(2)	601(3)	9288(1)	41(1)
O(3)	1316(2)	82(3)	9138(1)	52(1)
O(4)	3345(2)	1980(3)	6415(1)	34(1)
O(5)	2054(1)	1249(3)	6138(1)	31(1)
O(6)	3081(2)	-188(3)	6159(1)	33(1)
C(21)	2693(2)	-838(4)	9815(2)	37(1)
C(22)	3409(3)	-807(5)	10009(2)	52(1)
C(23)	3560(3)	-1017(7)	10533(2)	73(2)
C(24)	3028(4)	1224(5)	10837(2)	63(2)

Table **B3** Bond lengths [Á] for 5fbm2_0m. $[Co_2(CO)_6\{P(O\text{-}2\text{-}EtC_6H_4)_3\}_2]$ **(2b)**

Co(1)-C(01)	1.775(5)	Co(1)-C(03)	1.784(5)
Co(1)-C(02)	1.789(5)	Co(1)-P(1)	2.1265(12)
Co(1)-Co(2)	2.6607(7)	Co(2)-C(04)	1.779(4)
Co(2)-c(05)	1.786(5)	Co(2)-C(06)	1.788(5)
Co(2)-P(2)	2.1218(11)	P(1)-O(2)	1.578(3)
P(1)-O(1)	1.592(3)	P(1)-O(3)	1.604(3)
P(2)-O (5)	1.588(3)	P(2)-O(6)	1.598(3)
P(2)-O(4)	1.603(3)	C(01)-O(01)	1.150(5)
C(02)-O(02)	1.142(5)	C(03)-O(03)	1.145(5)
C(04)-O(04)	1.144(5)	C(05)-O(05)	1.143(5)
C(06)-O(06)	1.140(5)	O(1)-C(11b)	1.31(2)
O(1)-C(11a)	1.441(12)	O(2)-C(21)	1.406(5)
O(3)-C(31)	1.419(6)	O(4)-C(41)	.410(5)
O(5)-C(51)	1.421(4)	O(6)-C(61)	1.410(5)
C21)-C(22)	1.371(6)	C(21)-C(26)	1.380(6)
C(22)-C(23)	1.399(7)	C(22)-C(221)	1.488(8)
C(23)-C (24)	1.361(8)	C(24)-C(25)	1.366(8)
C(25)-C(26)	1.387(6)	C(31)-C(32)	1.286(11)
C(31)-C(36)	1.363(10)	C(32)-C(321)	1.487(13)
C(32)-C(33)	1.500(12)	C(33)-C(34)	1.376(14)
C(34)-C(35)	1.288(14)	C(35)-C(36)	1.349(9)
C(41)-C(46)	1.371(6)	C(41)-C(42)	1.385(6)
C(42)-C(43)	1.391(7)	C(42)-C(421)	1.488(7)
C(43)-C(44)	1.365(8)	C(44)-C(45)	1.365(8)
C(45)-C(46)	1.385(7)	C(51)-C(56)	1.375(6)
C(51)-C(52)	1.386(6)	C(52)-C(53)	1.402(6)
C(52)-C(521)	1.513(7)	C(53)-C(54)	1.377(8)
C(54)-C(55)	1.364(8)	C(55)-C(56)	1.384(6)
C(61)-C(66)	1.372(6)	C(61)-C(62)	1.386(7)
C(62)-C(63)	1.389(8)	C(62)-C(621)	1.576(8)
C(63)-C(64)	1.375(8)	C(64)-C(65)	1.356(7)
C(65)-C(66)	1.381(6)	C(221)-C(222)	1.510(11)
C(321)-C(322)	1.462(11)	C(421)-C(422)	1.520(7)
C(521)-C(522)	1.477(9)	C(521)-C(523)	1.581(18)
C(522)-C(523)	1.91(2)	C(621)-C(622)	1.455(10)
C(121)-C(12a)	1.522(14)	C(121)-C(122)	1.534(12)

C(11a)-C(16a)	1.376(13)	C(11a)-C(12a)	1.415(11)
C(12a)-C(13a)	1.392(17)	C(13a)-C(14a)	1.334(18)
C(14a)-C(15a)	1.296(17)	C(15a)-C(16a)	1.428(13)
C(123)-C(16b)	1.56(2)	C(123)-C(124)	1.56(3)
C(11b)-C(16b)	1.383(14)	C(11b)-C(12b)	1.410(14)
C(12b)-C(13b)	1.381(17)	C(13b)-C(14b)	1.31(2)
C(14b)-C(15b)	1.325(19)	C(15b)-C(16b)	1.400(18)

Table B3 Bond angles [º] for 5fbm2_0m. $[Co_2(CO)_6\{P(O\text{-}2\text{-}EtC_6H_4)_3\}_2]$ **(2b)**

C(01)-CO(1)-C(03)	124.8(2)	C(01)-CO(1)-C(02)	113.2(2)
C(03)-CO(1)-C(02)	119.4(2)	C(01)-CO(1)-P(1)	90.96(15)
C(03)-CO(1)-P(1)	96.96(14)	C(02)-CO(1)-P(1)	98.20(13)
C(01)-CO(1)-Co(2)	84.92(14)	C(03)-CO(1)-Co(2)	84.93(13)
C(02)-CO(1)-Co(2)	84.02(12)	P(1)-CO(1)-Co(2)	175.84(4)
C(04)-CO(2)-C(05)	118.6(2)	C(04)-CO(2)-C(06)	120.5(2)
C(05)-CO(2)-C(06)	119.2(2)	C(04)-CO(2)-P(2)	90.95(13)
C(05)-CO(2)-P(2)	96.27(14)	C(06)-CO(2)-P(2)	95.81(14)
C(04)-CO(2)-CO(1)	84.14(13)	C(05)-CO(2)-CO(1)	85.48(14)
C(06)-CO (2)-CO(1)	87.35(13)	P(2)-CO(2)-Co(1)	175.04(4)
O(2)-P(1)-O(1)	105.60(18)	O(2)-P(1)-O(3)	99.38(17)
O(1)-P(1)-O(3)	99.05(19)	O(2)-P(1)-CO(1)	110.32(12)
O(1)-P(1)-CO(1)	119.72(12)	O(3)-P(1)-CO(1)	120.07(13)
O(5)-P(2)-O(6)	99.49(14)	O(5)-P(2)-O(4)	105.84(15)
O(5)-P(2)-CO(2)	110.70(11)	O(6)-P(2)-CO(2)	119.54(11)
O(01)-C(01)-CO(1)	175.1(4)	O(02)-C(02)-CO(1)	176.1(4)
O(03)-C(03)-CO(1)	179.5(4)	O(04)-C(04)-CO(2)	177.3(4)
O(05)-C(05)-CO(2)	178.1(4)	O(06)-C(06)-CO(2)	179.1(4)
C(11b)-O(1)-C(11a)	15.5(10)	C(11b)-O(1)-P(1)	125(2)
C(11a)-O(1)-P(1)	123.0(11)	C(21)-O(2)-P(1)	133.2(3)
C(31)-O(3)-P(1)	121.5(3)	C(41)-O(4)-P(2)	123.5(2)
C(51)-O(5)-P(2)	125.7(2)	C(61)-O(6)-P(2)	124.5(3)
C(22)-C(21)-C(26)	123.1(4)	C(22)-C(21)-O(2)	113.9(4)
C(26)-C(21)-O(2)	122.9(4)	C(21)-C(22)-C(23)	116.2(5)
C(21)-C(22)-C(221)	121.6(4)	C(23)-C(22)-C(221)	122.2(5)
C(24)-C(23)-C(22)	122.4(5)	C(23)-C(24)-C(25)	119.6(5)
C(24)-C(25)-C(26)	120.6(5)	C(21)-C(26)-C(25)	118.1(5)
C(32)-C(31)-C(36)	120.8(7)	C(32)-C(31)-O(3)	119.3(8)

C(36)-C(31)-O(3)	119.6(7)	C(31)-C(32)-C(321)	119.5(8)
C(31)-C(32)-C(33)	120.1(10)	C(34)-C(33)-C(32)	110.8(9)
C(35)-C(34)-C(33)	129.5(12)	C(34)-C(35)-C(36)	115.2(12)
C(35)-C(36)-C(31)	123.1(10)	C(46)-C(41)-C(42)	122.8(4)
C(46)-C(41)-O(4)	120.6(4)	C(42)-C(41)-O(4)	116.5(4)
C(41)-C(42)-C(43)	115.7(4)	C(41)-C(42)-C(421)	122.1(4)
C(43)-C(42)-C(421)	122.2(4)	C(44)-C(43)-C(42)	122.5(5)
C(43)-C(44)-C(45)	120.2(5)	C(44)-C(45)-C(46)	119.5(5)
C(41)-C(46)-C(45)	119.2(5)	C(56)-C(51)-C(52)	124.0(4)
C(56)-C(51)-O(5)	119.5(4)	C(52)-C(51)-O(5)	116.4(4)
C(51)-C(52)-C(53)	115.3(4)	C(51)-C(52)-C(521)	121.2(4)
C(53)-C(52)-C(521)	123.5(4)	C(54)-C(53)-C(52)	121.6(5)
C(55)-C(54)-C(53)	120.7(4)	C(54)-C(55)-C(56)	119.9(5)
C(51)-C(56)-C(55)	118.5(5)	C(66)-C(61)-C(62)	122.1(4)
C(66)-C(61)-O(6)	120.5(4)	C(62)-C(61)-O(6)	117.3(4)
C(61)-C(62)-C(63)	116.6(5)	C(61)-C(62)-C(621)	122.9(5)
C(63)-C(62)-C(621)	120.4(5)	C(64)-C(63)-C(62)	121.6(5)
C(65)-C(64)-C(63)	120.4(5)	C(64)-C(65)-C(66)	119.8(4)
C(61)-C(66)-C(65)	119.5(4)	C(22)-C(221)-C(222)	112.3(6)
C(322)-C(321)-C(32)	124.7(11)	C(42)-C(421)-C(422)	112.2(4)
C(522)-C(521)-C(52)	116.1(5)	C(52)-C(521)-C(523)	112.4(7)
C(521)-C(522)-C(523)	54.0(6)	C(521)-C(523)-C(522)	49.1(6)
C(622)-C(621)-C(62)	107.4(7)	C(12a)-C(121)-C(122)	111.7(7)
C(16a)-C(11a)-C(12a)	124.7(11)	C(16a)-C(11a)-O(1)	113.3(8)
C(12a)-C(11a)-O(1)	122.0(10)	C(13a)-C(12a)-C(11a)	113.6(12)
C(13a)-C(12a)-C(121)	125.2(12)	C(11a)-C(12a)-C(121)	121.1(9)
C(14a)-C(13a)-C(12a)	122.1(16)	C(15a)-C(14a)-C(13a)	123.6(15)
C(14a)-C(15a)-C(16a)	120.3(11)	C(11a)-C(16a)-C(15a)	115.4(10)
C(16b)-C(123)-C(124)	100.9(16)	O(1)-C(11b)-C(16b)	126.0(15)
O(1)-C(11b)-C(12b)	110.6(15)	C(16b)-C(11b)-C(12b)	122.9(19)
C(13b)-C(12b)-C(11b)	117.5(18)	C(14b)-C(13b)-C(12b)	116.1(19)
C(13b)-C(14b)-C(15b)	129(2)	C(14b)-C(15b)-C(16b)	116(2)
C(11b)-C(16b)-C(15b)	116.4(18)	C(11b)-C(16b)-C(123)	112.3(15)
C(15b)-C(16b)-C(123)	131.3(17)		

Table **B4** Anisotropic displacement parameters (A^2 x 10^3) for 5fbm2_0m.The anisotropic displacement factor exponent takes the form: $-2\pi^2$ [$h^2 a^{*2}$ U11 + ... + 2 h k a* b* U12]

	U11	U22	U33	U23	U13	U12
CO(1)	37(1)	30(1)	21(1)	-2(1)	-2(1)	3(1)
CO(2)	34(1)	27(1)	22(1)	0(1)	-1(1)	0(1)
P(1)	29(1)	39(1)	23(1)	-3(1)	-1(1)	4(1)
P(2)	32(1)	27(1)	24(1)	0(1)	0(1)	3(1)
C(01)	72(3)	35(3)	27(2)	0(2)	0(2)	5(2)
C(02)	38(2)	38(2)	26(2)	6(2)	6(2)	2(2)
C(03)	47(3)	42(3)	24(2)	-1(2)	5(2)	5(2)
C(04)	42(2)	35(3)	30(2)	0(2)	7(2)	0(2)
C(05)	48(3)	40(3)	28(2)	0(2)	1(2)	2(2)
C(06)	46(3)	37(2)	28(2)	6(2)	1(2)	2(2)
O(01)	125(4)	32(2)	47(2)	-10(2)	1(2)	13(2)
O(02)	49(2)	47(2)	60(2)	18(2)	15(2)	15(2)
O(03)	39(2)	70(2)	39(2)	-5(2)	-6(2)	3(2)
O(04)	69(2)	32(2)	46(2)	-6(2)	6(2)	8(2)
O(05)	66(2)	53(2)	50(2)	4(2)1	2(2)	23(2)
O(06)	43(2)	65(2)	45(2)	11(2)	-12(2)	13(2)
O(1)	59(2)	46(2)	36(2)	-7(2)	21(2)	7(2)
O(2)	37(2)	65(2)	21(1)	5(1)	-4(1)	4(2)
O(3)	51(2)	71(2)	32(2)	-13(2)	2(1)2	4(2)
O(4)	37(2)	32(2)	32(2)	-2(1)	7(1)	3(1)
O(5)	35(2)	35(2)	22(1)	1(1)	-1(1)	5(1)
O(6)	37(2)	33(2)	27(1)	-2(1)	1(1)	9(1)
O(21)	48(3)	38(2)	23(2)	-1(2)	-3(2)	4(2)
C(22)	46(3)	74(4)	32(2)	-3(2)-	6(2)	19(3)
C(23)	63(4)	115(5)	36(3)	-6(3)-	14(3)	36(4)
C(24)	102(5)	63(3)	21(2)	1(2)	-2(3)	29(3)
C(25)	94(4)	55(3)	31(3)	9(2)	12(3)	7(3)
C(26)	58(3)	64(3)	34(2)	4(2)	6(2)	12(3)
C(31)	44(3)	118(6)	62(4)	-49(4)	-9(3)	37(4)
C(32)	71(5)	128(7)	112(6)	-22(6)	19(5)	23(5)
C(33)	60(5)	160(10)	172(10)	-58(8)	39(6)	5(6)
C(34)	83(6)	157(10)	133(9)	-72(8)	-5(6)	34(7)
C(35)	134(8)	145(9)	90(6)	-53(6)	-32(6)	93(7)
C(36)	115(6)	99(5)	50(3)	-26(3)	-27(3)	77(5)

C(41)	42(2)	24(2)	31(2)	2(2)	8(2)	2(2)
C(42)	41(3)	39(2)	35(2)	6(2)	5(2)	7(2)
C(43)	63(3)	47(3)	49(3)	1(2)	2(2)	19(3)
C(44)	90(4)	35(3)	51(3)	-7(2)	13(3)	16(3)
C(45)	78(4)	26(2)	59(3)	3(2)	27(3)	6(2)
C(46)	47(3)	31(2)	46(3)	5(2)	8(2)	0(2)
C(51)	37(2)	37(2)	25(2)	4(2)	1(2)	12(2)
C(52)	49(3)	36(2)	30(2)	-3(2)	-1(2)	15(2)
C(53)	69(4)	58(3)	33(2)	-12(2)	10(2)	18(3)
C(54)	72(4)	80(4)	25(2)	11(3)	2(2)	31(3)
C(55)	62(3)	64(3)	40(3)	25(3)1	2(21)	7(3)
C(56)	45(3)	42(3)	42(3)	9(2)	0(2)	7(2)
C(61)	36(2)	35(2)	36(2)	-4(2)	2(2)	9(2)
C(62)	70(4)	94(5)	44(3)	20(3)	23(3)	38(3)
C(63)	69(4)	129(6)	70(4)	32(4)	34(3)	49(4)
C(64)	50(3)	81(4)	62(3)	6(3)	10(3)	28(3)
C(65)	47(3)	47(3)	41(3)	4(2)	0(2)	11(2)
C(66)	41(2)	39(2)	36(2)	2(2)	5(2)	8(2)
C(221)	39(3)	183(8)	45(3)	3(4)	-5(2)	25(4)
C(222)	49(4)	197(10)	89(5)	58(6)	-3(3)	21(5)
C(321)	68(5)	144(8)	230(12)	-64(8)	85(7)	19(5)
C(322)	158(9)	148(9)	388(19)-	112(11)	185(12)	75(8)
C(421)	38(3)	62(3)	55(3)	1(3)	4(2)	5(2)
C(422)	56(4)	113(5)	59(4)	5(4)	20(3)	1(4)
C(521)	75(4)	35(3)	47(3)	-2(2)	-8(3)	7(2)
C(522)	69(6)	49(5)	84(7)	-4(5)	-22(5)	8(4)
C(523)	69(11)	68(11)	72(11)	26(9)	16(9)	15(9)
C(621)	70(4)	144(7)	62(4)	-1(4)	29(3)	38(5)
C(622)	99(6)	117(6)	82(5)	19(5)	34(4)	30(5)
C(121)	60(6)	62(6)	34(5)	14(4)	-11(4)	16(5)
C(122)	68(6)	68(6)	58(6)	11(5)	-7(5)	20(5
C(11a)	74(8)	34(7)	25(6)	0(5)	9(6)	2(6)
C(12a)	66(6)	29(5)	31(4)4	(3)4	(4)	0(4)
C(13a)	167(19)	59(12)	77(12)	-2(8)	62(15)	46(13)
C(14a)	132(14)	47(7)	63(8)	24(6)	56(9)	30(8)
C(15a)	71(7)	45(6)	67(6)	23(5)	25(5)	12(5)
C(16a)	60(8)	44(6)	38(6)	2(5)	5(5)	26(6)

C(123) 80(13)	112(14)	47(10)	22(10)	17(9)	6(11)
C(124) 73(11)	78(11)	114(13)	40(10)	42(10)	10(8)
C(11b) 81(14)	71(18)	58(14)	28(13)	19(12)	18(12)
C(12b) 67(12)	101(14)	53(9)	10(9)	-23(9)	37(11)
C(13b) 122(17)	121(17)	90(14)	-3(13)	22(13)	18(15)
C(14b) 95(13)	25(8)	54(10)	12(7)	40(10)	4(10)
C(15b) 100(18)	140(20)	90(20)	17(16)	-6(16)	24(17)
C(16b) 87(12)	20(7)	68(11)	3(6)	49(10)	1(8)

Table **C1**: Crystal data and structure refinement of bm1, $[HCo(CO)_2\{P(O\text{-}4\text{-}^tBuC_6H_4)_3\}_2]$ **(5a)**

Identification code	bm1_
Empirical formula	C_{60} H_{79} Co O_8 P_2
Formula weight	969.53
Temperature	293(2) K
Wavelength	0.71069 Å
Crystal system, space group	Triclinic, $P\bar{1}$
Unit cell dimensions	a = 12.014(5)Å α =92.368(5)°
	b = 12.863(5)Å β = 93.452(5)°
	c = 22.050(5)Å γ = 116.590(5)°
Volume ($Å^3$)	3032.7(19)
Z, Calculated density (Mg/m^3)	2, 1.175
Absorption coefficient (mm^{-1})	0.386
F(000)	1144
Crystal size	0.26 x 0.13 x 0.06 mm
θ range for data collection (°)	0.93 to 25.19
Limiting indices	-10≤*h*≤14
	-15≤*k*≤12
	26≤*l*≤26
Reflections collected / unique	26888 / 10794 [R(int) =0.0719]
Completeness to θ = 25.	98.8 %
Absorption correction	none
Refinement method	Full-matrix least-squares on F^2
Data / restraints / parameters	10794 / 111 / 681
Goodness-of-fit on F^2	0.965
Final R indices [I>2sigma(I)]	R1 = 0.0797, *wR2* = 0.1688
R indices (all data)	R1 = 0.1769, *wR2* = 0.2358
Extinction coefficient	0.0018(4)
Largest diff. peak and hole	0.979 and -1.610 $e.A^{-3}$

Table C2: Atomic coordinates (x 10^4) and equivalent isotropic displacement parameters ($Å^2$ x 10^3) for bm. U(eq) is defined as one third of the trace of the orthogonalized Uij tensor.

	x	y	z	U(eq)
Co	6373(1)	4330(1)	7170(1)	57(1)
P(1)	6713(2)	3014(2)	7571(1)	52(1)
P(2)	8182(2)	5732(2)	7327(1)	55(1)
O(1)	5621(6)	3350(6)	5915(3)	110(2)
O(2)	4462(7)	4323(6)	7909(4)	129(3)
O(11)	7231(4)	3335(4)	8266(2)	60(1)
O(12)	5566(5)	1731(4)	7577(2)	64(1)
O(13)	7710(4)	2621(4)	7329(2)	61(1)
O(21)	8588(5)	6699(4)	7894(2)	65(1)
O(22)	8631(4)	6731(4)	6848(2)	59(1)
O(23)	9287(4)	5348(4)	7367(2)	61(1)
C(1)	5892(7)	3712(7)	6416(4)	78(2)
C(2)	5242(10)	4301(7)	7629(4)	90(3)
C(11)	7317(7)	2598(6)	8699(3)	60(2)
C(12)	7908(9)	1937(8)	8629(3)	90(3)
C(13)	8003(9)	1289(8)	9101(4)	97(3)
C(14)	7520(8)	1290(7)	9643(3)	72(2)
C(15)	6934(10)	1972(9)	9692(4)	106(3)
C(16)	6805(9)	2613(8)	9227(3)	94(3)
C(17)	7657(9)	587(8)	10159(4)	89(3)
C(18)	8901(13)	599(14)	10211(6)	189(7)
C(19)	6651(13)	-610(11)	10076(6)	181(6)
C(21)	4261(6)	1474(6)	7545(3)	55(2)
C(22)	3642(6)	1183(7)	6995(3)	73(2)
C(23)	2367(7)	880(7)	6960(3)	77(2)
C(24)	1757(6)	874(6)	7469(3)	54(2)
C(25)	2473(7)	1173(7)	8016(3)	71(2)
C(26)	3765(7)	1484(7)	8062(3)	67(2)
C(27)	381(6)	622(7)	7428(3)	66(2)
C(28)	-303(9)	-37(10)	6824(5)	132(4)
C(29)	318(9)	1775(8)	7486(4)	101(3)
C(31)	7629(7)	2163(6)	6728(3)	55(2)
C(32)	8423(8)	2837(7)	6346(3)	80(2)
C(33)	8429(9)	2376(7)	5769(4)	90(3)

C(34)	7648(7)	1236(7)	5571(3)	69(2)
C(35)	6890(8)	596(7)	5977(4)	91(3)
C(36)	6861(8)	1047(7)	6557(4)	86(3)
C(37)	7696(10)	708(9)	4945(4)	98(3)
C(38)	7278(17)	1245(14)	4467(5)	197(7)
C(39)	9024(15)	959(17)	4855(7)	247(9)
C(41)	8369(8)	6403(6)	8495(3)	63(2)
C(42)	9034(8)	5984(8)	8823(3)	80(2)
C(43)	8864(9)	5792(8)	9423(3)	91(3)
C(44)	8017(8)	6004(7)	9715(3)	76(2)
C(45)	7320(11)	6395(10)	9369(4)	118(4)
C(46)	7523(10)	6613(9)	8766(4)	106(3)
C(47)	7819(11)	5811(9)	10391(4)	102(3)
C(48)	7964(18)	6875(13)	10728(5)	217(8)
C(49)	8673(15)	5385(16)	10685(5)	205(7)
C(51)	8349(7)	6415(6)	6224(3)	60(2)
C(52)	7566(7)	6734(7)	5904(3)	69(2)
C(53)	7270(8)	6414(7)	5290(3)	78(2)
C(54)	7775(7)	5789(7)	4978(3)	68(2)
C(55)	8591(8)	5520(8)	5313(3)	82(2)
C(56)	8904(8)	5837(7)	5929(3)	77(2)
C(57)	7356(8)	5387(9)	4305(3)	87(3)
C(58)	7572(13)	6435(11)	3936(4)	159(5)
C(59)	5963(10)	4580(11)	4238(4)	141(5)
C(61)	10601(6)	6027(6)	7481(3)	53(2)
C(62)	11185(7)	7208(6)	7454(4)	77(2)
C(63)	12493(8)	7788(7)	7569(4)	80(2)
C(64)	13167(7)	7196(6)	7700(3)	62(2)
C(65)	12534(7)	6003(6)	7724(3)	65(2)
C(66)	11226(7)	5409(6)	7615(3)	58(2)
C(67)	14559(8)	7830(7)	7826(5)	91(3)
C(68)	15251(11)	7425(13)	7427(6)	184(6)
C(69)	15116(10)	9106(9)	7923(7)	159(5)
C(110)	7626(17)	1135(13)	10774(5)	196(7)
C(210)	-277(9)	-100(9)	7948(5)	125(4)
C(310)	6921(16)	-547(11)	4851(6)	202(7)

C(410)	6522(13)	4884(14)	10451(6)	194(7)
C(510)	8027(11)	4755(11)	4040(4)	135(4)
C(610)	4965(12)	7542(12)	8472(6)	168(5)

Table **C3**: Bond lengths [Å] for bm1_.[$HCo(CO)_2\{P(O\text{-}4\text{-}^tBuC_6H_4)_3\}$] **(3b)**

Co-C(2)	1.731(9)	Co-C(1)	1.758(9)
Co-P(2)	2.108(2)	Co-P(1)	2.125(2)
P(1)-O(11)	1.584(4)	P(1)-O(13)	1.605(5)
P(1)-O(12)	1.610(5)	P(2)-O(23)	1.609(5)
P(2)-O(21)	1.613(5)	P(2)-O(22)	1.618(4)
O(1)-C(1)	1.150(9)	O(2)-C(2)	1.162(9)
O(11)-C(11)	1.404(7)	O(12)-C(21)	1.446(8)
O(13)-C(31)	1.407(7)	O(21)-C(41)	1.402(8)
O(22)-C(51)	1.395(7)	O(23)-C(61)	1.421(7)
C(11)-C(12)	1.340(10)	C(11)-C(16)	1.351(9)
C(12)-C(13)	1.391(10)	C(13)-C(14)	1.361(10)
C(14)-C(15)	1.354(11)	C(14)-C(17)	1.527(10)
C(17)-C(19)	1.466(14)	C(15)-C(16)	1.386(10)
C(17)-C(110)	1.513(14)	C(17)-C(18)	1.485(14)
C(21)-C(22)	1.329(9)	C(21)-C(26)	1.319(9)
C(23)-C(24)	1.375(9)	C(22)-C(23)	1.398(9)
C(24)-C(27)	1.531(9)	C(24)-C(25)	1.372(9)
C(25)-C(26)	1.416(9)	C(27)-C(29)	1.520(10)
C(27)-C(28)	1.523(11)	C(27)-C(210)	1.531(11)
C(31)-C(36)	1.335(10)	C(31)-C(32)	1.337(9)
C(32)-C(33)	1.382(10)	C(33)-C(34)	1.374(10)
C(34)-C(35)	1.339(10)	C(34)-C(37)	1.530(10)
C(35)-C(36)	1.392(10)	C(37)-C(38)	1.465(15)
C(37)-C(310)	1.456(14)	C(37)-C(39)	1.507(16)
C(41)-C(46)	1.329(11)	C(41)-C(42)	1.341(10)
C(42)-C(43)	1.367(10)	C(43)-C(44)	1.357(11)
C(44)-C(45)	1.366(11)	C(44)-C(47)	1.537(10)
C(45)-C(46)	1.385(11)	C(47)-C(48)	1.463(15)
C(47)-C(49)	1.492(16)	C(47)-C(410)	1.498(15)
C(51)-C(52)	1.356(9)	C(51)-C(56)	1.370(10)
C(52)-C(53)	1.378(10)	C(53)-C(54)	1.388(10)
C(54)-C(55)	1.365(10)	C(54)-C(57)	1.528(10)

C(55)-C(56)	1.382(10)	C(57)-C(510)	1.503(13)
C(57)-C(59)	1.518(12)	C(57)-C(58)	1.532(13)
C(61)-C(66)	1.344(9)	C(61)-C(62)	1.365(9)
C(62)-C(63)	1.406(10)	C(63)-C(64)	1.364(10)
C(64)-C(65)	1.379(9)	C(64)-C(67)	1.498(10)
C(65)-C(66)	1.406(9)	C(67)-C(68)	1.474(13)
C(67)-C(69)	1.469(12)	C(67)-C(610)	1.591(14)

Table **C3**: Bond angles [º] for bm1_.$[HCo(CO)_2\{P(O\text{-}4\text{-}^tBuC_6H_4)_3\}]$ **(3b)**

C(2)-Co-C(1)	118.0(4)	C(2)-Co-P(2)	118.1(3)
C(1)-Co-P(2)	116.7(3)	C(2)-Co-P(1)	97.7(3)
C(1)-Co-P(1)	100.3(3)	P(2)-Co-P(1)	99.09(8)
O(11)-P(1)-O(13)	99.3(2)	O(11)-P(1)-O(12)	103.0(2)
O(13)-P(1)-O(12)	97.4(3)	O(11)-P(1)-Co	113.30(18)
O(13)-P(1)-Co	121.89(18)	O(12)-P(1)-Co	118.6(2)
O(23)-P(2)-O(21)	102.6(3)	O(23)-P(2)-O(22)	103.4(3)
O(21)-P(2)-O(22)	91.3(2)	O(23)-P(2)-Co	114.26(19)
O(21)-P(2)-Co	122.9(2)	O(22)-P(2)-Co	118.44(18)
C(11)-O(11)-P(1)	128.4(4)	C(21)-O(12)-P(1)	124.9(4)
C(31)-O(13)-P(1)	123.2(4)	C(41)-O(21)-P(2)	122.6(4)
C(51)-O(22)-P(2)	119.7(4)	C(61)-O(23)-P(2)	130.7(4)
O(1)-C(1)-Co	177.0(8)	O(2)-C(2)-Co	175.4(8)
C(12)-C(11)-C(16)	119.4(7)	C(12)-C(11)-O(11)	124.3(6)
C(16)-C(11)-O(11)	116.3(6)	C(11)-C(12)-C(13)	119.8(7)
C(14)-C(13)-C(12)	122.9(8)	C(15)-C(14)-C(13)	115.0(7)
C(15)-C(14)-C(17)	123.0(8)	C(13)-C(14)-C(17)	122.0(8)
C(14)-C(15)-C(16)	123.4(8)	C(11)-C(16)-C(15)	119.4(8)
C(19)-C(17)-C(18)	111.0(11)	C(19)-C(17)-C(110)	109.5(11)
C(18)-C(17)-C(110)	102.5(10)	C(19)-C(17)-C(14)	109.9(8)
C(18)-C(17)-C(14)	112.5(8)	C(110)-C(17)-C(14)	111.3(8)
C(26)-C(21)-C(22)	125.3(7)	C(26)-C(21)-O(12)	117.8(6)
C(22)-C(21)-O(12)	116.8(6)	C(21)-C(22)-C(23)	117.5(6)
C(24)-C(23)-C(22)	122.2(7)	C(25)-C(24)-C(23)	116.0(6)
C(25)-C(24)-C(27)	121.6(6)	C(23)-C(24)-C(27)	122.3(6)
C(24)-C(25)-C(26)	122.7(6)	C(21)-C(26)-C(25)	116.3(6)
C(29)-C(27)-C(28)	109.2(8)	C(29)-C(27)-C(210)	108.3(7)
C(28)-C(27)-C(210)	108.8(8)	C(29)-C(27)-C(24)	108.5(6)

C(28)-C(27)-C(24)	111.3(6)	C(210)-C(27)-C(24)	110.6(7)
C(36)-C(31)-C(32)	120.3(7)	C(36)-C(31)-O(13)	120.9(6)
C(32)-C(31)-O(13)	118.6(6)	C(31)-C(32)-C(33)	119.6(7)
C(34)-C(33)-C(32)	122.2(7)	C(35)-C(34)-C(33)	115.6(7)
C(35)-C(34)-C(37)	122.0(8)	C(33)-C(34)-C(37)	122.3(8)
C(34)-C(35)-C(36)	123.1(8)	C(31)-C(36)-C(35)	119.2(7)
C(38)-C(37)-C(310)	107.3(11)	C(38)-C(37)-C(39)	107.8(12)
C(310)-C(37)-C(39)	108.1(12)	C(38)-C(37)-C(34)	109.8(9)
C(310)-C(37)-C(34)	114.2(9)	C(39)-C(37)-C(34)	109.5(8)
C(46)-C(41)-C(42)	118.4(7)	C(46)-C(41)-O(21)	118.9(7)
C(42)-C(41)-O(21)	122.6(7)	C(41)-C(42)-C(43)	121.1(8)
C(44)-C(43)-C(42)	122.1(8)	C(43)-C(44)-C(45)	116.0(7)
C(43)-C(44)-C(47)	123.1(8)	C(45)-C(44)-C(47)	120.8(9)
C(44)-C(45)-C(46)	121.2(9)	C(41)-C(46)-C(45)	121.1(8)
C(48)-C(47)-C(49)	110.0(11)	C(48)-C(47)-C(410)	107.6(12)
C(49)-C(47)-C(410)	105.7(11)	C(48)-C(47)-C(44)	111.1(9)
C(49)-C(47)-C(44)	112.4(9)	C(410)-C(47)-C(44)	109.8(9)
C(52)-C(51)-C(56)	119.9(7)	C(52)-C(51)-O(22)	119.6(7)
C(56)-C(51)-O(22)	120.5(6)	C(51)-C(52)-C(53)	120.0(7)
C(52)-C(53)-C(54)	121.8(7)	C(55)-C(54)-C(53)	116.3(7)
C(55)-C(54)-C(57)	123.7(8)	C(53)-C(54)-C(57)	119.9(7)
C(54)-C(55)-C(56)	122.8(8)	C(51)-C(56)-C(55)	119.1(7)
C(510)-C(57)-C(59)	108.8(9)	C(510)-C(57)-C(54)	112.5(8)
C(59)-C(57)-C(54)	109.0(7)	C(510)-C(57)-C(58)	109.0(8)
C(59)-C(57)-C(58)	107.3(9)	C(54)-C(57)-C(58)	110.2(8)
C(66)-C(61)-C(62)	122.6(6)	C(66)-C(61)-O(23)	114.5(6)
C(62)-C(61)-O(23)	122.9(6)	C(61)-C(62)-C(63)	117.9(7)
C(64)-C(63)-C(62)	121.4(7)	C(63)-C(64)-C(65)	118.5(7)
C(63)-C(64)-C(67)	120.7(7)	C(65)-C(64)-C(67)	120.8(7)
C(64)-C(65)-C(66)	120.9(7)	C(61)-C(66)-C(65)	118.6(6)
C(68)-C(67)-C(69)	113.2(10)	C(68)-C(67)-C(64)	114.6(8)
C(69)-C(67)-C(64)	116.6(8)	C(68)-C(67)-C(610)	100.6(10)
C(69)-C(67)-C(610)	99.4(9)	C(64)-C(67)-C(610)	109.9(8)

Symmetry transformations used to generate equivalent atoms

Table **C4**: Anisotropic displacement parameters ($Å^2$ x 10^3) for bm1_.The anisotropic displacement factor exponent takes the form:$-2\pi^2$ [$h^2 a^{*2}$ U11 + ... + 2 h k a* b* U12]

	U11	U22	U33	U23	U13	U12
Co	74(1)	54(1)	46(1)	11(1)	3(1)	31(1)
P(1)	74(1)	50(1)	36(1)	3(1)	5(1)	32(1)
P(2)	75(1)	51(1)	38(1)	8(1)	-1(1)	29(1)
O(1)	124(5)	127(6)	57(4)	-5(4)	-24(4)	43(4)
O(2)	129(6)	107(5)	186(7)	39(5)	86(5)	73(5)
O(11)	87(3)	56(3)	41(2)	5(2)	0(2)	37(3)
O(12)	84(3)	48(3)	64(3)	8(2)	10(3)	34(3)
O(13)	88(3)	72(3)	39(2)	1(2)	10(2)	50(3)
O(21)	94(4)	53(3)	45(3)	4(2)	-2(2)	32(3)
O(22)	65(3)	50(3)	47(3)	11(2)	-1(2)	14(2)
O(23)	73(3)	46(3)	62(3)	4(2)	-6(2)	27(2)
C(1)	70(5)	79(6)	72(5)	17(5)	-15(4)	23(4)
C(2)	132(8)	69(6)	105(7)	36(5)	55(6)	69(6)
C(11)	94(5)	53(4)	38(4)	5(3)	2(3)	40(4)
C(12)	130(8)	130(8)	54(5)	26(5)	25(5)	94(7)
C(13)	144(8)	132(8)	69(5)	21(5)	10(5)	109(7)
C(14)	92(6)	71(5)	52(4)	15(4)	2(4)	36(5)
C(15)	167(10)	141(9)	65(5)	46(6)	46(6)	111(8)
C(16)	150(9)	126(8)	59(5)	31(5)	35(5)	103(7)
C(17)	113(7)	90(7)	72(6)	31(5)	4(5)	49(6)
C(18)	162(11)	270(16)	190(12)	145(12)	32(9)	135(12)
C(19)	195(11)	132(9)	171(10)	80(8)	-40(8)	34(8)
C(21)	61(4)	48(4)	53(4)	5(3)	3(3)	23(3)
C(22)	57(4)	101(6)	50(4)	-11(4)	10(4)	27(4)
C(23)	76(5)	106(7)	45(4)	-11(4)	-7(4)	38(5)
C(24)	60(4)	51(4)	53(4)	4(3)	7(3)	26(3)
C(25)	77(5)	87(6)	45(4)	7(4)	17(4)	33(4)
C(26)	64(4)	90(6)	40(4)	9(4)	4(3)	28(4)
C(27)	54(4)	75(5)	75(5)	0(4)	3(4)	34(4)
C(28)	89(7)	161(11)	125(9)	-54(8)	-21(6)	47(7)
C(29)	107(7)	112(8)	117(8)	14(6)	19(6)	77(6)
C(31)	77(4)	58(4)	40(4)	2(3)	6(3)	39(4)
C(32)	100(6)	59(5)	59(5)	-6(4)	19(4)	15(4)

C(33)	117(7)	69(6)	66(5)	4(4)	33(5)	22(5)
C(34	)82(5)	72(5)	50(4)	-9(4)	2(4)	34(4)
C(35)	102(6)	67(5)	84(6)	-19(5)	22(5)	22(5)
C(36)	105(6)	59(5)	77(6)	-2(4)	36(5)	20(5)
C(37)	130(8)	99(7)	59(5)	-24(5)	4(5)	50(7)
C(38)	335(19)	236(15)	79(8)	-22(9)	-14(10)	187(15)
C(39)	197(15)	350(20)	176(13)	-140(13)	38(11)	117(14)
C(41)	94(5)	57(4)	40(4)	-1(3)	3(4)	36(4)
C(42)	104(6)	114(7)	50(4)	14(4)	10(4)	73(6)
C(43)	125(8)	124(8)	51(5)	10(5)	1(5)	81(7)
C(44)	102(6)	74(5)	45(4)	2(4)	4(4)	36(5)
C(45)	154(10)	188(12)	66(6)	18(7)	22(6)	123(9)
C(46)	143(9)	166(10)	62(5)	18(6)	7(6)	116(8)
C(47)	135(9)	111(8)	51(5)	11(5)	11(5)	45(7)
C(48)	400(20)	176(13)	83(8)	-19(8)	39(11)	136(14)
C(49)	246(16)	360(20)	73(7)	79(10)	33(8)	185(15)
C(51)	74(4)	52(4)	44(4)	16(3)	3(3)	20(4)
C(52)	90(5)	73(5)	58(4)	16(4)	9(4)	49(5)
C(53)	96(6)	94(6)	57(5)	21(4)	-3(4)	53(5)
C(54)	66(4)	83(5)	48(4)	21(4)	6(4)	27(4)
C(55)	104(6)	120(7)	51(5)	21(4)	22(4)	73(6)
C(56)	94(6)	102(6)	51(4)	21(4)	4(4)	59(5)
C(57)	90(6)	121(8)	46(4)	12(5)	11(4)	43(6)
C(58)	218(14)	187(12)	61(6)	55(7)	6(7)	80(11)
C(59)	124(9)	185(12)	74(7)	-20(7)	-10(6)	40(9)
C(61)	54(4)	43(4)	48(4)	6(3)	0(3)	10(3)
C(62)	65(4)	57(5)	112(7)	19(4)	-1(5)	29(4)
C(63)	80(5)	45(4)	111(7)	22(4)	3(5)	23(4)
C(64)	63(4)	43(4)	68(5)	13(3)	3(4)	15(3)
C(65)	77(5)	47(4)	70(5)	11(4)	1(4)	28(4)
C(66)	69(4)	41(4)	57(4)	10(3)	-2(3)	18(3)
C(67)	78(5)	56(5)	126(8)	11(5)	4(6)	20(4)
C(68)	103(7)	208(11)	201(11)	-74(9)	38(8)	39(8)
C(69)	101(8)	88(8)	254(15)	2(9)	-27(9)	18(6)
C(110)	351(19)	218(14)	83(8)	37(9)	-2(10)	187(14)
C(210)	94(7)	126(9)	147(10)	51(8)	36(7)	36(7)
C(310)	307(18)	122(10)	119(10)	-45(8)	63(11)	45(11)

C(410)	167(13)	257(16)	109(9)	55(10)	57(9)	44(12)
C(510)	154(10)	203(13)	64(6)	-12(7)	8(6)	99(10)
C(610)	123(9)	180(12)	183(12)	24(10)	-38(9)	58(9)

FOR DETERMINATION OF k_{obs}

// MicroMath Scientist Model File
IndVars: T
DepVars: Aaobs, Abobs, Acobs
Params: Koba, Aa1, Aa0, Kobb, Ab1, Ab0, Kobc, Ac1, Ac0
Aaobs=Aa1-(Aa1-Aa0)*exp((-Koba)*T)
Abobs=Ab1-(Ab1-Ab0)*exp((-Kobb)*T)
Acobs=Ac1-(Ac1-Ac0)*exp((-Kobc)*T)
***

Time	AAOBS	ABOBS	ACOBS
0.00	0.33863	0.27845	1.19726
600	0.33594	0.33662	1.18146
1200	0.33247	0.37665	1.14970
1800	0.32624	0.42677	1.12371
2400	0.31920	0.47126	1.08049
3000	0.31419	0.52539	1.04718
4200	0.30759	0.59343	1.00288
4800	0.30101	0.64057	0.96723
5400	0.29337	0.68254	0.93402
7800	0.28459	0.79098	0.87595
10200	0.27326	0.85978	0.81313
12600	0.26412	0.92395	0.75908
13800	0.25986	0.95220	0.74141
15000	0.25363	0.98596	0.71470
16800	0.25069	1.01306	0.69157
18000			

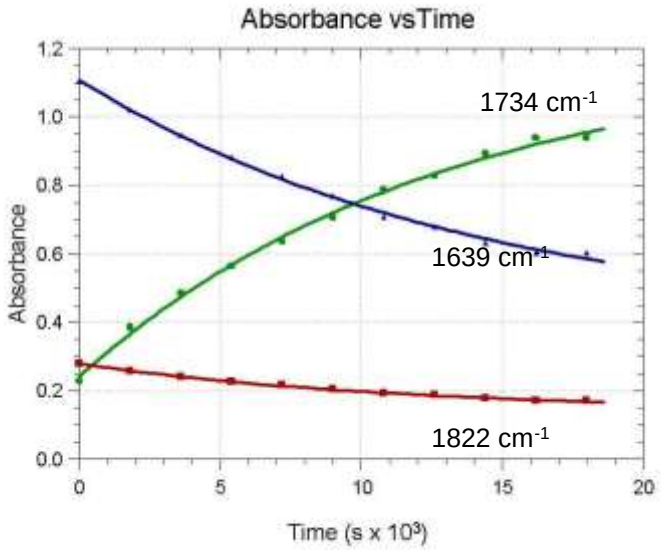

Figure 6.2a2: Representation of the data and kinetic plot of $P(OPh)_3$ ***(a),*** *as ligand in the hydroformylation of 1-octene.*

Time (s)	AAOBS	ABOBS	ACOBS
0.00	0.27916	0.22738	1.10397
1800	0.25783	0.38556	1.02019
3600	0.24066	0.48469	0.94618
5400	0.22558	0.56468	0.88057
7200	0.2156	0.63634	0.82651
9000	0.20363	0.70654	0.76883
10800	0.19170	0.78668	0.70791
12600	0.18690	0.82726	0.68012
14400	0.17690	0.89367	0.63142
16200	0.17020	.93782	0.60326
18000	0.17020	0.93782	0.60326
18600			

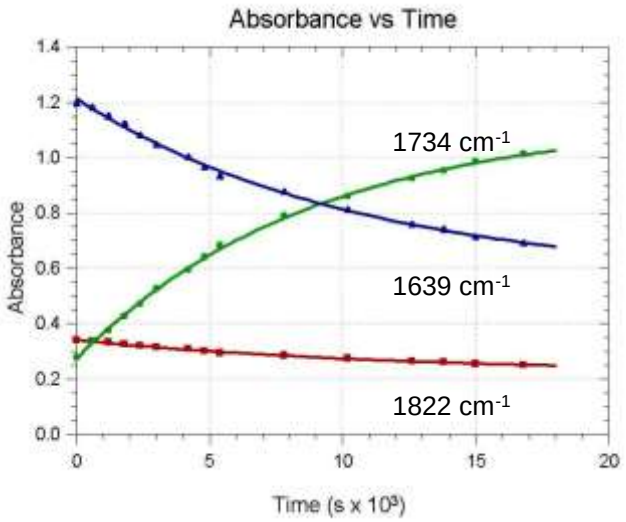

Figure 6.2b2: Representation of the data and kinetic plot of P(O-4-^{t}BuC$_6$H$_4$)$_3$ ***(b),*** *as ligand in the hydroformylation of 1-octene.*

Time	AAOBS	ABOBS	ACOBS
0.00	0.22466	0.42508	1.06445
300	0.21576	0.48883	1.02686
900	0.20288	0.59508	0.97385
1800	0.18555	0.75285	0.89716
2700	0.16985	0.87386	0.81965
3600	0.15879	0.98468	0.76258
4500	0.14877	1.07977	0.71144
5400	0.14010	1.16158	0.66788
6300	0.13223	1.23209	0.63106
7200	0.12590	1.30545	0.59673
8100	0.12007	1.35615	0.56761
9000	0.11491	1.42782	0.53805
9900	0.10967	1.45312	0.51192
10800	0.10370	1.52434	0.48070
11700	0.10040	1.55307	0.45991
12600	0.09689	1.60797	0.44685
13500	0.09254	1.63422	0.42192
18600			

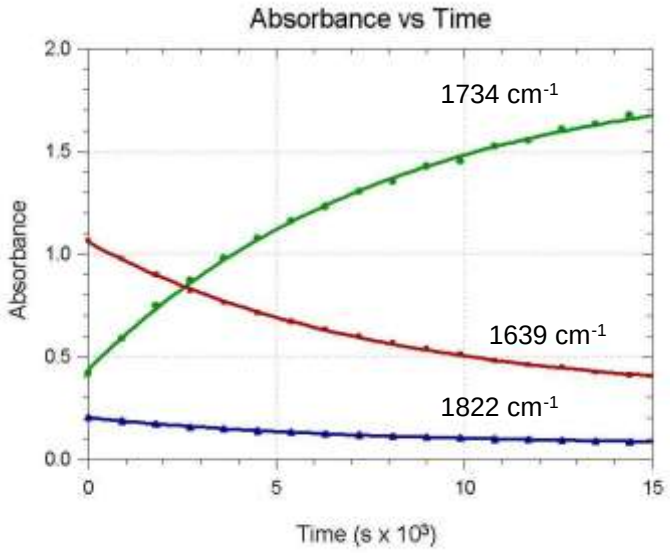

Figure 6.2c2: Representation of the data and kinetic plot of $P(O\text{-}2\text{-}EtC_6H_4)_3$ ***(c)****as ligand in the hydroformylation of 1-octene.*